Errata Sheet

for

David Taylor Model Basin Report 1857

(Aerodynamics Report 1077)

by Harvey R. Chaplin

June 1964

Page 92. Equations [B1] should be:

$$\Psi^*(x,\bar{x},r,\bar{r}) = \sqrt{r\,\bar{r}}\,\frac{2}{k}\left[\left(1 - \frac{k^2}{2}\right)K(k) - E(k)\right]$$

$$V_x^*(x,\bar{x},r,\bar{r}) = \frac{1}{\sqrt{(x - \bar{x})^2 + (\bar{r} + r)^2}}\left\{K(k) - \left[1 + \frac{2(\bar{r} - r)r}{(x - \bar{x})^2 + (\bar{r} - r)^2}\right]E(k)\right\}$$

$$V_r^*(x,\bar{x},r,\bar{r}) = \frac{\bar{x} - x}{\sqrt{(x - \bar{x})^2 + (\bar{r} + r)^2}}\left\{K(k) - \left[1 + \frac{2\bar{r}\,r}{(x - \bar{x})^2 + (\bar{r} - r)^2}\right]E(k)\right\}$$

The next to the last equation should be:

$$\sigma \equiv \sqrt{(x - \bar{x})^2 + (r - \bar{r})^2}\Big/\bar{r}$$

Page 133, Figure 10b: The dashed line was taken from Ref. 4 (not Ref. 1).

Page 135, Figure 11b: The data represented by the circle were taken from Figure 11a (not Figure 14a).

Aerodynamics Laboratory
David Taylor Model Basin

Issued August 6, 1964

A METHOD FOR NUMERICAL CALCULATION OF SLIPSTREAM CONTRACTION OF A SHROUDED IMPULSE DISC IN THE STATIC CASE WITH APPLICATION TO OTHER AXISYMMETRIC POTENTIAL FLOW PROBLEMS

by

Harvey R. Chaplin

Prepared under the direction of
Dr. G. D. Boehler
Professor of Aerospace Engineering
The Catholic University of America

June 1964

Report 1857
Aero Report 1077

Foreword

This report was prepared as a dissertation, under the direction of Dr. G. D. Boehler, Professor of Aerospace Engineering, The Catholic University of America. It was approved by Professor C. C. Chang and Dr. W. B. Morgan as readers. The author is indebted to the above named and to Dr. H. Pao, for their suggestions and encouragement, and to Mr. Dan M. Walker for his tireless assistance with the computer programming and data handling.

TABLE OF CONTENTS

TABLE OF CONTENTS (Concluded)

TABLE OF CONTENTS (Continued)

A Method for Numerical Calculation of SLIPSTREAM CONTRACTION OF A SHROUDED IMPULSE DISC IN THE STATIC CASE With Application to Other Axisymmetric Potential Flow Problems

by

Harvey R. Chaplin, Jr.

SUMMARY

The problem of the axisymmetric flow of an ideal incompressible fluid through an impulse disc bounded by a thin shroud is considered. A systematic calculation procedure is developed, suitable for use on a large electronic digital computer. The shroud and slipstream are represented by a continuous surface distribution of ring vortices. The correct slipstream shape is approached by successive approximations.

The results of calculations of the slipstream contraction ratio, in the static case, for cylindrical, conical, and parabolic-cambered shrouds, are presented. It is found that the slipstream contracts less severely, in the case of very short cylindrical shrouds, than had previously been supposed. Also for cylindrical shrouds, it is found that an excellent estimate of the slipstream contraction ratio can be obtained from a comparatively brief calculation, essentially equivalent to a calculation from the linearized theory, provided the estimate is based on the product of velocity and vortex density at the

trailing edge rather than on the vortex density alone. These results have practical interpretations, within the framework of the one-dimensional shrouded propeller theory, in terms of shrouded propeller static efficiency and thrust ratio. However, such interpretations must be made cautiously until the proper experimental evidence is developed. The theoretical results provide a useful guide for the planning and evaluation of proper experiments.

The method of calculation is also applicable to axisymmetric flows about (a) shrouded impulse discs at finite thrust coefficients, (b) circular inlets, and (c) arbitrary annular and solid bodies of revolution. Internal flows within circular ducts can be closely approximated by the internal flows within very long shrouds. A few calculative results are presented to illustrate these applications.

The accuracy of the method has not been definitely established because, in most of the cases considered, there were no exact solutions available for comparison. By all indications, however, careful application of the method can yield results which are, for ordinary engineering purposes, equivalent to exact solutions.

NOTATION

A_p	propeller disc area, square feet
A_t	shroud exit area, $\pi \bar{r}_N^2$, square feet
C_T	thrust coefficient, $T/(\frac{1}{2} \pi \bar{r}_N^2 \rho U^2)$
e	fractional error [(approximate value) ÷ (exact value) - 1]
F_i	ratio $\bar{\gamma}_i/\bar{\gamma}_N$
f(S)	ratio $\gamma(S)/\gamma(S_{t.e.})$
K(k), E(k)	complete elliptic integrals of the first and second kind, respectively
ℓ	shroud chord, feet
N,M	numbers of cone-frustum segments used to approximate the shroud and slipstream, respectively
P	power expended by the propeller, lb-ft/sec
R_∞	limiting slipstream radius, far downstream, feet
S	curvilinear coordinate of a point on the shroud or slipstream surface, measured along the surface from the shroud leading edge, feet
s	curvilinear coordinate of a point on a surface composed of cone-frustum segments, feet
T	total thrust, pounds
T_p	propeller thrust, pounds
U	free-stream velocity, feet per second
w u u, v	axial and radial components of the velocity at a general point
V	mean velocity at a point on the vortex sheet (that is, mean of the surface velocities on either side of the sheet) feet per second

$\bar{V}$	surface velocity, feet per second
V_j	axial velocity within the far slipstream
V_x, V_r	axial and radial components of the velocity V, feet per second
V_x^*, V_r^*	axial and radial velocity influence functions, feet^{-1}
X, R	axial and radial coordinates of a point on the shroud or slipstream surface, feet
x, r	axial and radial coordinates of a general point, feet
x_i, r_i, s_i	coordinates of the first point of the ith cone-frustum segment, feet
$\bar{x}_i$, $\bar{r}_i$, $\bar{s}_i$	coordinates of the midpoint of the ith segment (that is, $\bar{x}_i = \frac{1}{2}(x_i + x_{i+1})$, etc.) except, when i = 1, coordinates of the first point of the first segment, also the leading edge of the shroud, feet
$\bar{x}_N$, $\bar{r}_N$, $\bar{s}_N$	coordinates of the shroud trailing edge, feet
$a_{i,j}$	stream function influence coefficient, square feet ($a_{i,j}\bar{\gamma}_j$ is the value of the stream function at the point $(\bar{x}_i, \bar{r}_i)$, due to the pulse $\gamma_j(s)$)
$b_{i,j}$, $c_{i,j}$	axial and radial velocity influence coefficients, dimensionless
$a_{i,j-}$, $b_{i,j-}$, $c_{i,j-}$	partial values of the influence coefficients, corresponding to the first part of the pulse $\gamma_j(s)$ ($a_{i,j} = a_{i,j-} + a_{i,j+}$, etc.)
$a_{i,j+}$, $b_{i,j+}$, $c_{i,j+}$	partial values of the influence coefficients, corresponding to the second part of the pulse $\gamma_j(s)$ ($a_{i,j} = a_{i,j-} + a_{i,j+}$, etc.)

α_i	semi-vertex angle of the ith segment, radians (subscript omitted when not required for clarity)
γ	density of ring-vortex singularity distribution, divided by 2π, feet per second
$\gamma_i(s)$	pulse of continuously distributed ring-vortex singularities defined over the ith and (i-1)th cone-frustum segments, feet per second
$\bar{\gamma}_i$	characteristic value of $\gamma_i(s)$, feet per second
η_F	Froude efficiency ($\eta_F = TU/P$)
η_{st}	static efficiency $\left(\eta_{st} = \eta_{st} = \dfrac{T^{3/2}}{2\sqrt{\rho A_t}\, P}\right)$
ϕ	slipstream contraction ratio $(R_\infty / \bar{r}_N)^2$
ρ	fluid density, slugs per cubic foot
Ψ	value of Stokes' stream function, cubic feet per second
Ψ^*	stream-function influence function, feet

INTRODUCTION

The advent of the high speed electronic computer has made it practical to solve many problems in fluid mechanics which would have required prohibitive labor in an earlier era. The present investigation is concerned with bringing the power of this modern tool to bear against certain problems of the axisymmetric flow of an ideal incompressible fluid which have resisted previous efforts at solution.

In Part I, the problem of the axisymmetric potential flow through a shrouded impulse disc is considered. This is a boundary value problem of a non-classical mixed type which had previously been solved only in cases for which the second boundary condition could be disposed of by a simple assumption. A systematic method of calculation is developed, tried out, and discussed.

The motivation for the investigation of Part I comes from certain practical problems of the shrouded propeller, associated with the concept of slipstream contraction. However, Part I is confined primarily to consideration of the mathematical problem of the shrouded impulse disc. The practical aspects are discussed in Part II, in the context of the results of calculations.

It is found that the method of calculation developed to solve the problem of the shrouded impulse disc is also directly applicable to certain other problems; and that it could, by means of straightforward modifications and extensions, be developed into a rather general and powerful tool for axisymmetric potential flow calculations. These further applications and possible extensions are also discussed briefly in Part II.

PART I - A METHOD FOR CALCULATING THE AXISYMMETRIC POTENTIAL FLOW THROUGH A SHROUDED IMPULSE DISC IN THE STATIC CASE

The shrouded impulse disc is a mathematical idealization of the shrouded propeller, wherein the fluid which passes through the propeller is imagined to receive a uniformly discontinuous increase in total pressure, and to flow downstream in a sharply defined stream tube, called the slipstream. Further, the velocity is imagined to be free from azimuthal components, and to be continuous everywhere except at the boundaries of the flow; that is, at the shroud and slipstream surface.

This idealization obviously greatly enhances the possibilities of calculating the flow in detail. On the other hand, many of the details of the flow so calculated will differ markedly from those of a real flow through a real shrouded propeller.

The question of the applicability of shrouded impulse disc results to practical shrouded propeller problems will be discussed at length - in Part II of the present investigation. Part I is restricted to consideration of the mathematical problem of the idealized shrouded impulse disc.

In the exact theory of the shrouded impulse disc, the shroud shape is regarded as known. The flow and the slipstream shape are to be determined so that the shroud and slipstream are part of a common stream tube; and so that there is a uniform discontinuity in squared velocity across the slipstream boundary.

Previous theories have provided approximate solutions of this problem, subject to assumptions which can be justified only if the slipstream

diameter is nearly constant. Therefore, these theories have been of very limited value for estimating the slipstream contraction.

PREVIOUS THEORIES

Access to the technical literature related to shrouded propellers was greatly facilitated by Sacks' and Burnell's (Reference 1) comprehensive bibliography, which includes brief critiques of many of the important works

Current practical understanding of the shrouded propeller is based, in large part, on the one-dimensional momentum theory of the shrouded impulse disc. A fairly thorough account of this theory is given by Krüger (Reference 2). The essential elements are reviewed herein, at the beginning of Part II. A number of useful relationships between the thrust, power expenditure, and forward velocity are deduced by applying the principles of conservation of momentum and energy to the flow in the slipstream far downstream from the shroud. The one-dimensional theory gives no prediction of the slipstream contraction, however, and, to apply the theory successfully, one must have prior information on the slipstream contraction from some independent source.

A second theoretical approach, which can yield a prediction of the slipstream contraction, is provided by the method of singularities. This approach to the shrouded impulse disc problem appears to have been first developed to the point of application by a team of investigators in Germany during the World War II period. A lucid account of the main features of this work, with references to the original papers, was subsequently published by two of these investigators, Küchemann and Weber (Reference 3). The axisymmetric flow about a shrouded impulse disc with negligible shroud thickness and small (but not necessarily negligible) camber was

represented by a distribution of ring vortices on a semi-infinite cylinder, originating at the leading edge of the shroud. The vortex distribution was assumed to be uniform downstream of the shroud trailing edge. The vortex distribution along the length of the shroud was solved for, applying the boundary condition (equivalent to that applied by Glauert (Reference 4) in his thin-airfoil theory) that the flow at a point on the cylinder containing the singularities should be parallel to that at the corresponding point on the shroud. The solutions actually obtained were carried out by a numerical process, in which the boundary condition was satisfied at a finite number of points along the shroud. A second boundary condition, equivalent to the Kutta condition of airfoil theory, was shown to be satisfied merely by requiring that the vortex distribution be continuous at the trailing edge. (The numerical process involved the use of tables of the stream function and velocity components for an isolated vortex ring (Reference 5), based on the solution for flow around a vortex ring, which was given in terms of the complete elliptic integrals by Lamb (Reference 6).) It was argued that the solutions obtained in this manner afforded valid approximations in all cases in which the stream surface defining the shroud and slipstream deviated little from the cylinder on which the singularities were placed. This requirement was shown to be satisfied, in general, when the thrust coefficient was small. In the case of high thrust coefficients (including the static case), a valid approximation was assured only if the shroud was cylindrical and of sufficiently long chord to assure a slipstream contraction ratio of nearly unity. Thus, the application of such results to the prediction of the contraction ratio was severely limited.

This general approach to the problem is usually referred to as

"linearized shrouded propeller theory." The linearized theory has been further developed by a number of more recent investigators, who have also considered some of the effects of shroud thickness, finite center bodies, and propellers with finite numbers of blades and non-uniform loading. However, the limitations on application of the linearized theory to the prediction of slipstream contraction have not been alleviated. For an account of these developments, the reader is referred to Morgan (Reference 7).

Despite the known limitations of the linearized theory, it has nevertheless been applied by some investigators to the calculation of slipstream contraction of the shrouded impulse disc, even in the static case, because no alternative method of calculation was available. The most extensive such application was by Kriebel, Sacks, and Nielson (Reference 8), using a technique devised by Burggraf (Reference 9). They treated thin cylindrical shrouds of sufficiently short chord that the flow around the shroud could be considered essentially two-dimensional. (This work is particularly interesting, in that it is the only case in which explicit analytical solutions have been obtained.) Helmbold (Reference 10) presented results of numerical calculations (for shrouds with chords of 0.5, 1.0, and 2.0 propeller radii) in which the boundary condition was satisfied at only three points along the chord.

To whatever extent such calculations might be valid, most of the earlier analyses using the linearized theory also produced results which could be interpreted to give information on the slipstream contraction in the static case; but such interpretations were not offered by the earlier authors. For example, Küchemann and Weber (Reference 11, Figure 7) presented for cylindrical shrouds of chord/diameter ratios zero to unity a

graph of a nondimensional variable which is directly interpretable, in the static case, as twice the contraction ratio, less one. These authors made no such interpretation, however; and, in fact, stated in regard to their representation of the slipstream by a uniform vortex cylinder that ". . . the flow at advance ratio zero, of particular importance for the propeller with annular fairing, cannot be dealt with by this assumption."

FORMULATION OF THE PROBLEM

In this section we will formulate the problem of calculating a stationary irrotational flow of an incompressible, inviscid, homogeneous fluid of infinite extent through a shrouded impulse disc, in the static case. We will restrict ourselves to the case of a shroud which is a surface of revolution, this being the simplest case of practical interest. Effects of gravitational forces and other extraneous forces will be neglected, as is usual in problems of this kind.

We will use the cylindrical coordinate system (x, r, θ). It is evident from symmetry that none of the properties of the flow will depend on the azimuthal coordinate, θ, so the coordinates of a general point can be specified (x, r), provided that, when two or more points are specified without the aximuthal coordinate, they will be understood to lie in a common meridian plane.

The shroud can specified by an equation

$$r = R(x) \quad , \quad 0 \leq x \leq x_{t.e.}$$

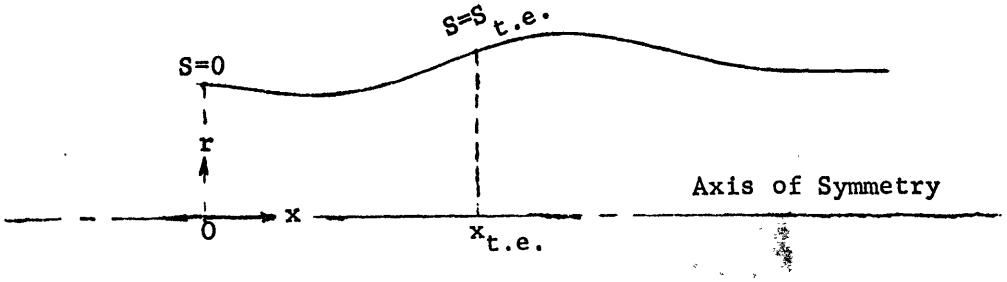

The function R(x) need not be single-valued. To avoid ambiguity, we will define a curvilinear coordinate S, measured along the shroud from the leading edge. The shroud can then be specified by the single-valued equation.

$$r = R(S) \quad , \quad 0 \leq S \leq S_{t.e.}$$

For the present, let us assume that the slipstream boundary is a simple continuation of the shroud surface, so that the shroud and slipstr boundary together constitute a continuous semi-infinite surface of revolu describable by a single-valued function

$$r = R(S) \quad , \quad 0 \leq S$$

although only the portion of this function which describes the shroud is known initially.

We regard the shroud as a rigid and impervious physical surface; whereas, as previously stated, the slipstream boundary is regarded as a hypothetical surface along which the normal velocity components vanish, b across which we admit the possibility of a discontinuity in tangential velocity. The role of the impulse disc now becomes apparent for, under t assumptions thus far stated in the present section, Bernoulli's equation

$$p + \tfrac{1}{2} \rho(u^2 + v^2) = p_o$$

would apply, with the same constant p_o, along every streamline of the flow. Thus a discontinuity of velocity across the slipstream surface

would imply a discontinuity in pressure, which is physically unreasonable. This difficulty is avoided by postulating the existence of a closed surface, the impulse disc, which is bounded by a closed line on the surface of the shroud, and which, together with the shroud and slipstream surface, divides the space into two regions, as follows:

The first region includes all of the points on the outer suface of the slipstream boundary. Within the first region, Bernoulli's equation applies in the form

$$p + \tfrac{1}{2} \rho(u^2 + v^2) = p_o$$

The second region includes all of the points on the inner surface of the slipstream boundary. Within the second region, Bernoulli's equation applies in the form:

$$p + \tfrac{1}{2} \rho(u^2 + v^2) = p_o + \Delta p$$

Now, a discontinuity in velocity across the slipstream boundary is permissible, provided the discontinuity in squared velocity is equal to $2 \Delta p/\rho$, for there will then be no discontinuity in static pressure.

On the other hand, if we now adopt the assumption that all velocity components are continuous across the impulse disc, it is evident that there is a uniform discontinuity in static pressure across that surface. We can argue that this is physically reasonable, if we consider the impulse disc to represent a propeller, on the grounds that an approximately similar difference in the static pressure is found between points just ahead of, and just behind, a real propeller.

It will be recognized that, under the assumptions which have been

introduced, we will be dealing with that class of fluid flows known as potential flow. Thorough treatments of the formulation and solution of the basic flow equations for such cases are given by Lamb, Reference 6, and appear in innumerable other books on fluid mechanics, applied mathematics, and potential theory. However, for the sake of clarity and completeness, the complete mathematical development of the problem will be outlined, starting from the equations of continuity and irrotationality. To avoid repetitious citation of references, it will be understood that Lamb can be referred to for all aspects of this development not unique to the present problem.

The governing equations of the flow are the equations of continuity and irrotationality:

$$\frac{\partial u}{\partial x} + \frac{1}{r}\frac{\partial}{\partial r}(rv) = 0 \qquad [$$

$$\frac{\partial u}{\partial r} - \frac{\partial v}{\partial x} = 0 \qquad [$$

It is convenient to introduce Stokes' stream function, $\Psi(x,r)$, defined so that

$$\left.\begin{aligned} u &= \frac{1}{r}\frac{\partial \Psi}{\partial r} \\ v &= -\frac{1}{r}\frac{\partial \Psi}{\partial x} \\ \Psi(x,r) &= \int_0^r u(x,r')\, r'dr' \end{aligned}\right\} \qquad [$$

(We denote these relations as Equations [1′] because, as can be verified by direct substitution, the existence of the function $\Psi(x,r)$ is a sufficient condition that the continuity Equation [1] is satisfied). Our boundary conditions can now be expressed

$$\Psi(x,R) = \Psi_o \quad , \quad 0 \le x \qquad [$$

$$\lim_{\epsilon \to 0} \left[u^2(x,R-\epsilon) + v^2(x,R-\epsilon) - u^2(x,R+\epsilon) - v^2(x,R+\epsilon) \right] = 2 \frac{\Delta p}{\rho} \qquad [4]$$

for $x_{t.e.} \leq x$.

Now, evidently the function R(S) is bounded, because if R increased without limit, the velocities within the slipstream must vanish and Equation (4) could not be satisfied. Moreover, it is evident that, as x increases without limit, the velocities outside the slipstream must vanish, so that the flow within the slipstream becomes uniform. This provides a relation between the quantities Ψ_o and $\frac{\Delta p}{\rho}$, for, if we denote the limiting velocity by u_∞ and the limiting radius by R_∞, we have

$$\Psi_o = \tfrac{1}{2} u_\infty R_\infty^2$$

from Equation [3]; and

$$u^2_\infty = 2\Delta p/\rho$$

from Equation [4]. Whence

$$R_\infty^2 = \Psi_o \sqrt{2/(\Delta p/\rho)}$$

Thus we are free to specify only one of the quantities, Ψ_o or $\frac{\Delta p}{\rho}$, arbitrarily, in stating the problem. We will choose to specify Ψ_o arbitrarily. (It may be noted further that the value given to Ψ_o, together with the arbitrary scale in which the shroud dimensions are given, serves merely to establish a scale of velocities. It will not influence the slipstream contraction.)

Let us now examine the assumption that the slipstream surface is a simple continuation of the shroud surface. This assumption could be justified by analogy with the Kutta condition of airfoil theory, but it appears that there is a better justification. Suppose the slipstream

surface met the shroud surface at a point other than the trailing edge.

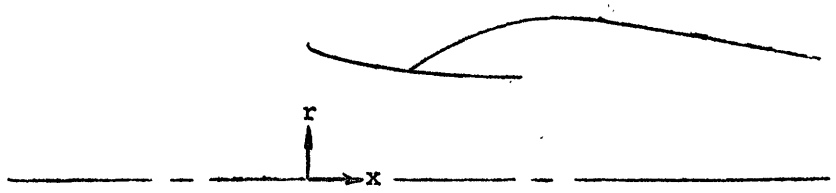

Evidently, the velocities must vanish in the corners on both sides of such a juncture, and Equation [4] could not be satisfied. Moreover, we see that the slipstream not merely must meet the shroud at the trailing edge, but that the function R(S) must have continuous first derivatives at all points $S \geq S_{t.e.}$. Otherwise, we would have a corner, at which the velocities would vanish on one side of the surface and become unbounded on the other side, and again Equation [4] could not be satisfied. (One can conceive of cases in which these simple arguments would not hold. For example, a shroud might have a cusp between the specified leading and trailing edges, at which the slipstream might meet without violation of Equation [4]; but such exceptions are evidently without practical interest.)

Now let us collect the pertinent relations together. Equations [1] and [2] can be replaced by a single equation expressing the condition of irrotationality in terms of the stream function.

$$\frac{\partial^2 \Psi}{\partial x^2} + \frac{\partial^2 \Psi}{\partial r^2} - \frac{1}{r} \frac{\partial \Psi}{\partial r} = 0 \qquad [2']$$

The boundary conditions can now be expressed

$$\Psi(x,R) = \Psi_o \quad , \quad 0 \le x \qquad [3]$$

$$\lim_{\epsilon \to 0} \left[u^2(x,R-\epsilon) + v^2(x,R-\epsilon) - u^2(x,R+\epsilon) - v^2(x,R+\epsilon) \right] = \text{a constant} \qquad [4']$$

for $x_{t.e.} \le x$. The velocities u and v are given in terms of the stream function by Equation [1′].

Given a shroud, and the boundary value Ψ_o of the stream function, one is to find a solution $\Psi(x,r)$ of Equation [2′] which has the value Ψ_o on the shroud surface, and which satisfies the condition [4′] along the rest of the stream surface $\Psi = \Psi_o$.

Equation [2′] is readily solved by the method of separation of variables, and has solutions of the form

$$\Psi(x,r) = r(A_k e^{kx} + B_k e^{-kx}) \; J_1(kr)$$

where J_1 is the Bessel function of first order and first kind, and where k can assume any value whatever, real or complex.

We require solutions corresponding to velocities which are continuous and bounded everywhere except on the surface

$$r = R(x) \quad , \quad 0 \le x$$

whereas it is found that individual solutions of the above type correspond to velocities which are unbounded at infinity. However, it is shown in Reference 6 that, by superposition of infinitely many of these elementary solutions in the form of a definite integral, a composite solution

$$\Psi(\bar{x},\bar{r}) = \frac{\Gamma}{2} r\bar{r} \int_o^\infty e^{-k|x-\bar{x}|} \; J_1(kr) \; J_1(k\bar{r}) \; dk$$

(with k real) can be formed, which corresponds to velocities which are

bounded and continuous at all points except on the circle (x,r). In fact, this expression gives the stream function at a point $(\bar{x}, \bar{r})$ due to a discrete vortex ring of circulation Γ at the position (x, r). (There are other solutions which satisfy this condition; for example, the stream functions of ring vortices and ring doublets. However, since we have to deal with a boundary condition on the discontinuity of tangential velocity across a surface, it will be seen that the ring vortex is a natural choice.)

Lamb also gives an equivalent and more convenient form of this solution, in terms of the complete elliptic integrals. A concise review of Lamb's derivation is given herein in Appendix E. The result is:

$$\Psi(\bar{x}, \bar{r}) = \frac{\Gamma}{2\pi} \sqrt{r\bar{r}} \frac{2}{k} \left[(1 - \frac{k^2}{2})K(k) - E(k) \right] \qquad [5]$$

where K(k) and E(k) are the complete elliptic integrals of the first and second kinds, with modulus

$$k = \sqrt{\frac{4r\bar{r}}{(x-\bar{x})^2 + (r+\bar{r})^2}}$$

We can now construct a solution of Equation [2'] which has the required properties, as a superposition of infinitely many solutions of the type given in Equation [5], in the form of another definite integral. In other words, we can consider that $\Psi(\bar{x}, \bar{r})$ arises from a distribution of coaxial ring vortices on the surface r = R(S). Since we are concerned only with points on this surface, it is convenient to write Equation [5] in the form

$$d\Psi(\bar{S}) = \gamma(S)\, dS\, \psi^*(S,\bar{S}) \qquad [5']$$

where $\gamma(S)dS$ has taken the place of $\frac{\Gamma}{2\pi}$, and is the circulation around the element of surface between S and S + dS, divided by 2π; and the

function $\psi^*(S,\bar{S})$, which we shall call the stream-function influence function, represents the remaining factors of the right-hand member of Equation [5].

The rather awkward notation of Equation [4′] can be avoided if we note that the magnitude of the velocity discontinuity across the surface $r = R(S)$ is precisely $2\pi\,\gamma(S)$.

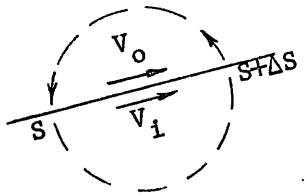

$$2\pi\,\gamma(S)\,dS = \oint (u\,dx + v\,dr) = (V_i - V_o)\,dS$$

$$V_i = V + \pi\gamma$$

$$V_o = V - \pi\gamma$$

$$V_i^2 - V_o^2 = 4\pi\,\gamma\,V$$

If we denote the mean tangential velocity at a point of this surface by $V(S)$, the discontinuity in squared velocity across the surface is

$$\left[V(S) + \pi\,\gamma(S)\right]^2 - \left[V(S) - \pi\,\gamma(S)\right]^2 = 4\pi\gamma(S)\,V(S) \qquad [6]$$

The axial and radial components V_x and V_r of the velocity V can be obtained by differentiating the stream function according to Equation [1′]. The results are given by Reference 3. We will write the results here in the form

$$dV_x(\bar{S}) = \gamma(S)\,dS\;V_x^*(S,\bar{S})$$
$$dV_r(\bar{S}) = \gamma(S)\,dS\;V_r^*(S,\bar{S}) \qquad [7]$$

analogous to Equation [5′] above. Detailed expressions for the axial and radial velocity influence functions are given herein in Appendix B.

We can now express the boundary conditions Equations [3] and [4′] in terms of solutions of the differential equation (Equation [2′]), with the aid of Equations [5′], [6], and [7]:

$$\psi(\bar{S}) = \int_0^\infty \psi^*(S,\bar{S})\,\gamma(S)\,dS = \psi_o \quad , \quad S \geq 0 \qquad [3']$$

$$\left.\begin{aligned} \gamma(\bar{S})V(\bar{S}) &= \text{a constant}, \quad S \geq S_{t.e.} \\ V(\bar{S}) &= \left\{\left[\int_0^\infty V_x^*(S,\bar{S})\ \gamma(S)\ dS\right]^2 + \left[\int_0^\infty V_r^*(S,\bar{S})\ \gamma(S)\ dS\right]^2\right\}^{\frac{1}{2}} \end{aligned}\right\} \quad [4'']$$

We must not lose sight of the fact that, in these equations, the influence functions Ψ^*, V_x^*, V_r^* have specific meaning only in terms of a specific function R(S), since the same thing may be said of the variables S, $\bar{S}$ themselves, and that the function R(S) is known initially only up to the point $S = S_{t.e.}$. Equations [3'] and [4''] thus constitute two equations in the two unknown functions

$$R(S) \quad , \quad S > S_{t.e.}$$

$$\gamma(S) \quad , \quad S \geq 0$$

It is evident, from the discussion of previous theory in the preceding section, that we cannot expect to find nontrivial analytic solutions of the pair of Equations [3'] and [4'']. Previous investigators, even by neglecting the second boundary condition entirely, and retaining a single equation equivalent to Equation [3'], have succeeded in obtaining analytic solutions (or numerical solutions, for that matter) only by means of still further simplifying assumptions regarding the representation of the slipstream; and even then, only in cases of small thrust coefficients or of cylindrical shrouds. We shall therefore proceed immediately to attempt solution of the problem by numerical approximation.

METHOD OF SOLUTION

We have seen that the successful previous treatments of the shrouded propeller and the shrouded impulse disc by the method of singularities proceeded on the following scheme: A sufficiently strong assumption was

made on the mathematical representation of the slipstream that the boundary condition on the shroud itself could be expressed by a single definite integral equation with finite limits of integration. This equation yielded a solution which was assumed, subject to appropriate restrictions, to be approximately consistent with the two boundary conditions on the slipstream.

We will begin with the same scheme; but then, since we must anticipate that, in general our first solution will not be consistent with the boundary conditions on the slipstream, we will seek to improve the mathematical representation of the slipstream by successive approximation.

A systematic calculating procedure along this line, suitable for execution on a large electronic digital computer, is developed in detail in Appendix A. For the sake of continuity, the essential elements of this development will be indicated briefly here.

The following simplifying assumptions are introduced:

1. It is assumed that the distribution of vortices on the shroud and slipstream can be represented by a continuous distribution $\gamma(S)$ on a continuous system of cone-frustum segments (N of which approximate the shroud shape and M of which approximate the slipstream shape), the function $\gamma(S)$ being further represented by a superposition of N+M simple pulse functions as illustrated in Figure 1.

2. It is assumed that, if such a representation is found so that the boundary condition $\Psi=\Psi_0$ is satisfied at the leading edge and at the midpoint of the second segment and each succeeding segment except the last (which is taken to be semi-infinite in length), and so that the second boundary condition of the slipstream (γV= a constant) is satisfied

at the midpoint of the Nth through (N+M-1)th segments, this representation will constitute an approximate solution of the exact problem, Equations [3′] and [4″].

These assumptions are justified initially by the fact that similar assumptions, introduced by Smith and Pierce in their treatment (Reference 12) of the Neumann problem for bodies of revolution, led to excellent approximations in the cases which they considered. (Smith and Pierce represented bodies of revolution by stepwise continuous distributions of ring sources on systems of cone-frustum segments.) Further justification will be provided, after the fact, by demonstrating that the method of calculation developed herein also gives excellent approximate solutions, in certain cases for which exact solutions are known.

With these assumptions, the stream function and mean velocity components at a point $s = \bar{s}_i$ of the system of cone-frustum segments (where $\bar{s}_i$ is a point on the leading edge, and otherwise $\bar{s}_i$ is a midpoint of the ith segment) can be expressed by linear algebraic equations,

$$\Psi(\bar{s}_i) = \sum_{j=1}^{N+M} a_{i,j}\,\bar{\gamma}_j \qquad [8]$$

$$\left.\begin{aligned} V_x(\bar{s}_i) &= \sum_{j=1}^{N+M} b_{i,j}\,\bar{\gamma}_j \\ V_r(\bar{s}_i) &= \sum_{j=1}^{N+M} c_{i,j}\,\bar{\gamma}_j \\ V(\bar{s}_i) &= [V_x^2(\bar{s}_i) + V_r^2(\bar{s}_i)]^{\frac{1}{2}} \end{aligned}\right\} \qquad [9]$$

where $\bar{\gamma}_j$ is a variable characterizing the vortex density of the pulse $\gamma_j(s)$; and the influence coefficients $a_{i,j}$, $b_{i,j}$, and $c_{i,j}$ depend only upon the geometry of the system of cone-frustum segments.

The development of practical and accurate procedures for calculating these influence coefficients, given the shape of the system of segments, constitutes a main problem of the present investigation. This problem (which resolves itself into five distinct cases, depending upon the nature of the pulse $\gamma_j(s)$ and the geometric relationship of the point $\bar{s}_i$ to the cone-frustum segments over which this pulse is defined) does not lend itself to brief discussion. The interested reader is referred to the detailed development in Appendix A.

Now suppose we have been given a shroud and the constant boundary value Ψ_o, and have chosen a system of N cone-frustum segments which approximates the shroud. As a first approximation, we choose a continuation of this system (M additional segments, the last of which is a semi-infinite cylinder) to represent the slipstream. Further, we choose a set of numbers ($F_i = \bar{\gamma}_i/\bar{\gamma}_n$, $N+1 \le i \le N+M$) to represent a first approximation to the shape of the vortex distribution on the slipstream. The influence coefficients now become known constants; and in Equation [8], the last M+1 terms of the summation reduce to a single known constant multiplied by $\bar{\gamma}_N$. Application of Equation [8] to the first N points $\bar{s}_i$ results in a system of N equations in the N unknown variables $\bar{\gamma}_j$, which can be solved for the values of these variables consistent with the condition

$$\Psi(\bar{s}_i) = \Psi_o \quad , \quad 1 \le i \le N$$

Now, Equations [8] and [9] can be applied to learn how nearly consistent our first approximation is, with the boundary conditions along the slipstream (which we have thus far neglected). That is, we tabulate the

sets of quantities

$$\left.\begin{array}{c} \Psi(\bar{s}_i) \\ \gamma(\bar{s}_i)\ V(\bar{s}_i) \end{array}\right\} \quad N+1 \le i \le N+M-1$$

If the first of these sets were uniformly equal to Ψ_o and the second were uniformly equal to $\gamma(\bar{s}_N)V(\bar{s}_N)$ we would consider the problem solved. In general, of course, this will not be the case, and we will seek to improve the first assumption on the shape of the slipstream and the shape of the vortex distribution on the slipstream. If we have a method of doing this, we can, of course, repeat the procedure described above as many times as we like, improving the assumptions after each cycle of calculation, until we have a solution as nearly consistent with the boundary conditions on the slipstream as desired.

The problem of deducing an improved estimate of the slipstream shape and vortex distribution is approached under the following tentative assumptions:

1. It is assumed that the radial coordinate of a general point on the slipstream surface is a single-valued function of the axial coordinate. Thus, the successive estimates of the slipstream shape need differ only in the radial coordinates.

2. It is assumed that, if the kth estimate, wherein the radius at the ith segment midpoint was taken to be $r_k(\bar{s}_i)$, leads to a boundary value $\Psi_k(\bar{s}_i)$ at this point, then a new estimate

$$r_{k+1}(\bar{s}_i) = r_k(\bar{s}_i) \quad \sqrt{\Psi_o/\Psi_k(\bar{s}_i)}$$

will lead to an improved approximation; or, if not, then some new estimate lying between these two values of $r(\bar{s}_i)$ will lead to an improved

approximation.

3. It is assumed that, if the kth estimate leads to a boundary value $V_k(\bar{S}_i)$ at this point, then a new estimate $F_i = V_k(\bar{S}_N)/V_k(\bar{S}_i)$ will lead to an improved approximation.

The first of these assumptions is rather obviously justified in cases of practical interest.

The second assumption is a generalization of the result that, for an infinitely long cylinder of uniformly distributed ring vortices, the value of the stream function at the boundary is proportional to the square of the radius (since the internal velocity in such a case is uniformly $2\pi\gamma$, independent of the radius). Thus the expression given in the second assumption can be expected to give a correction of the right order of magnitude; and in any case, it is in the correct sense to move the vortex tube for the (k+1)th cycle of calculation toward the location which the stream tube $\Psi=\Psi_o$ occupied at the kth cycle.

The third assumption reflects the consideration that the velocity at a point of the boundary of a long vortex tube is changed only slightly by a change in the vortex density in the immediate neighborhoo of the point. For example, while the mean velocity on the boundary of an infinite uniform vortex cylinder is $\pi\gamma$, it can be shown (Appendix A, Equation [A7c]) that the mean velocity at the midpoint of a short uniform vortex cylinder, with a length of two-tenths its radius, is only about 0.44γ. Thus, on the long cylinder, the effect of halving th vortex density everywhere within one-tenth radius of a given boundary point is to change the mean velocity at this point by only about seven percent.

Thus, while a procedure for successive estimates based on these assumptions may not be strictly and generally justified, the r-adjustment and F-adjustment indicated are at least plausible, when considered separately. It is much more difficult to justify applying both adjustments simultaneously. Especially, it might be expected that adjustments in the shape of the vortex tube would affect the mean velocity on the boundary appreciably. Indeed, we need not make the adjustments simultaneously; we can make them individually on alternate cycles of calculation. However, it was found by trial that a process of simultaneous adjustment is more efficient, under ordinary circumstances, and gives successive solutions which converge satisfactorily toward consistency with the boundary conditions on the slipstream. This procedure is described in detail in Appendix A.

In summary, we have replaced the integral equations [3′] and [4″], which express the boundary conditions at every point of the shroud and slipstream, with sets of algebraic equations (see Appendix A, Résumé of the Calculating Procedure, Equations [A1′] and [A2′] which express the boundary conditions at finite numbers of control points along the shroud and slipstream. Moreover, we have adopted a cyclic calculating procedure, at each cycle of which we use an "interim boundary condition"

$$\Psi(\bar{s}_i) = \sum_{j=1}^{N-1} a_{i,j}\,\bar{\gamma}_j + \bar{\gamma}_N \sum_{j=N}^{N+M} a_{i,j}\,F_j = \Psi_o \quad , \quad 1 \le i \le N$$

which applies at the control points of the shroud only.

The main features of this procedure are

1. Selection of a first approximate representation

$$(x_i, r_i \quad , \quad 1 \le i \le N+M)$$

$$(F_i \quad , \quad M+1 \le i \le N+M)$$

of the shape of the shroud and slipstream and relative vortex distribution along the slipstream.

2. Calculation of the influence coefficients $a_{i,j}$, $b_{i,j}$, and $c_{i,j}$.

3. Solution of N equations in N unknowns, from the "interim boundary condition" to yield values of $\bar{\gamma}_j$, $1 \le j \le N$.

4. Evaluation of the error in the boundary conditions along the slipstream, by calculating

$$\left.\begin{array}{l} \Psi(\bar{s}_i) \\ \gamma(\bar{s}_i)\, V(\bar{s}_i) \end{array}\right\} \quad N \le i \le N+M-1$$

These must ultimately become uniform sets.

5. Calculation of improved estimates

$$(x_i, r_i \quad , \quad M+2 \le i \le N+M)$$

$$(F_i \quad , \quad M+1 \le i \le N+M)$$

of the shape and vortex distribution of the slipstream. The cyclic procedure is to be continued until the errors, as evaluated at step 4, are suitably small. The details of the procedure are developed and summarized more explicitly in Appendix A.

PRELIMINARY CALCULATIONS

A limited series of calculations of slipstream contraction was undertaken, with the dual objectives of (a) confirming the feasibility of making such calculations by the procedure proposed and (b) providing improved quantitative knowledge of slipstream contraction, for future use in shrouded propeller theory and design.

For this purpose, the calculating procedure outlined in the preceding

section and developed in detail in Appendix A was translated into a FORTRAN language computer program for compilation and execution by the LARC digital computer system of the David Taylor Model Basin. The FORTRAN coding was performed by the writer, with substantial assistance from Model Basin staff mathematicians, especially Mr. Dan M. Walker. For each calculation, input data were supplied to the LARC system in the form of punched cards presenting the N+M pairs of initial coordinates (x_i, r_i) and the M initial values of F_i. Results were received from the system in the form of printed tabulations presenting the current values $\bar{\gamma}_i$, r_i , F_i , $\gamma(\bar{s}_i)V(\bar{s}_i)$, and $\Psi(\bar{s}_i)$ at the end of each iterative cycle, plus certain supplementary data, at the end of the last cycle, from which the surface velocities at each point $(\bar{x}_i, \bar{r}_i)$ could be found if desired. The target boundary value, Ψ_o, of the stream function, was defined by the program to be one-half. The slipstream contraction is, of course, independent of Ψ_o, and velocities scale linearly with Ψ_o.

Early trials of the computer program were directed toward a very brief investigation of the convergence of the iteration process, and toward obtaining a preliminary notion of the number and spacing of cone-frustrum segments required for adequate representation of the shroud and slipstream.

CONVERGENCE - As discussed in Appendix A, the first formulation of the iterative calculation procedure overestimated the required adjustments in slipstream radius at the end of each cycle, and did not produce acceptable convergence. However, after several fruitless efforts, a simple modification of the procedure (wherein the r-adjustments were, in effect, first estimated by the original formula, but then multiplied by

a variable factor, ranging from one-third for very small adjustments to nearly unity for large adjustments, before being applied) was found which did produce satisfactory convergence. This is illustrated by Figure 2, which presents for comparison the results from the first, second, fifth, and twentieth cycles of calculation, for a short cylindrical shroud ($\ell/\bar{r}_N = 0.20$). Tabulated results, from the first ten cycles of this calculation, and the twentieth cycle, are presented in Table 1.

As is evident from Table 1, the calculations could well have been terminated long before the twentieth cycle. However, an early decision was made to run all of the calculations of slipstream contraction for twenty iterative cycles, for the following reasons: The LARC computing system has no provision for on-line inspection of intermediate results. It is therefore necessary to decide in advance when the calculation will be terminated. (The alternative possibility, of programming the computer to terminate whenever some specified convergence criterion was satisfied, was rejected because no sufficiently simple and reliable convergence criterion was evident.) Moreover, once the computing sequence has been terminated, there is no convenient way to restart it, where it left off. Finally, it was considered desirable, in these first applications of the computing procedure, to carry the calculations on for a liberal number of iterative cycles in order to guard against the possibility that a sequence of successive solutions which appeared to be converging might not continue to converge, or might converge to a different destination than would be guessed from the first several cycles.

The convergence of successive solutions illustrated by Figure 2 and Table 1 turned out to be typical of that which occurred for all iterative

calculations reported herein, with the following qualification: The convergence was somewhat more rapid for longer shrouds (larger ratio $\ell/\bar{r}_N$), and somewhat slower for shorter shrouds (smaller ratio $\ell/\bar{r}_N$). (In fact, for the shortest shroud attempted thus far, $\ell/\bar{r}_N = 0.05$, it was not evident that the solutions were converging, by the end of a twenty-cycle calculation in which the slipstream was represented by a uniform vortex cylinder at the first cycle. Convergence was finally obtained by starting the calculation over again, with a better first estimate of the slipstream shape and vortex distribution.) For very short shrouds, unless a good first estimate is used, substantial changes occur in the "curvature" of the vortex sheet, as measured in the meridian plane, just downstream of the trailing edge of the shroud, during the first few cycles of calculation. (The meridian-plane section of the vortex sheet consists of straight-line segments, but is understood to approximate a smooth curve, whence the concept of "curvature.") Under these circumstances, the assumption implicit in the iteration process - that r-adjustment will affect $\Psi(s)$ primarily, and not affect $V(s)$ very much - does not hold true, and the situation is kept from getting out of hand only by "damping" the r-adjustments as discussed in Appendix A. Undoubtedly, the present method could be applied to still shorter shrouds than attempted herein, by using heavier damping, and careful first estimates; but, if it were desired to approach zero chord length, it would probably become necessary to take direct account, when estimating the r-adjustments after each cycle, of the effect of these adjustments on V. Undoubtedly, such a procedure could be devised. However, there is no known practical interest, at present, in shrouds of chord shorter

than perhaps $0.4\bar{r}_N$, so this question was not pursued in the present investigation.

REPRESENTATION OF THE SHROUD - In most of the calculations presented herein, the shroud was represented by a surface composed of 24 cone-frustum segments (N = 24). In order to have reasonable assurance that this provided an adequate representation, one of the early calculations was repeated, but with N = 12. The results of the two calculations are presented for comparison in Figure 3. The close correspondence in all features of the two results is regarded as strong evidence that the representation with N = 24 was adequate for the simple shroud shapes studied. The estimates of slipstream contraction ratio afforded by the two calculations were equal within 0.2 percent. (The same evidence might be used to justify making the succeeding calculations with N = 12. However, the saving in the expense of the calculations would not have been significant, so the more accurate representation was used.)

REPRESENTATION OF THE SLIPSTREAM - The spacing of segments immediately downstream of the shroud trailing edge is necessarily similar to that immediately upstream, because of the consideration (previously discussed) that the widths of adjacent segments should not differ drastically. Further downstream, all of the variables involved in the calculations vary more and more slowly, along the slipstream, so the successive segment widths can safely be increased, gradually, to the maximum allowable width of about twenty percent of the local radius. The main choice to be made, as to the representation of the slipstream, is how far downstream to continue the system of cone-frustum segments before terminating it in the final (N+Mth) semi-infinite, segment.

In most of the calculations presented herein, the N+Mth segment was begun at $x_{N+M} = 4\ \bar{r}_N$, where x was measured from the shroud leading edge, and $\bar{r}_N$ was the radius of the shroud trailing edge. In order to have reasonable assurance that this provided an adequate representation, one of the early calculations was repeated, with the same segment spacing but a reduced number of segments (reduced M) such that $x_{N+M} \doteq 2\ \bar{r}_N$. The results of the two calculations are presented for comparison in Figure 4. The close correspondence in all features of the two results is regarded as strong evidence that the representation of the slipstream with $x_{N+M} = 4\ \bar{r}_N$ was adequate. The estimates of slipstream contraction ratio afforded by the two calculations were equal within 0.1 percent.

It can be noted from Figure 4 that, if one elected to estimate the slipstream contraction ratio by taking r_{N+M} as an estimate of the limiting slipstream radius (or by taking $\bar{\gamma}_{N+M}$ as an estimate of the limiting slipstream vorticity, analogous to the usual practice in the linearized theory), the result would depend comparatively strongly on how far downstream the system of cone-frustum segments was carried. This dependence is largely avoided by basing the estimate of the slipstream contraction on the quantity γV.

(In this connection, it can be noted from Table 1 that, in the particular case represented there, the value of $\gamma(\bar{s}_N)V(\bar{s}_N)$ from the first cycle of calculation--in which the entire slipstream was represented by a single semi-infinite cylinder, as in the linearized theory--would already have provided a rather good estimate of the slipstream contraction. The possible significance of this circumstance will be investigated further in a later section.)

COMPUTING TIME - For any one of the calculations for which results are presented herein, the time required for the LARC Computer system to perform the calculation can be roughly approximated by the formula:
(Time in Minutes) $\doteq$ (Number of Iterative Cycles)

$$\times \left[\left(\frac{N+M}{60} \right)^2 + \left(\frac{N}{30} \right)^3 \right] + 2$$

The program will accommodate values of N up to 50, for iterative calculations, and up to 98 for single-cycle calculations. In either case, N+M cannot exceed 100.

(The program can be modified very easily to permit values of N up to, say, 90, for iterative calculations. However, N+M cannot be increased very much without fairly extensive modifications. In any event, as is apparent from the above formula, the calculations rapidly become more expensive as the numbers N and M are increased.)

REMARKS - It may be well to point out that it has not been proven that solutions of the exact problem, (Equations [3′] and [4″]) exist; nor that, if a solution is found, it will be unique. The facts that a numerical procedure has been found to yield apparently very close approximations to such solutions, and that these results seem entirely reasonable physically, constitute circumstantial evidence of existence and uniqueness, but hardly proof. This evidence will become stronger (but not conclusive) in a later section when it is found that the same numerical procedure also yields extremely close approximations to exact solutions of other problems, for which existence and uniqueness are well known.

This situation finds parallels in many other applications of

mathematics to physical problems. There is always the undeniable hazard, in such cases, that approximate methods of analysis may yield "solutions" of a problem which has no solution. This hazard is far outweighed by the advances in knowledge which such methods, in company with physical intuition, make possible.

PART II - APPLICATIONS AND EXTENSIONS

We have considered the problem of the axisymmetric potential flow of an incompressible fluid through a shrouded impulse disc, and have succeeded in finding a practical method of obtaining approximate numerical solutions.

We have treated the problem of the shrouded impulse disc as a special case of the more general problem of the axisymmetric potential flow about an arbitrary surface of revolution. We may suspect, therefore, that our method might have more general applications. This possibility will be examined in a later section. First, let us consider the possible applications of theoretical predictions of slipstream contraction to the problem of the shrouded propeller.

APPLICATIONS TO SHROUDED PROPELLERS

It was mentioned at the outset that the original motivation for the present investigation came from certain practical problems of the shrouded propeller.

It is found experimentally that shrouded propellers are more efficient, in terms of thrust delivered and power expended, than free propellers, in the static case. This advantage is of great practical interest in connection with "vertical take-off and landing" aircraft. It has been best understood, in terms of the concept of slipstream contraction, from the one-dimensional theory of the shrouded propeller.

THE ONE-DIMENSIONAL THEORY OF THE SHROUDED PROPELLER -- The assumptions introduced in Part I, in the section on Formulation of the Problem, are consistent with the assumptions of the one-dimensional theory of the shrouded propeller, often referred to as "simple momentum theory." Under these assumptions, a number of useful relationships for the shrouded propeller can be derived very simply, without considering the details of the flow. A treatment of this theory was given by Krüger, Reference 2, who also obtained experimental data tending to confirm some of the main conclusions.

One objection to the one-dimensional theory has been that most of the relationships deduced contain the slipstream contraction ratio as an unknown parameter, which must be estimated in order to apply the theory. In the past, there has been no very sound basis for making such estimates, except when ϕ was known to be nearly equal to unity.

Since we now have a tool for calculating slipstream contraction, it is of interest to review the essential features of the one-dimensional theory.

The Static Case -- In the static case (zero free-stream velocity), the energy, dynamic pressure, and momentum of the slipstream are entirely due to the action of the shrouded propeller.

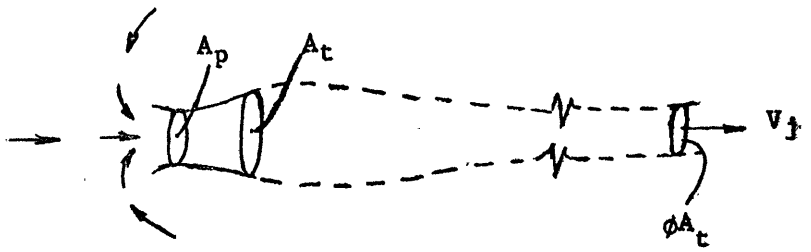

The momentum flux through a section of the slipstream, far downstream, is

$$T = \rho V_j^2 A_t \phi$$

The propeller thrust is

$$T_p = \frac{1}{2} \rho V_j^2 A_p$$

The kinetic energy flux is

$$P = \frac{1}{2} \rho V_j^3 A_t \phi = T^{3/2} / 2\sqrt{\rho A_t \phi}$$

Therefore, the static efficiency is given by

$$\eta_{st} \equiv \frac{T^{3/2}}{2\sqrt{\rho A_t} P} = \sqrt{\phi} \qquad [10]$$

For a propeller without shroud, the total thrust and propeller thrust are equated, and it is deduced that $\phi = \frac{1}{2}$. Thus the shrouded propeller enjoys the advantage of a static efficiency, better by a factor of $\sqrt{2\phi}$ than that of the free propeller, according to this theory. (The "static efficiency" is not a true efficiency, but a parameter which plays the same role for the shrouded propeller which is played by "figure of merit" for the hovering rotor.)

The ratio of total thrust to propeller thrust is given by

$$T/T_p = 2 \phi A_t/A_p \qquad [11]$$

It is sometimes cited as an advantage of the shrouded propeller that the total static thrust exceeds the thrust of the propeller. This is not in itself an advantage, except insofar as it is symptomatic of the real advantage of a superior static efficiency. The thrust on the shroud appears largely as a suction pressure around the leading edge,

with the result that there is usually an adverse pressure gradient in this neighborhood. This may be quite severe unless the shroud is rather thick, or is made artificially thick during static operation by means of flaps or inflatable sections.

The shrouded propeller's superior static efficiency is of great interest in connection with Vertical Take-Off and Landing (VTOL) aircraft. For propeller-driven VTOL aircraft, the operation of the propellers is essentially static during landing and take-off, at the times when the propeller thrust must offset the entire weight of the aircraft, and the maximum power is required.

If shrouded propellers are employed, to reduce the power required for take-off and landing, a penalty is incurred in terms of the weight and drag of the shrouds. From this standpoint, it seems advantageous to make the shrouds as small as possible. On the other hand, if the shrouds are too small, they may be less effective in preventing slipstream contraction. Moreover, it was suggested by Krüger, Reference 2, that a long, divergent (diffusing) shroud might produce a slipstream expansion, and provide an even greater advantage. Thus, it is of great interest to the designer to know the effects of the shroud geometry on slipstream contraction in the static case.

The Case of Finite Thrust Coefficients -- When there is a free-stream velocity, only a part of the energy, dynamic pressure, and momentum of the slipstream are due to the action of the shrouded propeller.

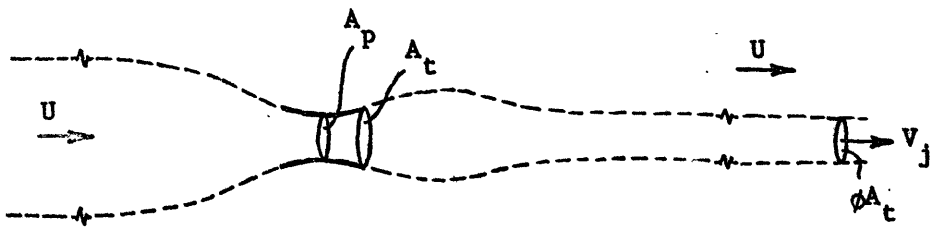

The mass flow through the propeller is $\rho V_j A_t \phi$, so that the portion of the momentum flux ascribed to the action of the shrouded propeller is

$$T = \rho V_j A_t \phi (V_j - U) \qquad [12]$$

The propeller thrust is

$$T_p = \left(\frac{1}{2} \rho V_j^2 - \frac{1}{2} \rho U^2\right) A_p \qquad [13]$$

The portion of the kinetic energy flux ascribed to the action of the shrouded propeller is

$$P = \frac{1}{2} \rho V_j A_t \phi (V_j^2 - U^2) \qquad [14]$$

The thrust coefficient is

$$C_T = \frac{T}{\frac{1}{2} \rho U^2 A_t} = 2 \phi \frac{V_j}{U} \left(\frac{V_j}{U} - 1\right) \qquad [15]$$

Whence

$$\frac{V_j}{U} = \frac{1}{2} \left[1 + \sqrt{1 + 2 C_T/\phi}\right] \qquad [16]$$

The Froude efficiency is, from Equations [12] and [14]

$$\eta_F \equiv \frac{TU}{P} = \frac{2 U}{V_j + U}$$

and by application of Equation [16] becomes

$$\eta_F = \frac{2}{1 + \frac{1}{2}\left[1 + \sqrt{1 + 2C_T/\phi}\right]} \qquad [17]$$

The ratio of total thrust to propeller thrust is, from Equations [12] and [13]

$$\frac{T}{T_p} = \frac{2 \phi V_j}{V_j + U}$$

and, by application of Equation [16] becomes

$$\frac{T}{T_p} = 2 \phi \left(\frac{1 + \sqrt{1 + 2 C_T/\phi}}{3 + \sqrt{1 + 2 C_T/\phi}} \right) \qquad [18]$$

For a free propeller, the ratio T/T_p is equated to unity, giving the relationship between ϕ and C_T, which is plotted as the dashed curve in Figure 10b. The contraction ratio for the free propeller approaches unity as the thrust coefficient approaches zero, as would be intuitively expected.

Equation [17] may be written, for low thrust coefficients

$$\eta_F \approx 1 - \frac{C_T}{4\phi} \quad , \quad C_T \ll 1 \qquad [17']$$

Thus, it is seen that

a. At low thrust coefficients, there is substantially less difference between the slipstream contraction of a free propeller and that of a shrouded propeller than there is in the static case.

b. The slipstream contraction ratio has a weaker influence on the Froude efficiency, in the case of low thrust coefficients, than it has on the static efficiency, in the static case.

Both of these considerations tend to indicate that, even when the drag of the shroud is ignored, there is little advantage in shrouding the propeller unless the performance in the static case is important. When the drag of the shroud is considered, the shrouded propeller is found to

be at a definite disadvantage, at low thrust coefficients, so far as the Froude efficiency is concerned. However, in some applications, the shroud may take the place of stabilizing or lifting surfaces, or provide sound reduction, so as to retain an advantage despite the drag.

Experimental Evidence -- Krüger's experiments, Reference 2, and all subsequent experience (see Reference 1) confirm the general conclusions of the one-dimensional theory, using $\phi \approx 1$ for the shrouded propeller, as regards the advantage of the shrouded propeller over the free propeller in the static case. Moreover, in the case of reasonably long, nearly cylindrical shrouds, the total thrust is found to be divided approximately evenly between the shroud and the propeller, as expected from this theory.

We were concerned, in Part I, with developing a method to predict in detail, under assumptions consistent with those of the one-dimensional theory, the effects on ϕ of shroud geometry variables. It would seem that it must be possible to establish the more important of these effects by proper experiments. However, while the shrouded propeller literature (see Reference 1) contains a great quantity of experimental data, one finds no correlations of these data wherein these effects are systematically identified.

Since it can hardly be believed that no such correlations have been attempted, during two decades of shrouded propeller research, it may be appropriate to speculate on the reasons why none are found in the literature. First of all, one cannot measure the slipstream contraction directly, because the slipstream (in the sense in which we are using this word) does not really exist. Instead, one must measure effects which

imply slipstream contraction, such as changes in the static efficiency and the ratio of propeller thrust to total thrust. However, these quantities may be influenced by a great many other variables besides slipstream contraction. These include the numerous variables of propeller geometry and location, centerbody geometry and location, and shroud support strut geometry and location, as well as viscous effects on all these components and the shroud. Even when two experiments are performed with essentially the same model, a change in the geometry of the shroud might--in addition to changing the slipstream contraction--also change the flow through the propeller and around the centerbody, and change the character of the boundary layers on any or all components. Obviously, comparative interpretation of experiments with different models is still more uncertain. The large effects which occur when the shroud is added to a free propeller, or removed from a shrouded propeller, are comparatively easy to observe and interpret; but if one compares a propeller with a long shroud to one with a short shroud, or one with a cylindrical shroud to one with a divergent shroud, the differences in measurable quantities which might properly be associated with differences in slipstream contraction may be of the same order of magnitude as--or even much smaller than--numerous other possible effects. Experimental isolation of these effects is possible only by means of very painstaking measurements, if it is possible at all. It has evidently not yet been accomplished, to any significant extent. Hopefully, future experiments may be planned and interpreted more successfully, with the advantage of better theoretical information on the effects of shroud geometry.

In summary, very significant differences in performance are found, experimentally, between free propellers and shrouded propellers, in the

static case. The general character and magnitude of these differences are explained very conveniently and successfully in terms of the concept of slipstream contraction. It seems reasonable to expect that some of the important effects of variations in the shroud geometry of a shrouded propeller might also be conveniently and successfully predicted in terms of the concept of slipstream contraction. The available experimental evidence neither confirms nor denies this expectation. At the minimum, knowledge of the effects of shroud geometry on the slipstream contraction of shrouded impulse discs should be useful for planning and interpreting new shrouded propeller experiments. At the maximum, if experimental confirmation is forthcoming, this knowledge might be extremely useful in the design of shrouded propellers for VTOL applications.

It is the author's opinion that the predictions of the one-dimensional theory regarding changes in static efficiency associated with changes in shroud geometry, using values of the slipstream contraction ratio calculated by the present method, will be found to be reasonably valid; provided,

a. There is no flow separation from the shroud.

b. The pressure rise across the propeller disc is approximately uniform.

c. Any changes in the efficiency of the propeller itself are either prevented, by adjusting the propeller geometry, or are accounted for separately.

It should not be imagined that, even if this opinion is confirmed, the design of shrouded propellers would then become straightforward. The uncertainty regarding the slipstream contraction is only one of a large

number of complications which plague the shrouded propeller designer. (Perhaps the greatest of these is the difficulty of predicting the circumstances under which flow separation will or will not occur. It will be seen later that the present method of calculation, by providing information on the velocity distribution over the shroud, might possibly provide the basis for a future approach to this problem.)

SYSTEMATIC CALCULATIONS OF SLIPSTREAM CONTRACTION -- In order to provide some immediate quantitative information on the effects of shroud geometry on slipstream contraction, a limited series of calculations was undertaken for certain interrelated families of cylindrical, conical, and parabolic-cambered shrouds.

The Static Case -- It was of particular interest to obtain results for cylindrical shrouds, in the static case, because the previously available estimates of slipstream contraction, from the linearized theory, pertained to cylindrical shrouds.

The results of twenty-iterative-cycle calculations for cylindrical shrouds, over a wide range of chord/radius ratios, are presented in Figure 5. Also presented, for comparison, are:

a. The estimate provided by the linearized, short-chord theory of Kriebel, Sacks, and Nielsen (Reference 8).

b. The estimate available from the first cycle of calculation by the present method, based on $\bar{\gamma}_{N+M}$; that is,

$$\phi \approx \frac{\Psi_o}{\pi \bar{\gamma}_{N+M} \bar{r}_N^2}$$

c. The estimate available from the first cycle of calculation by the present method, based on $\gamma(\bar{s}_N)V(\bar{s}_N)$; that is,

$$\phi \approx \frac{\Psi_o}{\bar{r}_N^2\sqrt{\pi\,\gamma(\bar{s}_N)V(\bar{s}_N)}}$$

In the calculations by the present method, the slipstream was represented, at the first cycle of calculation, by a uniform vortex cylinder, just as in the linearized theory. Thus, the estimates available from the first cycle of calculation are essentially linearized-theory estimates.

These estimates are based on the relationship

$$\Psi_o = \frac{1}{2}\,u_\infty R_\infty^2$$

where u_∞ is the limiting velocity within the slipstream, far downstream, and R_∞ is the limiting slipstream radius. In the linearized theory it is assumed a priori that γ is constant along the slipstream, and the relationship

$$u_\infty = 2\pi\,\gamma(=)$$

leads directly to the estimate given in "b" above. However, one is not compelled to continue to assume a posteriori that γ is constant along the slipstream. The relationship

$$u_\infty^2 = 4\pi\,\gamma(=)\,V\,(\infty)$$

together with an a posteriori assumption that γV is constant along the

slipstream with the value calculated at the trailing edge, leads to the estimate given in "c" above.

The results given in Reference (8) were derived without any modification of the a priori assumption concerning the representation of the slipstream, and so would be expected to merge, at small chord/radius ratios, with the first-cycle estimate from $\bar{\gamma}_{N+M}$. It is seen in Figure 5 that this does, indeed, appear to be the case. (The identification of this estimate with $\bar{\gamma}_{N+M}$ is, of course, somewhat arbitrary since, at the first cycle of calculation, all of the $\bar{\gamma}_i$'s from i = N to i = N+M were equal.)

As anticipated earlier, Figure 5 shows that a comparatively good estimate is afforded by the value of $\gamma(\bar{s}_N)V(\bar{s}_N)$ at the end of the first cycle. From the special vantage point afforded by hindsight, it seems quite reasonable that an extrapolation along the slipstream to infinity should be based on the quantity γ V, which is supposed to be uniform along the slipstream, rather than on the quantity γ, which is not supposed to be uniform.

The only available and comparable results of previous theory for larger chord/radius ratios were those of Heimbold (Reference 10), which were obtained from linearized-theory calculations in which the boundary conditions were applied at only three axial stations along the shroud. Thus, they are not really representative of the linearized theory. As a matter of fact, however, Helmbold's results, which were for chord/radius ratios of 0.5, 1.0, and 2.0, agreed rather closely with the results of the present twenty-cycle calculations. Helmbold did use the value of γ V at the trailing edge for his estimate of slipstream contraction.

Vortex distributions for certain of the cylindrical shrouds, taken from the twentieth cycles of calculation, are presented in Figure 6. It is easily shown that in the case represented ($\Psi_o = 0.5$, $\bar{r}_{\infty} = 1.0$), the function $\gamma(S)$ for a semi-infinite shroud must approach the value $1/2\pi$. This asymptote is shown on Figure 6. A line is also shown which represents the variation $\gamma(S) \sim S^{-\frac{1}{2}}$, which must necessarily prevail at the leading edge of any thin shroud, and which evidently prevails for a significant distance downstream from the leading edge. It would seem that, as cylindrical shrouds of shorter and shorter chord are considered, the functions $\gamma(S)$ change smoothly, and only slightly, from that which would be found for a semi-infinite cylindrical shroud. Also it would seem that, for cylindrical shrouds of sufficiently long chord, representation of the entire slipstream by a uniform vortex cylinder could be justified, even in the static case. (This latter conclusion is also supported by Figure 5.)

Twenty-cycle calculations of slipstream contraction were carried out for a few members of a family of diffusing conical shrouds and a family of parabolic-cambered shrouds. These families were chosen so that the cylindrical shrouds of Figure 5 would be limiting-case members of both families. Moreover, corresponding members of the conical and parabolic-cambered shroud familes were chosen to have equal trailing-edge divergence angles; namely, $\tan \alpha_N = 0$, 0.08, 0.16, and 0.24, in the various cases.

The results are presented in Figures 7 and 8 and in Table 2. It is seen that shrouds with positive trailing-edge divergence angles can provide significantly more favorable contraction ratios.

Weinig (Reference 13) gave an approximate formula for estimating the effect of trailing-edge divergence on slipstream contraction; namely, $\phi \approx \frac{1}{1 - 0.45\ \alpha_N}$. (This formula was based on two-dimensional free-boundary calculations. The application to axisymmetric flow was justified on the basis of an investigation by Trefftz (Reference 14), who showed that approximately the same contraction occurred in the flow through a circular orifice, as in the flow through a long narrow slit.) The formula is compared with present results in Figure 9. It is seen that the formula gives a fairly good approximation in cases of long-chord conical and parabolic-cambered shrouds.

The Case of Finite Thrust Coefficients -- While only the static case has been considered in the preceding discussion (since it is in the static case that slipstream contraction is especially interesting), the extension of the method to include the case of axisymmetric flow in a free stream is very easy. This extension was included in the computer program. (If the free-stream velocity is U, it is necessary only to add $\frac{1}{2}Ur^2$ to the expressions for stream function, and to add U to the axial velocities.)

The computer program was arranged to permit specification of a non-zero value of free-stream velocity, U. This allows calculations for arbitrary finite thrust coefficients, by the same procedure employed in the static case. (It is not possible, by the present method, to specify the thrust coefficient C_T precisely; but U is specified precisely, and it is easily shown that

$$C_T = \frac{4\ \Psi_o}{\bar{r}_N^2\ U}\left(\frac{2\ \Psi_o}{\bar{r}_N^2\ U\phi} - 1\right)$$

Thus, C_T can be specified approximately before the calculation, from a preliminary estimate of the slipstream contraction ϕ, and can be determined precisely after the calculation.)

Results of calculations sufficient to provide a preliminary indication of the variation of slipstream contraction with thrust coefficient, for a cylindrical shroud of chord/radius ratio 0.40, are presented in Figure 10a. The slipstream contraction ratio was plotted versus the reciprocal of the thrust coefficient, so that the static case, $\frac{1}{C_T} = 0$, could be included on the graph.

In the calculations with finite thrust coefficient, the shroud was represented by twelve segments (N = 12), and the slipstream was represented with $X_{N+M} = 2.05\ \bar{r}_N$. The calculation with finite thrust coefficient is much easier than in the static case, because there is less difference between the initial and final slipstream shapes, and because the quantity $V(\bar{s}_i)$, along the slipstream, contains the constant component U, and hence is less sensitive, fractionally, to the successive r-adjustments.

Figure 10a shows the (perhaps) surprising result that, as one moves away from the static $\left(\frac{1}{C_T} = 0\right)$, to finite thrust coefficients, the slipstream contraction ratio ϕ at first declines; and then, as $1/C_T$ is increased (C_T decreased) further, ϕ increases again, approaching unity asymptotically. While this result was not expected, it is readily understood, in terms of the evolution of the static pressure, on the outer surface of the vortex sheet, in the neighborhood of the shroud trailing edge. Consider, for example, a case in which the mean axial velocity within the shroud is held constant and equal to unity. At zero free-stream velocity, the axial velocity at a point just outside the slipstream boundary near the trailing edge will have a negative value, say, $-\beta$. To the first approximation, at finite free-stream velocities, the axial velocity at this point will be $U - \beta(1-U)$; and the gage static pressure at this point will be $\frac{1}{2}\ \rho\left\{U^2 - \left[(1 + \beta)\ U - \beta\right]^2\right\}$. This quantity is

negative at U = 0, goes to a maximum positive value at a small value of U, and approaches zero again as U approaches unity (that is, as C_T approaches zero). Thus, in a range of large but finite thrust coefficients, the static pressure in the neighborhood of the trailing edge is perceptibly higher than ambient; and the mean internal axial velocity, across the trailing-edge plane, may well be lower (compared with the limiting velocity, far downstream, where the static pressure becomes uniform and equal to ambient) at some thrust coefficient, in this neighborhood, than at higher or lower thrust coefficients. Thus, it should not be surprising that the slipstream contraction ratio could be at a minimum at a finite thrust coefficient.

This result lends emphasis to the fundamental and perceptible difference between the classical "free streamline" problems (in which a uniform static pressure is imposed along the "free" surface, and hence only the flow on one side of the surface need be considered), and the present problem (in which the static pressure is continuous across the "free" surface, but may vary along it, and hence a flow field which occupies all space must be considered).

(It might be pointed out that it has been elected to consider, herein, that the static pressure is continuous across the slipstream surface, and that the quantity $\bar{V}^2$, and hence the total pressure, are uniformly discontinuous across this surface, the uniform jump in total pressure corresponding to an equal jump across an impulse disc spanning the interior of the shroud. This viewpoint is most nearly consistent with the physical processes of a real shrouded propeller. However, one could elect, with exactly equivalent results, to consider that the slipstream surface consists of a rigid, impervious membrane, across which there is a uniform

jump in static pressure, the total pressure being uniform throughout the entire field. In this case, the concept of an impulse disc need not enter at all, until one wishes to justify the application of the results to shrouded propeller theory.)

For a cylindrical shroud, at the first cycle of calculation, the shape of the vortex distribution is independent of the forward velocity, U, since the shroud is automatically coincident with a stream surface of the undisturbed free stream. Hence, the induced velocity at any point has a fixed direction and a magnitude proportional to, say, $\gamma(\bar{s}_N)$. Thus, one can write

$$V\,\bar{s}_N = C_1 \left(\ell/\bar{r}_N\right) \gamma\left(\bar{s}_N\right) + U$$

$$\Psi_o = \left[C_2 \left(\ell/\bar{r}_N\right) \gamma\left(\bar{s}_N\right) + U/2\right] \bar{r}_N^{\,2}$$

whence

$$\gamma\left(\bar{s}_N\right) V\left(\bar{s}_N\right) = \frac{1}{C_2}\left[\left(\frac{\Psi_o}{\bar{r}_N^{\,2}} - U/2\right)\frac{C_1}{C_2} + U\right]\left(\frac{\Psi_o}{\bar{r}_N^{\,2}} - U/2\right)$$

For each chord/radius ratio, the constants C_1 and C_2 can be determined from the first cycle of the static-case calculation, and the slipstream contraction can then be estimated for any arbitrary value of U. The estimate obtained in this way is equivalent to the first-cycle estimate from $\gamma(\bar{s}_N)V(\bar{s}_N)$, obtained from a calculation in which the desired U is specified. In fact, in Figure 10a, the upper dotted curve was deduced from the first cycle of the static-case calculation, and was found to practically contain the points with triangular symbols, which were obtained from the first cycles of the finite C_T (finite U) calculations. (In the absence of all errors, that line would contain those points, exactly.)

prone to have flow separation. However, this difficulty might be circumvented by use of inflatable leading edges or other devices.

OTHER APPLICATIONS AND EXTENSIONS

The emphasis in the preceding discussions has been placed on the calculation of slipstream contraction. However, the method developed for calculating slipstream contraction involves the construction of a close approximation to an entire flow field bounded by a surface of revolution. We may thus consider applying this method to other problems of axisymmetric potential flow, including some for which slipstream contraction may be of little or no interest, and even some in which a slipstream is not involved at all.

While exploring the possibilities of further applications, the opportunity will be taken to apply the present method to some problems for which exact solutions are known. In this way we may obtain a few direct checks on its accuracy.

INTERNAL FLOW IN CIRCULAR DUCTS -- Axisymmetric flow through a section of circular ducting, of arbitrary radius distribution, can be approximated very readily, simply by representing a long "shroud" which has the desired radius distribution along a part of its length. It is advisable to let the shroud continue for some distance upstream and downstream of the section under study, to minimize end effects; and to specify values of W and Ψ_o which avoid any strong leading-edge singularity, for the same reason. (A specification such that $\Psi_o = \frac{1}{2} Ur^2$ should serve nicely, under most circumstances.)

For an example of this application, a duct studied by Thwaites (Reference 15) was chosen. Thwaites considered a class of potential flows for which the radial coordinate of an arbitrary point on a given stream surface is a periodic function of the axial coordinate. Thus, one of the stream surfaces may be chosen to represent the wall of an infinitely long periodic duct, for which an exact solution for the internal flow is available.

Of course, it is not possible to represent an infinitely long periodic duct by the present method, because an infinite number of cone-frustum segments would be required. However, only the solution for a single half-period of the internal flow is required, since the rest of the internal flow then follows by symmetry.

For the present example, as shown in Figure 11a, three half-periods of the duct were represented, on the assumption that the flow in the middle half-period would be essentially the same as for a truly periodic duct. (The duct represented is from the third of the three examples presented in Reference 15.) As shown in Figure 11a, the results of calculations of the velocity distribution on the wall, by the present method, agree extremely well with Thwaites' results (by the exact method, for a truly periodic duct).

Thwaites' practical interest in this periodic duct lay in the assumption that the flow within a half-period of the duct would approximate the flow within a transition section, of the same shape, joining two cylindrical ducts. By the present method, of course, such a transition section can be represented directly, as shown in Figure 11b. It would appear, on the basis of the results presented in Figure 11b, that Thwaites' assumpti was reasonable; although, of course, the velocity distribution in the

immediate neighborhoods of the junctures with the cylindrical ducts is perceptibly different from that in the corresponding neighborhoods of the periodic duct. (Thwaites' interest was in effusing transitions, whereas the example of Figure 11b represents a diffusing transition. However, since we are dealing with potential flow, this makes no material difference.)

At the first attempt to calculate the flow through the periodic duct, a noticeable discrepancy was found between the velocity distribution given by the present method and that given by Thwaites, in the neighborhood of the section of minimum radius. Thwaites' calculations were then partially rechecked, and a single ordinate -- the minimum radius itself -- was found to be very slightly in error. Specifically, it is given by Reference 16 to be 0.487, whereas a more nearly correct value is 0.4858, less than one-fourth of one percent different. Using this value, excellent agreement was obtained, as shown in Figure 11a. This incident points up a need for extreme care in specifying the coordinates x_i, r_i for applications of the present method; and suggests that, in many practical applications, the accuracy of the results may be limited by the precision with which the coordinates can be determined, rather than by errors inherent in the method itself.

CLOSED BODIES -- The development of the method of calculation, detailed in Appendix A, was specifically limited to a flow bounded by an open surface of revolution. This limitation arises primarily from the handling of the leading-edge singularity (Case II and Case IV of the Determination of the Influence Coefficients, Appendix A). It was expected from the beginning that an effort would eventually be made to extend the method to

include solid and annular bodies of revolution. However, it was only realized in retrospect that this extension could very easily have been included in the original computer program, and in fact consists primarily of simply bypassing the segments of the program dealing with the leading-edge singularity. Proposed methods of doing this, and of dealing with other less serious obstacles in the present computer program, so as to permit calculations of flows about closed bodies (literally, closed vortex sheets) will be outlined in a later section, along with other possible extensions.

The representation of a closed body by a distribution of vortices over its surface appears to have been applied rather rarely to practical problems, although the validity of such representation has long been recognized. Lamb stated, in Reference 6, Art. 151, that " . . . every continuous irrotational motion, whether cyclic or not, of an incompressible substance occupying any region whatever, may be regarded as due to a certain distribution of vortices over the boundaries which separate it from the rest of infinite space." We do not wish to review here the intricate reasoning by which Lamb justified this statement, but the elements of the argument required for our less general case are rather simple, if we may appeal to certain well-known theorems of the potential theory. First, note that the flow about a closed body in a uniform stream can be reduced to the flow about a body moving through a fluid which is at rest at infinity. Next, we note that, in Lamb's words, "No continuous irrotational motion is possible in an incompressible fluid filling infinite space, and subject to the condition that the velocity vanishes at infinity." From this it follows that the whole velocity field is determinate if the curl of the velocity is known at every point; for, suppose there were two

velocity fields $\vec{V}_1$, $\vec{V}_2$ satisfying a given specification on the curl, and vanishing at infinity, then the field $\vec{V}_3 = \vec{V}_1 - \vec{V}_2$ would have vanishing curl everywhere, and would also vanish at infinity; and hence, by the above theorem, would vanish everywhere. Let us suppose our body to be a closed surface filled with the fluid. We have assumed the motion outside the surface to be irrotational, and to vanish at infinity, and we now suppose the motion within the surface to be irrotational also, except in a thin stratum of thickness, t, next to the surface. Now, any possible motion of the outside fluid, consistent with our assumptions, can be associated with some - not necessarily unique - distribution of curl within this stratum; in other words, with a space distribution of vorticity. The argument is in no way changed if we let t tend to zero, so that the space distribution of vorticity becomes a surface distribution of vortex density. Now if we return to the stationary surface in a uniform stream, and require that the normal velocity vanish on the surface, we have, by another well-known theorem of the potential theory, that the velocity vanishes everywhere in the region enclosed by the surface. In this case, the vortex density at any point of the surface is equal in magnitude to the velocity just outside the surface, divided by 2π. If the velocity field is unique, the distribution of vortex density is also unique. Since the space outside an annular airfoil is doubly connected, the velocity field is not uniquely determined unless some suitable constraint - such as the Kutta condition - is placed on the circulation around the airfoil.

Vandrey, Reference 17, calculated plane-symmetrical and axisymmetric flows about closed bodies by representing the bodies by surface distributions of vortices.

Without any modification of the present computer program, we may seek to approximate the flow about a closed body by representing a significant part of its surface by a vortex sheet.

Circular Inlet -- A very simple example of this application is afforded by the problem of calculating the velocity distribution on the inlet to a thick semi-infinite pipe. (This problem may be thought of as an idealization of the problem of calculating the flow at the inlet of a jet engine or a shrouded propeller.) We may hope to approximate

the flow at the inlet by representing the inlet profile, a portion of the outer surface of the pipe and the whole interior surface of the pipe by a vortex sheet. Essentially, this amounts to representing the pipe by a shrouded impulse disc with a shroud in the shape of the specified portion of the pipe surface and with a very long chord.

An example is presented in Figure 12. A circular pipe of internal radius $\bar{r}_N$ and thickness $0.16125\bar{r}_N$, with an inlet profile composed of a quarter-circle and a quarter-ellipse, was represented as sketched in Figure 12. The tick marks on the sketch identify the joints of the system of cone-frustum segments chosen for this representation.

Squared velocity distributions on the inlet for the static case, and for the case of free-stream velocity equal to seven-tenths of the mean internal axial velocity, are presented in Figure 12. The scale of velocities was chosen so that the mean internal axial velocity was unity.

Also shown in Figure 12, for comparison, are results of calculations, for the static case, by the method of Smith and Pierce (Reference

In those calculations, the outer surface of the pipe was continued downstream past the "trailing edge" shown in the sketch and then in to the axis, capping off the pipe in the form of an urn. The inner surface was capped off by a sink disc, on which was prescribed a uniform normal velocity. (These calculations were performed on the IBM 7090 computer at the David Taylor Model Basin, using a modified version of a computer program which had previously been made available to the Model Basin by the Douglas Aircraft Company). As pointed out by Reference 12, the method of Smith and Pierce is not fully successful in calculations of inlet flows, because the boundary conditions are applied to the normal velocities rather than to the stream function, and a cumulative "leakage of fluid" can occur through the walls of the duct. (The normal velocity at the center of each segment is required to be zero; but the mean normal velocity along the segment is not necessarily zero.) This is presumably responsible for the unrealistic decrease of surface velocity, below unity, along the inner duct wall. It is seen, however, that the agreement with results of the present method is rather good, along the inlet profile itself.

Annular Airfoil -- We may carry the idea of the preceding paragraph a step further, and seek to approximate the flow about a closed body of finite dimensions by representing the major portion of its surface by a vortex sheet. We will call such a representation a "nearly closed" surface. A particularly natural application of this idea is the application to an annular airfoil, because an annular airfoil may be regarded as a shrouded impulse disc in the limiting case of zero thrust coefficient, and hence zero vortex density on the slipstream surface.

As discussed previously, in connection with the calculation of slipstream contraction in cases of finite thrust coefficients, the thrust coefficient can be made to come out nearly to zero by proper choice of Ψ_o and U. The specification on U can then be modified on successive calculations to make the thrust coefficient -- and hence the vortex density on the slipstream -- as nearly zero as desired. Inasmuch as the shape of the part of the vortex sheet representing the slipstream will be immaterial, once the vortex density has vanished, it is unnecessary to iterate for the shape of the slipstream.

The results of a calculation in which the flow around an annular airfoil was approximated are presented in Figure 13. Also shown are experimental data from Reference 16. The agreement between calculated and experimental velocity distributions is seen to be satisfactory. (The airfoil represented in the figure was that given in Reference 16. It was ten percent thick, with four percent camber, on an NACA a = 0.8 mean line, and had an NACA 66-010 thickness distribution over the forward 45 percent of the chord and parabolic thickness distribution over the after 55 percent.) As sketched in Figure 13, the cone-frustum system was begun on the upper (outer) surface of the airfoil at the 96-percent-chord station, extended forward, around the leading edge, and back along the lower (inner) surface to the trailing edge. Then, in order to establish the trailing-edge flow in a direction more representative of that which would obtain with a closed airfoil, a 2.5-percent-chord extension was added in the direction of the airfoil mean line extended. (It is believed that, unless some such measure were employed, the gap in the upper surface at the trailing edge would produce an effect similar to that of a reflexed

trailing edge, and the nearly closed airfoil would have appreciably less circulation than the corresponding [redacted]osed [redacted]. However, only the arrangement sketched in Figure 12 was tried.)

The results of this example of the "nearly closed" annular airfoil, and the preceding example of the circular inlet, strongly suggest that, by proper extensions and modifications of the present method, axisymmetric flows about arbitrary finite annular bodies, including thick annular airfoils and impulse discs with thick shrouds, can be approximated very closely. Previously, only linearized-theory methods were available for these problems. The linearized theory is limited to rather thin, nearly cylindrical bodies, and cannot correctly represent the velocity distribution around the leading edge, because of the leading-edge singularity which is present in that theory. This velocity distribution is of practical interest in connection with the problem of leading-edge flow separation.

Sphere -- The results of calculating the velocity distribution on a "nearly closed" sphere are presented in Figure 14.

The method of representing the sphere is most easily described in the following terms: A shrouded impulse disc was represented, with the shroud coinciding with that portion of the sphere sketched in Figure 14 from $\theta = 0.01$ radian to $\theta = (\pi - 0.01)$ radian. At the rear, a short transition to a cylinder of radius 0.0075 times the radius of the sphere was added, and then a semi-infinite uniform vortex cylinder "slipstream," of this same radius, completed the representation. There was thus no internal flow through the sphere, but Ψ_0 and U were chosen so that the mean internal axial velocity at the maximum cross section was only $10^{-6} \cdot U$.

It was assumed that this internal flow, and the extremely thin "slipstream" would have negligible effect, except in the immediate neighborhoods of "nose" and "tail" of the sphere.

It is seen in Figure 14 that the results of the calculations agreed extremely well with exact theory, except in these neighborhoods.

FURTHER POSSIBLE EXTENSIONS -- The computer program which was developed for the present investigation does not permit full exploitation of the potential applications of the method. The following improvements to the program are contemplated for the near future:

1. Provisions for representation of a closed annular body by a closed system of cone-frustum segments, rather than by a "nearly closed" system, by allowing the points s_1 and s_N to coincide. Tentative plans include:

a. Removal of the present limitation (discussed in Case III of the determination of influence coefficients) on allowable proximity of the midpoint of one segment to another segment.

b. In the case of an annular body with slipstream (that is, a shrouded impulse disc with a shroud of arbitrary finite thickness), replacement of the singular pulse $\gamma_1(s)$ by a triangular pulse, and definition $\bar{s}_1 = s_2/2$. (The trailing edge will be considered to lie at the point $\bar{s}_N$, just downstream of the coincident points s_1 and s_N.)

c. In the case of an annular airfoil without a slipstream, specification of the Kutta condition by specifying $\bar{\bar{\gamma}}_1 = \bar{\bar{\gamma}}_N = 0$; and replacement of $\bar{\bar{\gamma}}_1$ by the boundary value Ψ_0 of the stream function, as an unknown variable in the solution of N-1 simultaneous equations. (The trailing edge will be considered to lie at the coincident points s_1 and s_N

2. Provisions for representation of a closed solid body by a closed system of cone-frustum segments, by allowing the points s_1 and s_{N+1} to lie on the axis of symmetry. Tentative plans include

a. Replacement of the singular pulse $\gamma_1(s)$ by a triangular pulse, and definition $\bar{s}_1 = s_2/2$. (The pulse $\gamma_{N+1}(s)$ will be suppressed by specifying $F_{N+1} = 0$.)

b. Optional definition, $\Psi_o = 0$.

c. Removal of the present limitation (twenty percent of the mean segment radius) on the permissible length of a segment. (This limitation is presently imposed because of applying analytic formulas for the influence coefficients to entire segments, and can be removed by applying these formulas only to a short mid-section of each segment, and integrating numerically over the remaining portions of the segment.)

3. Provisions for calculating the velocity components and stream function at arbitrary points in the flow field, not on the system of cone-frustum segments.

4. Provisions for calculating the flow about a system of two or more coaxial bodies, such as, for example, a shrouded impulse disc with a leading-edge slat, or with a centerbody.

The above modifications and extensions appear to be fairly trivial in difficulty, although the improvements in utility of the method of calculation would not necessarily be trivial.

Another extension which would appear to be of potential value, but is not trivial, is the following: Provision for successive modification of the shape of a section of a closed body of revolution to approach a prescribed velocity distribution. Since, in the representation of a

closed body by a surface distribution of vortices, the vortex density distribution is directly proportional to the velocity distribution, this representation would appear to be especially well suited to this problem. (A semi-infinite body is a closed body in this context.) This class of problems includes certain classical free-streamline problems (wake flow, cavity flow, flow through an orifice, etc.) in which the prescribed velocity is uniform, as well as other possibilities, such as the design of laminar-flow annular airfoils, design for minimum adverse pressure gradient of separation-prone components such as inlets and diffusers, and many others. Although these problems might seem simpler than the slipstream problem to the extent that the vortex distribution is given along the unknown boundary, the problem of successively adjusting the boundary shape to obtain converging solutions would in general be much more difficult. Moreover, in many cases, the question of the existence of a solution would be a matter of real practical concern, since one can easily specify a velocity distribution which is impossible of attainment.

CONCLUSIONS

The following conclusions have been drawn:

1. A practical method of obtaining approximate numerical solutions of the mathematical problem of the axisymmetric potential flow through a shrouded impulse disc, using a high-speed computer, has been developed. In particular, it is now possible to examine in detail the theoretical effects of shroud geometry on slipstream contraction.

2. The assumptions of the theory of the shrouded impulse disc are consistent with those of the one-dimensional theory of the shrouded propeller. That theory has been extremely useful in the past, even though it was necessary to use rough estimates of the slipstream contraction for its application. It is a reasonable presumption that the one-dimensional theory will be still more useful, now that it is possible to make detailed predictions of the slipstream contraction. However, a definite conclusion on this must await experimental confirmation.

3. The results of systematic calculations of slipstream contraction for families of cylindrical, conical, and parabolic-cambered shrouds, in the static case, have been presented.

4. It is found that the slipstream contracts less severely, in the case of very short cylindrical shrouds, than had previously been predicted.

5. In the case of cylindrical shrouds, a good estimate of the slipstream contraction in the static case can be obtained from linearized-theory calculations, by using the calculated discontinuity in squared velocity (which is proportional to the quantity γW) across the slipstream at the trailing edge. This technique was used without substantiation by at least one previous investigator, but has not been used by more recent

investigators. However, there is no possibility of similarly accurate estimates from the linearized theory for non-cylindrical shrouds, because the linearized theory cannot apply to the static case unless the shrouds are cylindrical.

6. The computer program developed for the shrouded impulse disc problem is generally applicable to axisymmetric potential flows about and through arbitrary open surfaces of revolution. A sample calculation of the velocity distribution on the interior wall of a long duct of varying radius agreed extremely well with a previous exact solution.

7. Annular and solid bodies of revolution can be approximated by "nearly closed" surfaces of revolution. A sample calculation of the velocity distribution on an annular airfoil agreed quite well with experiment. A sample calculation of the velocity distribution on a sphere agreed extremely well with exact theory.

8. By means of fairly straightforward modifications and extensions, which are discussed briefly, the present method can become a rather general and powerful tool for making axisymmetric potential flow calculations. In particular, it appears that problems of flow about arbitrary thick annular bodies, with circulation or slipstreams, not amenable to treatment by previous methods can be treated accurately and conveniently.

APPENDIX A

PRACTICAL METHOD OF CALCULATION

It is desired to develop a systematic calculating process, suitable for execution on an electronic digital computer, for approximate solution of the equations

$$\int_o^\infty \Psi^*(S,\bar{S})\ \gamma(S)\ dS = \Psi_o \quad , \quad S \geq 0 \qquad [A1]$$

$$\left.\begin{aligned} \gamma(\bar{S})\ V(\bar{S}) &= \text{a constant} \quad , \quad S \geq S_{t.e.} \\ V(\bar{S}) &= \left[V_x^2(\bar{S}) + V_r^2(\bar{S})\right]^{\frac{1}{2}} \\ V_x(\bar{S}) &= \int_o^\infty V_x^*(S,\bar{S})\ \gamma(S)\ dS \\ V_r(\bar{S}) &= \int_o^\infty V_r^*(S,\bar{S})\ \gamma(\bar{S})\, dS \end{aligned}\right\} \qquad [A2]$$

where it is understood that the influence functions Ψ^*, V_x^*, and V_r^* have definition in terms of a function R(S) with a range $0 \leq S$. However, this function is given initially only in the range $0 \leq S \leq S_{t.e}$.

This becomes practical if each of the functions R(S) and $\gamma(S)$ can be characterized adequately by a finite number of variables. To this end, the following simplifying assumptions are introduced

1. It is assumed that the function R(S) can be represented with sufficient accuracy by a function r(s), the graph of which is composed of N + M straight-line segments. The first segment originates at the leading edge of the shroud, s = S = 0. The midpoint of the Nth segment coincides with the trailing edge of the shroud, $s = \bar{s}_N$, $S = S_{t.e.}$. The (N + M) th segment is semi-infinite at $r = r_{N+M}$ = constant. Thus, the function r(s) defines a system of cone-frustum segments terminating in a semi-infinite cylinder (see Figure 1).

2. It is assumed that the vortex distribution $\gamma(S)$ on the stream surface $\Psi = \Psi_o$ can be represented by a continuous distribution $\gamma(s)$ which varies linearly along each of these segments except the first; remains constant along the (N + M)th; and varies as $c_1 s^{-\frac{1}{2}} + c_2 s$ along the first (where c_1 and c_2 are arbitrary constants).

3. It is assumed that a pair of functions r = r(s) and $\gamma = \gamma(s)$, which when substituted for R(S) and $\gamma(S)$ satisfy Equations [A1] and [A2] at the shroud leading edge and at the midpoint of each of the second through (N+M-1)th segments, will constitute a sufficiently accurate approximation to a solution of these equations.

The validity of these assumptions will depend, of course, upon a suitable choice of the spacing of the N + M segments, including choice of sufficiently large numbers N and M.

The three assumptions stated above are similar to assumptions introduced by Smith and Pierce (Reference 12) in their treatment of axially symmetric, inviscid, irrotational flow about bodies of revolution. At the present stage, the hope that these assumptions will lead to accurate approximations to the exact solutions rests largely upon the notable

success of the work of those authors. (Smith and Pierce approximated the body surface by a system of cone-frustum segments. They employed a distribution of ring sources, which they took to be uniform over each segment, and hence discontinuous at the junctures between segments, and applied the boundary conditions at the midpoint of each segment. They dealt with fully-specified surface geometry; i.e., with the ordinary Neumann problem, so that iteration was not required.)

Following the second of the above assumptions, it is convenient to write $\gamma(s)$ as the sum of N + M overlapping pulse functions (triangular pulses, except for the first and last) as follows:

$$\gamma(s) \equiv \sum_{i=1}^{N+M} \gamma_i(s) \qquad [A3a]$$

where

$$\left.\begin{aligned} \gamma_1(s) &\equiv \bar{\gamma}_1 \left[\sqrt{\frac{s_2}{s}} - \frac{s}{s_2}\right] \quad , \quad 0 < s < s_2 \\ &\equiv 0 \quad , \quad \text{otherwise} \end{aligned}\right\} \qquad [A3b]$$

$$\left.\begin{aligned} \gamma_i(s) &\equiv \bar{\gamma}_i \left(\frac{s - s_{i-1}}{s_i - s_{i-1}}\right) \quad , \quad s_{i-1} < s < s_i \\ &\equiv \bar{\gamma}_i \left(\frac{s_{i+1} - s}{s_{i+1} - s_i}\right) \quad , \quad s_i < s < s_{i+1} \\ &\equiv 0 \quad , \quad \text{otherwise} \end{aligned}\right\} \quad 1 < i < N+M \qquad [A3c]$$

$$\left.\begin{aligned}
\gamma_{N+M}(s) &\equiv \bar{\gamma}_{N+M}\left(\frac{s - s_{N+M-1}}{s_{N+M} - s_{N+M-1}}\right), && s_{N+M} < s < s_{N+M} \\
&\equiv \bar{\gamma}_{N+M}, && s_{N+M} < s \\
&\equiv 0, && \text{otherwise}
\end{aligned}\right\} \quad [A3d]$$

(Note that $\bar{\gamma}_i = \gamma(s_i)$, except when $i = 1$)

With these definitions, the continuous function $\gamma(s)$ is completely specified, for all values of s, by specifying a set of N + M numbers, the values of $\bar{\gamma}_i$.

(These definitions involve no further approximation beyond the approximation introduced by the second of the above assumptions. They merely introduce a convenient way of expressing this assumption.)

The integral equations

$$\Psi(\bar{s}) = \int_0^\infty \Psi^*(s,\bar{s})\ \gamma(s)\ ds$$

$$V_x(\bar{s}) = \int_0^\infty V_x^*(s,\bar{s})\ \gamma(s)\ ds$$

$$V_r(\bar{s}) = \int_0^\infty V_r^*(s,\bar{s})\ \gamma(s)\ ds$$

now reduce to systems of linear algebraic equations as follows:

$$\Psi(\bar{s}_i) = \sum_{j=1}^{N+M} a_{i,j}\,\bar{\gamma}_j$$

$$V_x(\bar{s}_j) = \sum_{j=1}^{N+M} b_{i,j}\,\bar{\gamma}_j$$

$$V_r(\bar{s}_i) = \sum_{j=i}^{N+M} c_{i,j}\,\bar{\gamma}_j$$

where

$$a_{i,j} \equiv \frac{1}{\bar{\gamma}_j} \int_o^{\infty} \Psi^*(s,\bar{s}_i)\,\gamma_j(s)\,ds$$

$$b_{i,j} \equiv \frac{1}{\bar{\gamma}_j} \int_o^{\infty} V_x^*(s,\bar{s}_i)\,\gamma_j(s)\,ds$$

$$c_{i,j} \equiv \frac{1}{\bar{\gamma}_j} \int_o^{\infty} V_r^*(s,\bar{s}_i)\,\gamma_j(s)\,ds$$

These integrals, in turn, are expressed more conveniently by further defining

$$\left.\begin{aligned} a_{i,j} &\equiv a_{i,j-} + a_{i,j+} \\ b_{i,j} &\equiv b_{i,j-} + b_{i,j+} \\ c_{i,j} &\equiv c_{i,j-} + c_{i,j+} \end{aligned}\right\} \qquad [A4]$$

where

$$a_{i,1-} = 0 \qquad [A5a]$$

$$a_{i,1+} = \int_0^{s_2} \left(\sqrt{\frac{s_2}{s}} - \frac{s}{s_2} \right) \Psi^*(s, \bar{s}_i)\, ds \qquad [A5b]$$

$$a_{i,j-} = \int_{s_{j-1}}^{s_j} \left(\frac{s - s_{j-1}}{s_j - s_{j-1}} \right) \Psi^*(s, \bar{s}_i)\, ds \quad , \quad 1 < j < N+M \qquad [A5c]$$

$$a_{i,j+} = \int_{s_j}^{s_{j+1}} \left(\frac{s_{j+1} - s}{s_{j+1} - s_j} \right) \Psi^*(s, \bar{s}_i)\, ds \quad , \quad 1 < j < N+M \qquad [A5d]$$

$$a_{i,N+M-} = \int_{s_{N+M-1}}^{s_{N+M}} \left(\frac{s - s_{N+M-1}}{s_{N+M} - s_{N+M-1}} \right) \Psi^*(s, \bar{s}_i)\, ds \qquad [5e]$$

$$a_{i,N+M+} = \int_{s_{N+M}}^{\infty} \Psi^*(s, \bar{s}_i)\, ds \qquad [A5f]$$

The expressions for $b_{i,j\pm}$ and $c_{i,j\pm}$ are exactly the same as those given for $a_{i,j\pm}$, but with $V_x^*(s,\bar{s}_i)$ and $V_r^*(s,\bar{s}_i)$, respectively, appearing in place of $\Psi^*(s,\bar{s}_i)$.

Thus, a main problem of the task of developing a practical method of calculation consists of finding usable expressions for these influence coefficients.

DETERMINATION OF THE INFLUENCE COEFFICIENTS

The influence coefficient $a_{i,j}$ gives the value of the stream function at the point $s = \bar{s}_i$ due to the pulse function $\gamma_j(s)$, in the special case $\bar{\gamma}_j = 1$. (Similarly $b_{i,j}$ gives the value of the axial velocity component, and $c_{i,j}$ gives the value of the radial velocity component at this point due to this pulse.) In the great majority of instances, when j is equal to neither unity nor N+M, and $\bar{s}_i$ is outside the range of $\gamma_j(s)$ (i.e., $i \neq j$, and $i \neq j-1$), the influence coefficients can be determined by straightforward numerical integration of Equations [A5], it being necessary only to establish suitable rules to assure efficient and accurate performance of the numerical integration by the computer. In each remaining instance, however, the definite integral defining the influence coefficient is improper for one or more reasons, and special care is necessary. The various contingencies which arise are grouped in five separate cases, in the following discussion.

CASE I. $\bar{s}_i$ WITHIN TRIANGULAR PULSE -- The point denoted $\bar{s}_i$ falls within the ranges of the pulse $\gamma_i(s)$ and $\gamma_{i+1}(s)$.

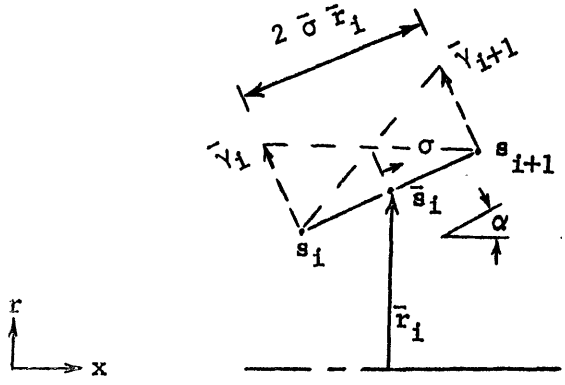

$$\sigma \equiv \frac{s - \bar{s}_i}{\bar{r}_i}$$

$$\bar{\sigma} \equiv \frac{s_{i+1} - s_i}{2\bar{r}_i}$$

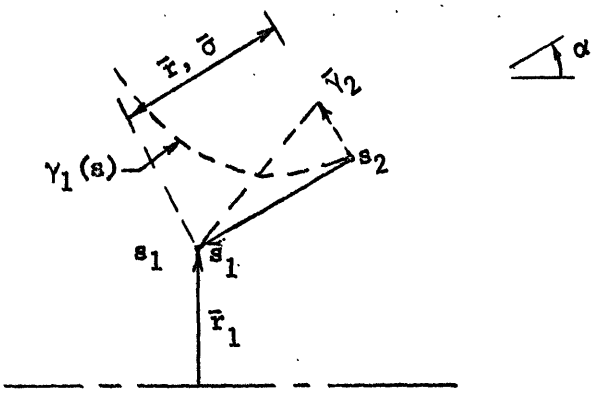

$$s_1 = 0$$

$$\sigma \equiv \frac{s}{\bar{r}_1}$$

$$\bar{\sigma} \equiv \frac{s_2}{\bar{r}_1}$$

The flow in the neighborhood of the leading edge of the shroud is quite similar to that in the neighborhood of the leading edge of a thin airfoil at incidence. Just as in the problem of the thin airfoil, as treated by Glauert (Reference 4), it is necessary to take careful account of the fact that the point $\bar{s}_1$, even though situated at the leading edge, is nevertheless to be considered an interior point of the shroud contour. This is facilitated by writing:

$$a_{1,1+} = \bar{r}_i \lim_{\epsilon \to 0} \int_0^{\bar{\sigma}} \left(\sqrt{\frac{\bar{\sigma}}{\sigma}} - \frac{\sigma}{\bar{\sigma}} \right) \gamma^*(\sigma - \epsilon)\, d\sigma$$

$$a_{1,2-} = \bar{r}_i \lim_{\epsilon \to 0} \int_0^{\bar{\sigma}} \frac{\sigma}{\bar{\sigma}}\, \gamma^*(\sigma - \epsilon)\, d\sigma \qquad [A9]$$

$$b_{1,1+} \equiv \bar{r}_i \lim_{\epsilon \to 0} \int_0^{\bar{\sigma}} \left(\sqrt{\frac{\bar{\sigma}}{\sigma}} - \frac{\sigma}{\bar{\sigma}} \right) \gamma_x^*(\sigma - \epsilon)\, d\sigma$$

etc.

Now, if series expansions of the influence functions (see Appendix B) are substituted into these integrals, it is found that the resulting terms are readily evaluated, except for terms which lead to integrals of the form

$$\lim_{\epsilon \to 0} \int_0^{\bar{\sigma}} \frac{\sqrt{\bar{\sigma}}}{\sqrt{\sigma}\,(\sigma-\epsilon)}\, d\sigma$$

With the aid of formulas given by Pierce (Reference 18), this integral is evaluated as follows:

Let $y = \sigma/\epsilon$; then

$$\int_0^{\bar{\sigma}} \frac{\sqrt{\bar{\sigma}}}{\sqrt{\sigma}\,(\sigma-\epsilon)}\, d\sigma = \sqrt{\frac{\bar{\sigma}}{\epsilon}} \int_1^{\bar{\sigma}/\epsilon} \frac{dy}{(y-1)\sqrt{y}} - \sqrt{\frac{\bar{\sigma}}{\epsilon}} \int_0^1 \frac{dy}{(1-y)\sqrt{y}}$$

But

$$\int_0^1 \frac{dy}{(1-y)\sqrt{y}} = \int_1^{\infty} \frac{dy}{(y-1)\sqrt{y}}$$

Thus

$$\int_0^{\bar{\sigma}} \frac{\sqrt{\bar{\sigma}}}{\sqrt{\sigma}\,(\sigma-\epsilon)}\, d\sigma = -\sqrt{\frac{\bar{\sigma}}{\epsilon}} \int_{\bar{\sigma}/\epsilon}^{\infty} \frac{dy}{(y-1)\sqrt{y}} = \sqrt{\frac{\bar{\sigma}}{\epsilon}} \log_e \frac{1+\sqrt{\epsilon/\bar{\sigma}}}{1-\sqrt{\epsilon/\bar{\sigma}}}$$

$$= -2\sqrt{\frac{\bar{\sigma}}{\epsilon}}\left[\sqrt{\frac{\epsilon}{\bar{\sigma}}} + \frac{1}{3}\left(\sqrt{\frac{\epsilon}{\bar{\sigma}}}\right)^3 + \frac{1}{5}\left(\sqrt{\frac{\epsilon}{\bar{\sigma}}}\right)^5 + \cdots\right]$$

Whence

$$\lim_{\epsilon \to 0} \int_0^{\bar{\sigma}} \frac{\sqrt{\bar{\sigma}}}{\sqrt{\sigma}\,(\sigma-\epsilon)}\, d\sigma = -2$$

The final results are:

$$a_{1,1+} = \bar{r}_1^2 \left\{ \log_e \frac{8}{\bar{\sigma}} \left[\frac{3}{2}\bar{\sigma} + \left(\frac{1}{6}\sin\alpha\right)\bar{\sigma}^2 - \left(\frac{3}{160}\sin^2\alpha - \frac{9}{320}\right)\bar{\sigma}^3 + \ldots \right] + \left[\frac{3}{4}\bar{\sigma} + \left(\frac{81}{3200}\sin^2\alpha + \frac{57}{6400}\right)\bar{\sigma}^3 + \ldots \right] \right\} \quad [A10a]$$

$$a_{1,2-} = \bar{r}_1^2 \left\{ \log_e \frac{8}{\bar{\sigma}} \left[\frac{1}{2}\bar{\sigma} + \left(\frac{1}{6}\sin\alpha\right)\bar{\sigma}^2 - \left(\frac{1}{32}\sin^2\alpha - \frac{3}{64}\right)\bar{\sigma}^3 + \ldots \right] - \left[\frac{3}{4}\bar{\sigma} + \left(\frac{1}{9}\sin\alpha\right)\bar{\sigma}^2 - \left(\frac{7}{128}\sin^2\alpha - \frac{1}{256}\right)\bar{\sigma}^3 + \ldots \right] \right\} \quad [A10b]$$

$$b_{1,1+} = \frac{1}{2} \left\{ \log_e \frac{8}{\bar{\sigma}} \left[\frac{3}{2}\bar{\sigma} - \left(\frac{1}{12}\sin\alpha\right)\bar{\sigma}^2 + \left(\frac{3}{80}\sin^2\alpha - \frac{9}{320}\right)\bar{\sigma}^3 + \ldots \right] - \left[6\sin\alpha - \left(\frac{3}{2}\sin^2\alpha + \frac{3}{2}\right)\bar{\sigma} + \left(\frac{1}{12}\sin^3\alpha - \frac{1}{8}\sin\alpha\right)\bar{\sigma}^2 - \left(\frac{3}{160}\sin^4\alpha - \frac{3}{50}\sin^2\alpha + \frac{123}{6400}\right)\bar{\sigma}^3 + \ldots \right] \right\} \quad [A10c]$$

$$b_{1,2-} = \frac{1}{2} \left\{ \log_e \frac{8}{\bar{\sigma}} \left[-\left(\frac{1}{12}\sin\alpha\right)\bar{\sigma}^2 + \left(\frac{1}{16}\sin^2\alpha - \frac{3}{64}\right)\bar{\sigma}^3 + \ldots \right] + \left[2\sin\alpha + \left(\frac{1}{2}\sin^2\alpha + \frac{1}{2}\right)\bar{\sigma} - \left(\frac{1}{12}\sin^3\alpha - \frac{13}{72}\sin\alpha\right)\bar{\sigma}^2 + \left(\frac{1}{32}\sin^4\alpha - \frac{1}{8}\sin^2\alpha + \frac{13}{256}\right)\bar{\sigma}^3 + \ldots \right] \right\} \quad [A10d]$$

$$c_{1,1+} = \frac{1}{2}\left\{\cos\alpha \log_e \frac{8}{\bar{\sigma}}\left[\frac{1}{4}\bar{\sigma}^2 - \left(\frac{9}{160}\sin\alpha\right)\bar{\sigma}^3 + \ldots\right]\right.$$

$$+ \left[6 - \left(\frac{3}{2}\sin\alpha\right)\bar{\sigma} + \left(\frac{1}{12}\sin^2\alpha + \frac{1}{24}\right)\bar{\sigma}^2\right.$$

$$\left.\left. - \left(\frac{3}{160}\sin^3\alpha - \frac{213}{3200}\sin\alpha\right)\bar{\sigma}^3 + \ldots\right]\right\} \qquad [A10e]$$

$$c_{1,2-} = \frac{1}{2}\left\{\cos\alpha \log_e \frac{8}{\bar{\sigma}}\left[\frac{1}{4}\bar{\sigma}^2 - \left(\frac{3}{32}\sin\alpha\right)\bar{\sigma}^3 + \ldots\right]\right.$$

$$- \left[2 + \left(\frac{1}{2}\sin\alpha\right)\bar{\sigma} - \left(\frac{1}{12}\sin^2\alpha - \frac{1}{8}\right)\bar{\sigma}^2\right.$$

$$\left.\left. + \left(\frac{1}{32}\sin^3\alpha - \frac{19}{128}\sin\alpha\right)\bar{\sigma}^3 + \ldots\right]\right\} \qquad [A10f]$$

It will be found that these expressions (with only the given leading terms of the infinite series) provide sufficiently accurate approximations for our purpose, if $\bar{\sigma}$ does not exceed 0.2.

CASE III. $\bar{s}_i$ OUTSIDE TRIANGULAR PULSE -- In this case, the integrals appearing in Equations [A5] are proper, and can be evaluated conveniently by numerical integration.

Simpson's rule (Reference 19) is particularly well suited for numerical integration by electronic digital computers because of its simplicity and the resulting flexibility with which it may be applied. This rule may be expressed

$$\int_{y_1}^{y_1+2h} fn(y)dy \doteq \frac{h}{3}\left[fn(y_1) + 4fn(y_1+h) + fn(y_1+2h)\right]$$

The approximate equality becomes exact if the fourth derivative of the integrand is zero over the interval of integration. Moreover, so long as the fourth derivative is finite, the fractional error incurred by applying the rule can be made as small as desired, by confining application to sufficiently small intervals, 2h. Thus, an integration over a given interval is split into integrations over an appropriate number of "subintervals" as follows:

$$\int_{y_1}^{y_k} \text{fn}(y)\, dy = \sum_{i=1}^{k-1} \int_{y_i}^{y_{i+1} = y_i + 2h_i} \text{fn}(y)\, dy \qquad [A11]$$

$$\doteq \sum_{i=1}^{k-1} \frac{h_i}{3} \left[\text{fn}(y_i) + 4\text{fn}(y_i + h_i) + \text{fn}(y_i + 2h_i) \right]$$

where each subinterval, $2h_i$, is to be chosen sufficiently small to assure the desired degree of accuracy.

In the present case, the integrands which are involved in Equations [A5] are well-behaved functions except for singularities of the influence functions situated at the point denoted $\bar{s}_i$. The most unfavorable circumstance (since we have excluded those cases in which the point $\bar{s}_i$ is encountered in the interval of integration) occurs when $\bar{s}_i$ is collinear with, and near one end of the line segment along which the integration is performed, and the integrand has a simple pole at $s = \bar{s}_i$. (The nature of the singularities of the influence functions is most readily apparent

in the series expansions, Appendix B.) Therefore, we consider the integral

$$\int_{y_i}^{y_i + 2h_i} \frac{1}{y}\, dy = \log_e \left(1 + \frac{2h_i}{y_i}\right) \qquad \text{(Exactly)}$$

$$\doteq \frac{h_i}{3}\left[\frac{1}{y_i} + \frac{4}{y_i + h_i} + \frac{1}{y_i + 2h_i}\right] \qquad \text{(By Simpson's rule)}$$

The fractional error is

$$e = \frac{\frac{2y_i}{h_i}\left[\frac{1}{6} + \frac{2}{3}\left(1 + \frac{h_i}{y_i}\right)^{-1} + \frac{1}{6}\left(1 + \frac{2h_i}{y_i}\right)^{-1}\right]}{\log_e \left(1 + \frac{2h_i}{y_i}\right)} - 1$$

The fractional error is seen to be a function of $\frac{2h_i}{y_i}$, the ratio of the length of the subinterval to the distance between the nearer end of the subinterval and the location of the pole of the integrand. Some values of e are given in the following table:

$\frac{2h_i}{y_i}$	Fractional Error, e
0.2	0.000018
0.4	0.000113
0.6	0.000409
0.8	0.000970
1.0	0.001865
2.0	0.011379

For the present case, it is chosen to evaluate Equations [A5] by Simpson's rule, in the form given by Equation [A11], with the subintervals $2h_i$ chosen to be of equal width within each particular interval. Thus

$$2h_i = \frac{y_k - y_1}{k - 1}$$

It is further chosen to select the number of subintervals, k-1, as the smallest (non-zero) integer satisfying the condition

$$2h_i = \leq 1/2\ d_{min}$$

where d_{min} is the distance from the point $\bar{s}_i$ to the nearest end of the line segment over which the integration is performed.

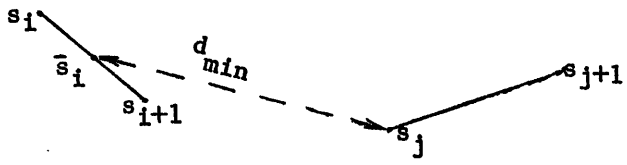

Finally, it is chosen to select the spacing of the points s_i, so that none of the points $\bar{s}_i$ shall fall closer to any point of any other line segment (that is, other than the line segment containing $\bar{s}_i$) than 0.7 times its distance from the nearest end of that other line segment.

(Application of the procedure described above involves accurate numerical evaluation of the influence functions Ψ^*, V_x^*, and V_r^* at discrete points along the path of integration. The method employed for this purpose is described in Appendix D.)

CASE IV. $\bar{s}_i$ OUTSIDE SINGULAR PULSE -- In this case, the singularities of the influence functions are located outside the interval of integration; but the singularity of $\gamma_1(s)$, of order $s^{-1/2}$, is located at one end of the interval.

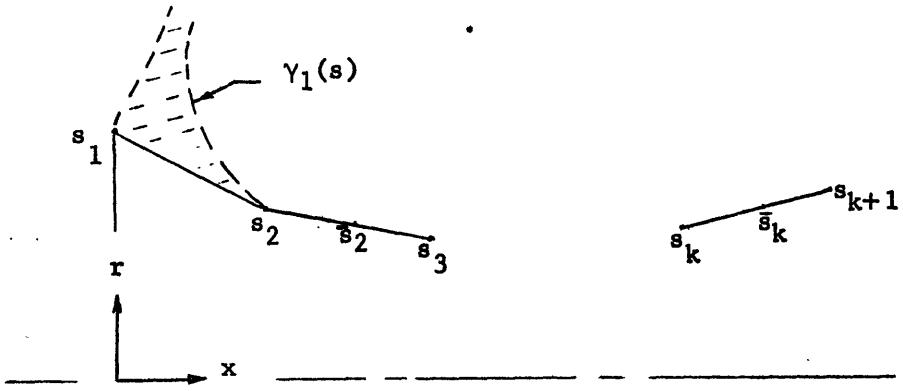

Since the point $\bar{s}_i$ is in general not collinear with the line segment over which integration is performed, and may be either close to or distant from this segment, it is not practical to expand the integrands in series. Numerical evaluation is practical, however, by the following device: Consider, for example, the influence coefficient

$$c_{2,1+} = \int_0^{s_2} \left(\sqrt{\frac{s_2}{s}} - \frac{s}{s_2} \right) V_r^*(s, \bar{s}_2) \, ds$$

As an approximation, this can be written

$$c_{2,1+} \doteq V_r^*(0, \bar{s}_2) \int_\sigma^{\beta s_2} \left(\sqrt{\frac{s_2}{s}} - \frac{s}{s_2} \right) ds + \int_{\beta s_2}^{s_2} \left(\sqrt{\frac{s_2}{s}} - \frac{s}{s_2} \right) V_r^*(s, \bar{s}_2) \, ds$$

where the error arises from neglecting any fractional change in $V_r^*(s,\bar{s}_2)$ over the interval $0 < s < \beta s_2$. This error can be made as small as desired by choosing the coefficient β sufficiently small. The first integral can then be evaluated analytically, and the second can be evaluated numerically, by Simpson's rule, after splitting it into appropriate subintervals. (In an instance in which $V_r^*(s,\bar{s}_2)$ is dominated by a singular term of order $(\bar{s}_2 - s)^{-1}$, the fractional error in the first integral will not exceed that of the approximation

$$\int_0^\beta (s^{-\frac{1}{2}} - s)(1 + s)\, ds \doteq \int_0^\beta (s^{-\frac{1}{2}} - s)\, ds$$

It is chosen to take $\beta = 0.01$. Then this approximation becomes

$$0.20061634 \doteq 0.19995$$

Thus, the fractional error in the evaluation of the first integral would be of the order 0.003; and the contribution of this error to the total fractional error in the evaluation of $c_{2,1+}$ would be acceptably small.)

With regard to application of Simpson's rule to the second integral, the permissible width, $2h_i$, of the ith subinterval of the second integral is related to the closest distance from this subinterval to any singularity of the integrand. If the width of the subinterval is taken equal to its closest distance from s_1 (the site of a singularity of order $s^{-1/2}$), then, to the approximation that the integrand is dominated by this singularity, the fractional error in evaluating the integral over this subinterval is

$$e \doteq \frac{\frac{y_1}{6}\left[\frac{1}{\sqrt{y_1}} + \frac{4}{\sqrt{1.5y_1}} + \frac{1}{\sqrt{2y_1}}\right]}{\int_{y_1}^{2y_1} \frac{1}{\sqrt{y}}\, dy} - 1 \doteq 0.0005$$

Taking $\beta = 0.01$ in the first integral, the width of the first subinterval of the second integral can be $2h_1 = 0.01\ s_2$. It is convenient to progressively increase the width of successive subintervals, so that the number required is not excessive. These considerations are applied in the following choice of a formal procedure for calculation of the influence coefficients, in the case at hand:

$$a_{i,1+} = 0.19995\ \Psi^*(0, \bar{s}_i)s_2 + \sum_{k=1}^{7} \frac{h_k}{3}\left[\left(\sqrt{\frac{s_2}{y_k}} - \frac{y_k}{s_2}\right)\Psi^*(y_k, \bar{s}_i)\right.$$

$$+ 4\left(\sqrt{\frac{s_2}{y_k + h_k}} - \frac{y_k + h_k}{s_2}\right)\Psi^*(y_k + h_k, \bar{s}_i)$$

$$\left. + \left(\sqrt{\frac{s_2}{y_k + 2h_k}} - \frac{y_k + 2h_k}{s_2}\right)\Psi^*(y_k + 2h_k, \bar{s}_i)\right] \qquad [A12]$$

where

$$h_1 = 0.00495\ s_2$$

$$h_k = 2^{k-1}h_1 \quad , \quad 2 \le k \le 6$$

$$h_7 = 0.18315\ s_2$$

$$y_1 = 0.01\ s_2$$

$$y_k = y_{k-1} + 2h_{k-1} \quad , \quad 2 \le k \le 7$$

The coefficients $b_{i,1+}$ and $c_{i,1+}$ are given by exactly similar expressions, in which V_x^* and V_r^*, respectively, appear in place of Ψ^*.

CASE V. $\bar{s}_i$ OUTSIDE SEMI-INFINITE PULSE -- In this case, the integrals appearing in Equations [A5] are improper because the upper limit of integration extends to infinity; that is,

$$a_{i,N+M+} = \int_{s_{N+M}}^{\infty} \Psi^*(s,\bar{s}_i)\, ds$$

$$b_{i,N+M+} = \int_{s_{N+M}}^{\infty} V_x^*(s,\bar{s}_i)\, ds$$

$$c_{i,N+M+} = \int_{s_{N+M}}^{\infty} V_r^*(s,\bar{s}_i)\, ds$$

The series expansions of the influence coefficients used in the preceding cases, are useful only over intervals collinear with the point $\bar{s}_i$, and not extending too far from this point. Alternative (asymptotic) expansions, valid at points sufficiently far removed from the point $\bar{s}_i$, are possible and are developed in Appendix C. Thus it is possible to evaluate a portion of any of the above integrals by numerical integration, from s_{N+M} to a point s', sufficiently far removed from $\bar{s}_i$ to assure validity of the asymptotic expansions; and to evaluate the remaining portion, from s' to infinity, by analytic term-by-term integration.

In the course of developing this procedure, however, and attempting to test its accuracy, it was discovered that a purely numerical procedure, much better adapted to automatic computing, is feasible. This consists of dividing each integral into an infinite number of subintervals, so that the successive subintervals increase in width in geometric progression. With appropriate choice of the width of the first subinterval, and of the ratio between the widths of successive subintervals, Simpson's rule can be successfully applied, so that the infinite integration is approximated by an infinite summation of algebraic terms.

The actual procedure to be followed is chosen as follows:

$$a_{i,N+M+} \doteq \sum_{k=1}^{k_f} \frac{h_k}{3} \left[\Psi^*(y_k, \bar{s}_i) + 4\Psi^*(y_k + h_k, \bar{s}_i) + \Psi^*(y_k + 2h_k, \bar{s}_i) \right]$$

where

$$h_1 = \frac{1}{4} \left[x(s_{N+M}) - x(\bar{s}_i) \right]$$

$$h_k = (1.5)^{k-1} h_1$$

$$y_1 = s_{N+M}$$

$$y_k = y_{k-1} + 2h_{k-1}$$

and where the k_fth term of the summation is the first term encountered which is smaller than 0.000001.

The coefficients $b_{i,N+M+}$ and $c_{1,N+M+}$ are evaluated by the same procedure, replacing Ψ^* by V_x^*, and V_r^*, respectively.

(Still another possibility for the handling of this case was considered; namely, replacing the semi-infinite uniform vortex cylinder, by its "equivalent" uniform sink disc, as discussed by Küchemann and Weber (Reference 3). In principle, this would be the best approach, because only proper definite integrals would be involved. However, this approach was rejected because it would have required an additional computer subprogram to evaluate the influence functions for ring sinks.)

ACCURACY CHECKS

Before attempting calculations of slipstream contraction, preliminary calculations were undertaken to uncover any significant errors in the

influence coefficients given by the procedures prescribed in each of the five cases. First, a procedure for numerical evaluation of the influence functions was developed and checked, as described in Appendix D. The numerical integration procedure prescribed for Case III was checked by applying the procedure exactly as prescribed; then applying it again, but taking five times as many subintervals; then comparing the two results. Precisely the same technique was used to check the numerical integration procedures prescribed for Cases IV and V.

The analytical formulas given for Cases I and II were checked by first applying the formulas over a certain interval; then dividing that interval into subintervals, applying the formulas over the singular subinterval, and integrating numerically over the other subintervals; then, comparing the two results.

No discrepancies larger than a few tenths of one percent were encountered in any of these checks. (Checks of the formulas given for Cases I and II were confined to cone-frustum segments for which the segment length was, at most, two-tenths of the radius at the segment midpoint. The accuracy of these formulas would, of course, deteriorate, if the segment length were increased very much.)

In addition, qualitative checks were made in all five cases by means of hand calculations using the tabulated properties of ring vortices, and certain special ring-vortex distributions, given in References 3 and 5. The results of these checks were also quite satisfactory. (Precise checks by this technique were not attempted, because the tables themselves are not very accurate. The object of these checks was merely to preclude the possibility of major errors.)

It was concluded that the procedures prescribed for calculation of the influence coefficients in each of these five cases were satisfactory.

RÉSUMÉ OF THE CALCULATION PROCEDURE

It is desirable, at this point, to give a concise, step-by-step summary of the procedure which was employed in the calculations.

The exact problem involves finding the shape of the slipstream of a shrouded impulse disc with a thin shroud of given shape and size. In principle, the flow field can be exactly represented by a distribution of ring-vortex singularities on the shroud and slipstream surface, in which case a solution of Equations [A1] and [A2] would constitute an exact solution of the exact problem.

It has been assumed that the exact problem can be replaced by an "approximate problem" in which the flow field is represented by a continuous distribution (of a certain restricted functional type) of singularities on a continuous surface composed of N+M cone-frustum segments (the first N of which approximate the shape of the shroud, and the N+Mth of which is a semi-infinite circular cylinder); and, further, that an exact solution of this approximate problem would afford an approximate solution of the exact problem. It follows that an approximate solution of this approximate problem will also afford an approximate solution of the exact problem.

The governing equations of the approximate problem (analogous to Equations [A1] and [A2] for the exact problem) are:

$$\Psi(\bar{s}_i) = \sum_{j=1}^{N-1} a_{1,j}\,\bar{\gamma}_j + \bar{\gamma}_N \sum_{j=N}^{N+M} a_{i,j}\,F_j = \Psi_o \quad , \quad 1 \le i \le N+M-1 \qquad [A1']$$

$$V(\bar{s}_i)\left(\frac{F_i + F_{i+1}}{2}\right) = V(\bar{s}_N)\left(\frac{1 + F_{N+1}}{2}\right) \quad , \quad N+1 \le i \le N+M-1 \qquad [A2']$$

where

$$V(\bar{s}_i) = \left[V_x^2 (\bar{s}_i) + V_r^2 (\bar{s}_i) \right]^{\frac{1}{2}}$$

$$V_x (\bar{s}_i) = \sum_{j=1}^{N+M} b_{i,j} \bar{\gamma}_j$$

$$V_r (\bar{s}_i) = \sum_{j=1}^{N+M} c_{i,j} \bar{\gamma}_j$$

Let us assume that a shroud shape has been given; that a set of points (x_i , r_i) , $1 \le i \le N+1$, defining a continuous system of cone-frustum segments which approximates the given shape has been selected; and further that a continuatuon of this set (x_i, r_i) , $N+2 \le i \le N+M$, representing a first estimate of the slipstream shape, and a set of numbers (F_i) , $N+1 \le i \le N+M$, representing a first estimate of the slipstream relative vortex distribution, have been selected. One can then proceed as follows:

1. Calculate the coordinates s_i of the points (x_i, r_i), using the relations:

$$s_1 = 0$$

$$s_i = s_{i-1} + \left[(x_i - x_{i-1})^2 + (r_i - r_{i-1})^2 \right]^{\frac{1}{2}}$$

2. Calculate the influence coefficients $a_{i,j}$, $b_{i,j}$, and $c_{i,j}$ for the values $1 \le i \le N+M-1$ and $1 \le j \le N+M$ by the procedures specified in the immediately preceding sections.

3. From Equation [A1'] , for $1 \leq i \leq N$, from a set of N simultaneous linear algebraic equations in the N unknowns, $\bar{\gamma}_j$, for $1 \leq j \leq N$; and solv for these values of $\bar{\gamma}_j$. (In the actual calculations subsequently describe this solution of simultaneous equations was performed by a standard subroutine (Reference 20) of the automatic computing facility employed.) Tabulate the remaining members of the set $\bar{\gamma}_j$, using the relation

$$\bar{\gamma}_j = F_j \, \bar{\gamma}_N \quad , \quad N+1 \leq j \leq N+M$$

4. Using Equations [A1'] and [A2'], tabulate the quantities

$$\left.\begin{array}{l} \Psi(\bar{s}_i) \\ \\ \gamma(\bar{s}_i) \;\; V(\bar{s}_i) \end{array}\right\} \quad N \leq i \leq N+M-1$$

(If these were uniform sets, then the most recently specified sets of values of x_i, r_i, and $\bar{\gamma}_i$ would constitute an exact solution of Equations [A1'] and [A2'].)

5a. Replace the most recent estimate of the slipstream relative vortex distribution with the following new estimate:

$$F'_i = G'_i \div \left[G'_{N+1} + \frac{s_{N+1} - s_N}{s_{N+2} - s_{N+1}} \left(G'_{N+1} - G'_{N+2} \right) \right] , \quad N+1 \leq i \leq N+M$$

where

$$G'_i = V(\bar{s}_N) \frac{s_{i+1} - s_{i-1}}{(s_{i+1} - s_i) V(\bar{s}_i) + (s_i - s_{i-1}) V(\bar{s}_{i-1})} , \quad N+1 \leq i \leq N+$$

$$G'_{N+M} = G'_{N+M-1}$$

5b. Replace the most recent estimate of the slipstream shape with the following new estimate:

$$r_i' = r_i \left[Q_i - 0.06 \tanh \left(\frac{Q_i - 1}{0.09} \right) \right] , \quad N+2 \leq N+M-1$$

$$r_{N+M}' = r_{N+M-1}$$

$$x_i' = x_i$$

where

$$Q_i = \left[\frac{\left(s_{i+1} - s_{i-1} \right) \Psi_o'}{\left(s_{i+1} - s_i \right) \left(\bar{s}_{i-1} \right) + \left(s_i - s_{i-1} \right) \Psi \left(\bar{s}_i \right)} \right]^{\frac{1}{2}}$$

5c. Return to Step 1 and begin a new cycle of calculation.

(Note: In regard to step 5b, it was originally planned to perform the r-adjustment by means of the simpler and more natural formula $r_i' = r_i Q_i$. It was found, however, that the values of Q_i tended to oscillate around unity on successive cycles of calculation, converging toward unity rather slowly, if at all, after the first two or three cycles. The more artificial formula given for Step 5b makes essentially the same r-adjustment as the simpler formula when Q_i differs substantially from unity, but "damps out" the small adjustments which would otherwise retard final convergence. While the given formula was quite satisfactory for purposes of the limited series of calculations undertaken for this dissertation, further improvement

in the rate of convergence could undoubtedly be achieved by systematic modification of this formula.)

This five-step cycle of calculations is to be repeated until the two sets of quantities calculated at Step 4

$$\left.\begin{array}{ll} \Psi(\bar{s}_i) & \\ \gamma(\bar{s}_i) & V(\bar{s}_i) \end{array}\right\} N \le i \le N+M-1$$

both approach uniformity, indicating that an exact solution of Equations [A1′] and [A2′] is being approached. When it becomes apparent to what uniform value γV this set $\gamma(\bar{s}_i)V(\bar{s}_i)$ is converging, to within the required accuracy, the calculations can be terminated. (Strictly speaking, of course, even if the iteration process were continued without limit, and if the sets under discussion became absolutely stationary, they would still not be absolutely uniform, because the successive adjustments at Step 5 are based on linear interpolation between conditions at adjacent points $\bar{s}_i$ and $\bar{s}_{i-1}$, rather than on conditions at individual points $\bar{s}_i$. The remarks of this paragraph, and the next, are thus to be interpreted in a practical sense, not in a rigorous mathematical sense.)

The estimate of the final uniform value γV of this set is then taken as an approximation to the uniform value of $\gamma(S)\ V(S)$, $S \ge S_{t.e.}$, which would be found from an exact solution of the exact problem.

The required estimate of the slipstream contraction ratio follows from this estimate of γV, as follows: It is shown in Reference 3 that: If

$$S \to \infty$$

then

$$V(S) \rightarrow \pi \gamma(S)$$

$$\Psi(S) \rightarrow \pi \gamma(S) \left[R(S)\right]^2$$

Thus the slipstream contraction ratio is given by

$$\phi = \frac{R^2(\infty)}{\bar{r}_N^2} = \frac{\Psi_o}{\bar{r}_N^2 \sqrt{\pi \gamma V}}$$

The five-step calculating procedure itself has been completely specified, in a form suitable for direct translation into a digital computer program.

The steps preceding initiation of the calculation procedure (that is, the selection of the number and location of points to represent the shroud shape and first estimate of the slipstream shape and relative vortex distribution) remain largely a matter of personal judgment. One arbitrary rule has been introduced in the interest of simplifying the calculation procedure:

a. No segment midpoint should fall closer to any point of any other segment than 0.7 times its distance from the nearest end of that other segment.

Beyond this, it has been pointed out that:

b. The accuracy of calculation of the influence coefficients may deteriorate if the length of a segment (other than the N+Mth) exceeds, say, twenty percent of the distance $\bar{r}_i$ of its midpoint from the axis of symmetry.

c. The efficiency of the calculation procedure is impaired (that is, it will take longer to complete the calculations) if the lengths of adjacent segments (other than the N+Mth) are not of the same order of magnitude.

Beyond this are still less precisely defined considerations, such as:

d. The accuracy of the final result will presumably improve as the number of segments is increased.

e. The lengths of the segments should presumably be relatively shorter in regions where the vortex density, $\gamma(s)$, and/or the slope of the stream surface Ψ_o are expected to change rapidly. The neighborhoods of the leading and trailing edges, and of points of rapid curvature of the shroud, are presumably such regions.

The decision on when to terminate the calculations also remains largely a matter of personal judgment. Only a general description has been given of how one should decide whether or not the iteration process has proceeded far enough.

It is possible that experience gained through long usage of this method of calculation might eventually lead to the formulation of further specific rules to diminish or remove these elements of personal judgment.

The preceding discussion was limited to the static case. However, the extension to the case of finite free-stream velocities is quite trivial Equation [A1′] gives the stream function as the sum of the contributions of N+M vortex distribution pulses; one adds to these the contribution $\frac{1}{2}\ U\ \bar{r}_i^2$ of the free stream. Similarly, Equation [A2′] gives the axial velocity component as the sum of N+M terms, to which one simply adds U.

The only other modification required is in the formula

$$\phi = \frac{\Psi_o}{\bar{r}_N^2 \sqrt{\pi \gamma V}}$$

which was used to estimate the slipstream contraction ratio in the static case. With U not zero this becomes

$$\phi = \frac{2 \Psi_o}{\bar{r}_N^2 \sqrt{U^2 + 4\pi \gamma V}}$$

APPENDIX B

SERIES EXPANSION OF THE INFLUENCE FUNCTIONS FOR A NEARBY RING VORTEX

The influence functions for an isolated vortex ring of strength 2π, as given by Küchemann and Weber (Reference 3), can be written

$$\left.\begin{aligned}
\psi^*(x,\bar{x},r,\bar{r}) &= \sqrt{r\,\bar{r}}\,\frac{2}{k}\left[\left(1-\frac{k^2}{2}\right)K(k) - E(k)\right] \\
V_x^*(x,\bar{x},r,\bar{r}) &= \frac{1}{\sqrt{(x-\bar{x})^2+(\bar{r}+r)^2}}\left\{K(k) - \left[1+\frac{2(\bar{r}-r)r}{(x-\bar{x})^2+(\bar{r}-r)^2}\right]E(k)\right\} \\
V_r^*(x,\bar{x},r,\bar{r}) &= \frac{\bar{x}-x}{\bar{r}\sqrt{(x-\bar{x})^2+(\bar{r}+r)^2}}\left\{K(k) - \left[1+\frac{2\bar{r}\,r}{(x-\bar{x})^2+(\bar{r}-r)^2}\right]E(k)\right\}
\end{aligned}\right\} \quad [B1]$$

where

$$k \equiv \frac{2\sqrt{\bar{r}\,r}}{\sqrt{(x-\bar{x})^2+(\bar{r}+r)^2}} \equiv \sqrt{1-k'^2}$$

and K(k) and E(k) are the complete elliptic integrals of the first and second kinds, as defined and tabulated by Jahnke and Emde (Reference 21), for example.

It is convenient to define the variables σ and α as follows (see the sketch):

$$\sigma \equiv \sqrt{(x-\bar{x})^2+(r-\bar{r})^2}$$

$$\alpha \equiv \sin^{-1}\left(\frac{r-\bar{r}}{\sigma\bar{r}}\right)$$

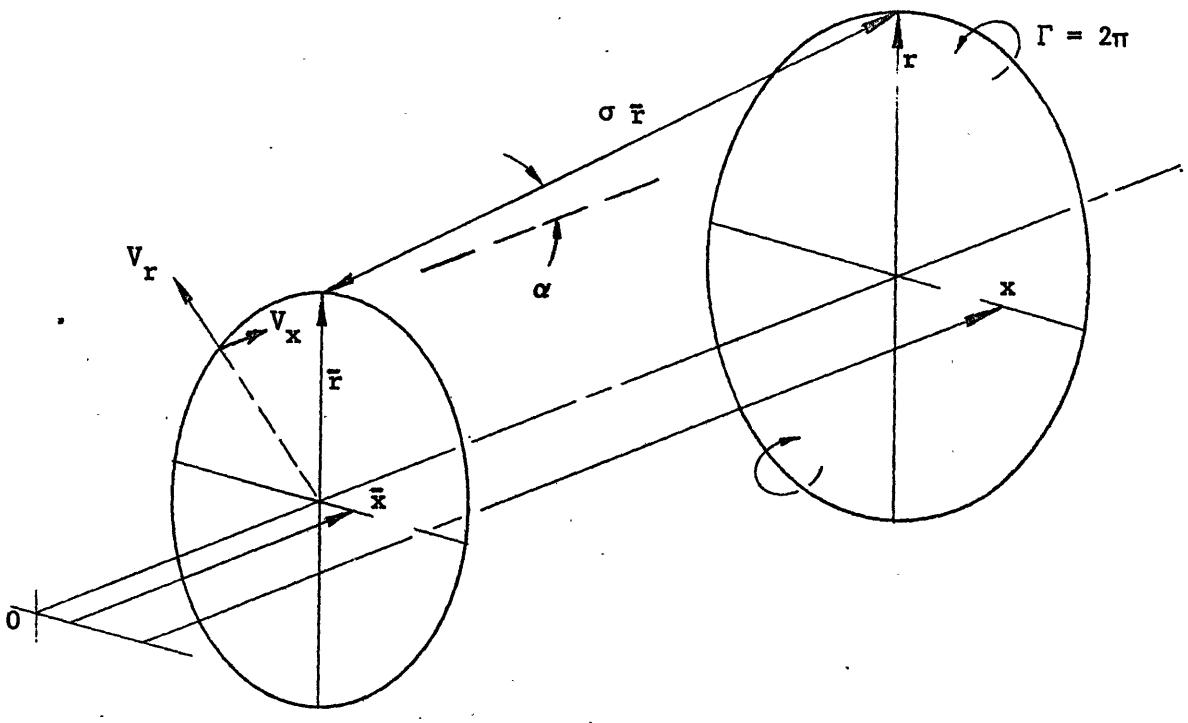

The influence functions are rewritten as follows:

$$\left.\begin{aligned}
\Psi^*(\sigma,\alpha) &= 2\bar{r}\sqrt{1+\sigma(\sin\alpha+\sigma/4)}\left[\left(1-\frac{k^2}{2}\right)K(k)-E(k)\right] \\
V_x^*(\sigma,\alpha) &= \frac{1}{2\bar{r}}\frac{1}{\sqrt{1+\sigma(\sin\alpha+\sigma/4)}}\left[K(k)+\left(\frac{2}{\sigma}\sin\alpha+\sin^2\alpha-\cos^2\alpha\right)E(k)\right] \\
V_r^*(\sigma,\alpha) &= -\frac{\cos\alpha}{2\bar{r}}\frac{1}{\sqrt{1+\sigma(\sin\alpha+\sigma/4)}}\left[\sigma K(k)-\left(\sigma+2\sin\alpha+\frac{2}{\sigma}\right)E(k)\right]
\end{aligned}\right\}$$

where

$$k^2 = 1 - \frac{\sigma^2/4}{1+\sigma(\sin\alpha+\sigma/4)} = 1 - k'^2$$

It is desired to expand these functions into infinite series, valid for small values of σ. Appropriate expansions of the elliptic integrals, as given by Curtis and Sparks (Reference 22), can be written:

$$K(k) = \frac{1}{2}\log_e\left(\frac{16}{k'^2}\right)\left[1 + \left(\frac{1}{2}\right)^2 k'^2 + \left(\frac{1\cdot3}{2\cdot4}\right)^2 k'^4 + \left(\frac{1\cdot3\cdot5}{2\cdot4\cdot6}\right)^2 k'^6 + \cdots\right]$$

$$- \left[\left(\frac{1}{2}\right)^2 \frac{2}{1\cdot2}\, k'^2 + \left(\frac{1\cdot3}{2\cdot4}\right)^2 \left(\frac{2}{1\cdot2} + \frac{2}{3\cdot4}\right) k'^4 + \left(\frac{1\cdot3\cdot5}{2\cdot4\cdot6}\right)^2 \left(\frac{2}{1\cdot2} + \frac{2}{3\cdot4} + \frac{2}{5\cdot6}\right) k'^6 + \cdots\right]$$

$$E(k) = \frac{1}{2}\log_e\left(\frac{16}{k'^2}\right)\left[\frac{1}{2}k'^2 + \left(\frac{1}{2}\right)^2 \frac{3}{4} k'^4 + \left(\frac{1\cdot3}{2\cdot4}\right)^2 \frac{5}{6} k'^6 + \cdots\right]$$

$$+ 1 - \left[\frac{1}{2}\left(\frac{1}{1\cdot2}\right) k'^2 + \left(\frac{1}{2}\right)^2 \frac{3}{4}\left(\frac{2}{1\cdot2} + \frac{2}{3\cdot4}\right) k'^4 + \left(\frac{1\cdot3}{2\cdot4}\right)^2 \frac{5}{6}\left(\frac{2}{1\cdot2} + \frac{2}{3\cdot4} + \frac{2}{5\cdot6}\right) k'^6 + \cdots\right]$$

Substituting these expressions into Equations [B2], suitable series expansions of the remaining factors which appear are readily obtained with the aid of formulas given by Pierce (Reference 18) as follows:

$$k'^2 = \frac{\sigma^2}{4}\left[1 - (\sin\alpha)\,\sigma + \left(\sin^2\alpha - \frac{1}{4}\right)\sigma^2 - \left(\sin^3\alpha - \frac{1}{2}\sin\alpha\right)\sigma^3\right.$$

$$\left. + \left(\sin^4\alpha - \frac{3}{4}\sin^2\alpha + \frac{1}{16}\right)\sigma^4 - \left(\sin^5\alpha - \sin^3\alpha + \frac{3}{16}\sin\alpha\right)\sigma^5 + \cdots\right]$$

$$\log_e\frac{16}{k'^2} = \log_e\frac{64}{\sigma^3} + \left[\left(\sin\alpha\right)\sigma - \left(\frac{1}{2}\sin^2\alpha - \frac{1}{4}\right)\sigma^2 + \left(\frac{1}{3}\sin^3\alpha - \frac{1}{4}\sin\alpha\right)\sigma^3\right.$$

$$- \left(\frac{1}{4}\sin^4\alpha - \frac{1}{4}\sin^2\alpha + \frac{1}{32}\right)\sigma^4$$

$$\left. + \left(\frac{1}{5}\sin^5\alpha - \frac{1}{4}\sin^3\alpha + \frac{1}{16}\sin\alpha\right)\sigma^5 + \cdots\right]$$

$$\sqrt{1+\sigma\,(\sin\alpha+\sigma/4)} \;=\; 1+\left(\tfrac{1}{2}\sin\alpha\right)\sigma-\left(\tfrac{1}{8}\sin^2\alpha-\tfrac{1}{8}\right)\sigma^2+\left(\tfrac{1}{16}\sin^3\alpha-\tfrac{3}{32}\sin\alpha\right)\sigma^3+\cdots$$

$$\frac{1}{\sqrt{1+\sigma(\sin\alpha+\sigma/4)}} \;=\; 1-\left(\tfrac{1}{2}\sin\alpha\right)\sigma+\left(\tfrac{3}{8}\sin^2\alpha-\tfrac{1}{8}\right)\sigma^2-\left(\tfrac{5}{16}\sin^3\alpha-\tfrac{3}{16}\sin\alpha\right)\sigma^3+\cdots$$

The desired expansions of the influence functions can then be obtained by a straightforward process of multiplying together the expansions of the various factors, as indicated by Equations [A2], and collecting terms in like powers of σ. The results are:

$$\left.\begin{aligned}
\Psi^*(\sigma,\alpha) \;&=\; \tfrac{1}{\pi}\left\{\tfrac{1}{2}\log_e\frac{64}{\sigma^2}\left[1+\left(\tfrac{1}{2}\sin\alpha\right)\sigma-\left(\tfrac{1}{8}\sin^2\alpha-\tfrac{3}{16}\right)\sigma^2+\left(\tfrac{1}{16}\sin^3\alpha-\tfrac{3}{32}\sin\alpha\right)\sigma^3+\cdots\right]\right.\\
&\qquad\left.-\left[2+\left(\tfrac{1}{2}\sin\alpha\right)\sigma-\left(\tfrac{1}{4}\sin^2\alpha-\tfrac{1}{16}\right)\sigma^2+\left(\tfrac{7}{48}\sin\alpha-\tfrac{1}{8}\sin\alpha\right)\sigma^3+\cdots\right]\right\}\\
V_x^*(\sigma,\alpha) \;&=\; \tfrac{1}{2\pi}\left\{\tfrac{1}{2}\log_e\frac{64}{\sigma^2}\left[1-\left(\tfrac{1}{4}\sin\alpha\right)\sigma+\left(\tfrac{1}{4}\sin^2\alpha-\tfrac{3}{16}\right)\sigma^2+\cdots\right]\right.\\
&\qquad\left.+\left[\left(2\sin\alpha\right)\tfrac{1}{\sigma}-\cos^2\alpha-\left(\tfrac{1}{4}\sin^3\alpha-\tfrac{5}{8}\sin\alpha\right)\sigma+\left(\tfrac{1}{8}\sin^4\alpha-\tfrac{9}{16}\sin^2\alpha+\tfrac{1}{4}\right)\sigma^2+\cdots\right]\right\}\\
V_r^*(\sigma,\alpha) \;&=\; \tfrac{\cos\alpha}{2\pi}\left\{\tfrac{1}{2}\log_e\frac{64}{\sigma^2}\left[\tfrac{3}{4}\sigma-\left(\tfrac{3}{8}\sin\alpha\right)\sigma^2+\cdots\right]\right.\\
&\qquad\left.-\left[\tfrac{2}{\sigma}+\sin\alpha-\left(\tfrac{1}{4}\sin^2\alpha-\tfrac{5}{8}\right)\sigma+\left(\tfrac{1}{8}\sin^3\alpha-\tfrac{11}{16}\sin\alpha\right)\sigma^2+\cdots\right]\right\}
\end{aligned}\right\}\quad[B3]$$

We are not concerned with investigating the conditions for convergence of these series, because we will be using only the given leading terms, as approximations. The limitations necessary to assure accuracy of the approximations, for our purposes, are discussed elsewhere.

APPENDIX C

SERIES EXPANSION OF THE INFLUENCE FUNCTIONS FOR A DISTANT RING VORTEX

For the problem of evaluating the stream function and velocity components induced at a point by a uniform distribution of ring vortices on a semi-infinite cylinder, it is convenient to have series expansions of the influence functions for an isolated ring vortex (Appendix B, Equations [B1]) which are valid at points sufficiently far removed from the ring vortex in question. It is necessary to consider only expansions of the Ψ^* and V_x^* functions, since there is a convenient exact solution which may be used to find the radial velocity induced by a semi-infinite uniform vortex cylinder; namely,

$$V_r(\bar{x},\bar{r}) = -\sqrt{\frac{r}{\bar{r}}}\,\frac{2}{k}\left[\left(1 - \frac{k^2}{2}\right)K(k) - E(k)\right]$$

where

$$k = \frac{2\sqrt{\bar{r}\,r}}{\sqrt{(x - \bar{x})^2 + (\bar{r} + r)^2}}$$

and (x, r) are the coordinates of a point on the leading edge of the semi-infinite cylinder, and $(\bar{x}, \bar{r})$ are the coordinates of the point where the radial velocity is measured. This formula is given by Reference 23, but with an error, presumably typographical.

Introducing the notation:

$$a \equiv 4r\bar{r}$$

$$b \equiv \bar{r} + r$$

$$c \equiv \bar{r} - r$$

$$\Delta x \equiv x - \bar{x}$$

Equations [B1] can be written

$$\left.\begin{aligned} \Psi^*(\Delta x) &= \frac{\sqrt{a}}{k}\left[\left(1-\frac{k^2}{2}\right)K(k) - E(k)\right] \\ V_x^*(\Delta x) &= \frac{1}{\sqrt{(\Delta x)^2+b^2}}\left[K(k) - \left(1+\frac{c(b-c)}{(\Delta x)^2+c^2}\right)E(k)\right] \end{aligned}\right\} \quad [C1]$$

where

$$k^2 = \frac{a}{(\Delta x)^2}\,\frac{1}{1+\left(\frac{b}{\Delta x}\right)^2}$$

Appropriate series expansions of the complete elliptic integrals are given by Pierce (Reference 18) as follows:

$$K(k) = \frac{\pi}{2}\left[1+\left(\frac{1}{2}\right)^2 k^2 + \left(\frac{1\cdot 3}{2\cdot 4}\right)^2 k^4 + \left(\frac{1\cdot 3\cdot 5}{2\cdot 4\cdot 6}\right)^2 k^6 + \ldots\right]$$

$$E(k) = \frac{\pi}{2}\left[1-\left(\frac{1}{2}\right)^2 k^2 - \left(\frac{1\cdot 3}{2\cdot 4}\right)^2 \frac{k^4}{3} - \left(\frac{1\cdot 3\cdot 5}{2\cdot 4\cdot 6}\right)^2 \frac{k^6}{5} - \ldots\right]$$

With the further expansions

$$k^2 = \frac{a}{(\Delta x)^2}\left[1-\left(\frac{b}{\Delta x}\right)^2+\left(\frac{b}{\Delta x}\right)^4 - \left(\frac{b}{\Delta x}\right)^6 + \ldots\right]$$

$$\frac{1}{\sqrt{(\Delta x)^2+b^2}} = (\Delta x)^{-1} - \frac{b^2}{2}(\Delta x)^{-3} + \frac{3b^4}{8}(\Delta x)^{-5} - \frac{5b^6}{16}(\Delta x)^{-7} + \ldots$$

$$\frac{c(b-c)}{(\Delta x)^2+c^2} = \frac{c(b-c)}{(\Delta x)^2}\left[1-\left(\frac{c}{\Delta x}\right)^2 + \left(\frac{c}{\Delta x}\right)^4 - \left(\frac{c}{\Delta x}\right)^6 \ldots\right]$$

one is again in position, simply by multiplying together the various factors and collecting like terms, to obtain the results:

$$\left.\begin{aligned}
\Psi^*(\Delta x) &= \frac{\pi}{2}\left[\frac{a^2}{16}(\Delta x)^{-3} - \left(\frac{3a^2b^2}{32} - \frac{a^3}{128}\right)(\Delta x)^{-5} + \cdots\right] \\
V_x^*(\Delta x) &= \frac{\pi}{2}\left[\left(\frac{a}{2} + c^2 - bc\right)(\Delta x)^{-3}\right. \\
&\quad \left. - \left(\frac{3ab^2}{4} - \frac{3a^2}{16} - \frac{abc}{4} + c^4 - bc^3 + \frac{b^2c^2}{2} - \frac{b^3c}{2}\right)(\Delta x)^{-5} + \cdots\right]
\end{aligned}\right\} \text{[C2]}$$

The given leading terms of these series will provide an adequate approximation when Δx is sufficiently large. When r and $\bar{r}$ are roughly equal (as is always the case in the present investigation), an approximation within about one percent is afforded by the given leading terms, provided $\Delta x/b \geq 4$. The fractional error tends to zero when $\Delta x/b$ increases without limit.

APPENDIX D

NUMERICAL EVALUATION OF THE INFLUENCE FUNCTIONS

In those cases in which an influence coefficient was determined by a numerical integration along a definite path, it was necessary to obtain numerical values of the influence functions (ψ^*, V_x^*, and V_r^*) at discrete points along this path. This was done by direct application of the formulas given in Appendix B, Equations [B1]. Values of the complete elliptic integrals appearing in those formulas were obtained as follows:

1. The squared modulus of the elliptic integrals was calculated:

$$k^2 = \frac{4\bar{r}r}{(x-\bar{x})^2 + (\bar{r}+r)^2} = 1 - k'^2$$

2a. If $k^2 \leq \frac{1}{2}$, the following series expansions given by Pierce (Reference 18) were applied:

$$K(k) = \frac{\pi}{2}\left\{1 + \sum_{n=1}^{\infty}\left[\left(\frac{1\cdot3\cdot5\cdot\cdots(2n-1)}{2\cdot4\cdot6\cdot\cdots(2n)}\right)^2 k^{2n}\right]\right\}$$

$$E(k) = \frac{\pi}{2}\left\{1 - \sum_{n=1}^{\infty}\left[\left(\frac{1\cdot3\cdot5\cdot\cdots(2n-1)}{2\cdot4\cdot6\cdot\cdots(2n)}\right)^2 \frac{k^{2n}}{2n-1}\right]\right\}$$

The summations were terminated at a value of n for which neither summand was greater than 10^{-7}.

2b. If $k^2 > \frac{1}{2}$, the following series expansions given by Curtis and Sparks (Reference 22) were applied:

$$K(k) = \frac{1}{2}\log_e\left(\frac{16}{k'^2}\right)\left\{1 + \sum_{n=1}^{\infty}\left[\left(\frac{1\cdot3\cdot5\cdot\cdots(2n-1)}{2\cdot4\cdot6\cdot\cdots(2n)}\right) k'^{2n}\right]\right\}$$

$$- \sum_{n=1}^{\infty}\left[\left(\frac{1\cdot3\cdot5\cdot\cdots(2n-1)}{2\cdot4\cdot6\cdot\cdots(2n)}\right)^2 \left(\frac{2}{1\cdot2} + \frac{2}{3\cdot4} + \cdots + \frac{2}{(2n-1)(2n)}\right) k'^{2n}\right.$$

$$E(k) = \frac{1}{2} \log_e \left(\frac{16}{k'^2}\right) \sum_{n=1}^{\infty} \left[\left(\frac{1\cdot3\cdot5\cdot\ \cdot\ \cdot\ (2n-3)}{2\cdot4\cdot6\cdot\ \cdot\ \cdot\ (2n-2)}\right)^2 \quad \frac{2n-1}{2n} \quad k'^{2n}\right] + 1$$

$$- \sum_{n=1}^{\infty} \left[\left(\frac{1\cdot3\cdot5\cdot\ \cdot\ \cdot(2n-3)}{2\cdot4\cdot6\cdot\ \cdot\ \cdot(2n-2)}\right)^2 \frac{2n-1}{2n} \quad \left(\frac{2}{1.2} + \frac{2}{3.4} + \cdot\ \cdot\ \cdot + \right.\right.$$

$$\left.\left.\frac{2}{(2n-3)(2n-2)} + \frac{1}{(2n-1)(2n)}\right) k'^{2n}\right]$$

The summations were terminated at a value of n for which none of the four summands was greater than 10^{-7}.

Values of the complete elliptic integrals computed in this manner were found to agree, to five significant figures, with the values given by Dwight's "Mathematical Tables," over a range of values of the squared modulus, $0 < k^2 < 0.9999998$.

(Note: The series given in paragraphs 2a and 2b are equivalent to those given in Appendix B and Appendix C, respectively.)

APPENDIX E

DERIVATION OF THE STREAM FUNCTION FOR AN ISOLATED VORTEX RING

The following derivation is adapted from one given by Lamb, Reference 6. Lamb's derivation was intermingled with a more general discussion of vortex motion. For this reason it was felt that a concise review of the essential steps might be helpful.

Consider the motion of a fluid of infinite extent due to a vortex tube of uniform vorticity, in the form of a torus centered on the x-axis. Let us seek to express the velocity at any point as the curl of a vector function $\vec{S}(x,y,z)$

$$\vec{V} = \nabla \times \vec{S}$$

Continuity will be satisfied, since $\nabla \cdot \vec{V} = \nabla \cdot (\nabla \times \vec{S}) = 0$, by definition. Taking the curl of both sides of this equation

$$\nabla \times \vec{V} = \nabla \times (\nabla \times \vec{S})$$
$$= \nabla(\nabla \cdot \vec{S}) - \nabla^2 \vec{S}$$

Since only the curl of $\vec{S}$ has significance, we may add to, or subtract from $\vec{S}$ any irrotational vector function we please. In particular, we may arrange that $\nabla \cdot \vec{S}$ = a constant, and so write

$$\nabla^2 \vec{S} = - \nabla \times \vec{V}$$

In the present case, we will have $\nabla^2 \vec{S} = 0$, except within the torus, where $\nabla^2 \vec{S}$ will be at every point a vector of constant magnitude, and in the direction normal to the x-axis, and the radius, and forming a right-hand set with them. An analogous problem occurs in the Newtonian potential theory, where the scalar equation

$$\nabla^2 \phi = - 4\pi\kappa$$

applies at points occupied by matter of density κ, and $\nabla^2\phi = 0$ elsewhere. It is well known that a solution is

$$\phi(\bar{x},\bar{y},\bar{z}) = \iiint \frac{\kappa(x,y,z)}{\rho}\, dx\, dy\, dz$$

where ρ is the distance between the points $(\bar{x}, \bar{y}, \bar{z})$ and (x, y, z), and the integral is taken over all space occupied by matter. By analogy, we have a solution

$$\vec{S} = \frac{1}{4\pi} \iiint \frac{\nabla \times \vec{V}}{\rho}\, dx\, dy\, dz$$

where the integral is taken over the volume of the torus. If we let the cross-sectional area of the torus tend to zero, while keeping the product of the area and the curl equal to a constant, say $\vec{\Gamma}$, we have

$$\vec{S}(\bar{x},\bar{r},\bar{\theta}) = \frac{1}{4\pi} \int_0^{2\pi} \frac{\vec{\Gamma}(x,r,\theta)\ r\, d\theta}{\rho}$$

The vector function $\vec{S}$ is related to the scalar function Ψ as explained below.

We have, by Stokes' theorem

$$\oint_\ell \vec{S} \cdot d\vec{\ell} = \iint_A (\nabla \times \vec{S}) \cdot d\vec{A} = \iint_A \vec{V} \cdot d\vec{A}$$

The right hand member is the flux across the area A. Choosing A to be the plane area enclosed by the circle $(\bar{x}, \bar{r})$, we have

$$\oint_\ell \vec{S} \cdot d\vec{\ell} = 2\pi \int_0^{\bar{r}} u\, y\, dy = 2\pi\ \Psi(\bar{x}, \bar{r})$$

since, by definition,

$$\Psi(\bar{x},\bar{r}) = \int_0^{\bar{r}} u(\bar{x},y)\, y\, dy$$

(See Equations [1'].)

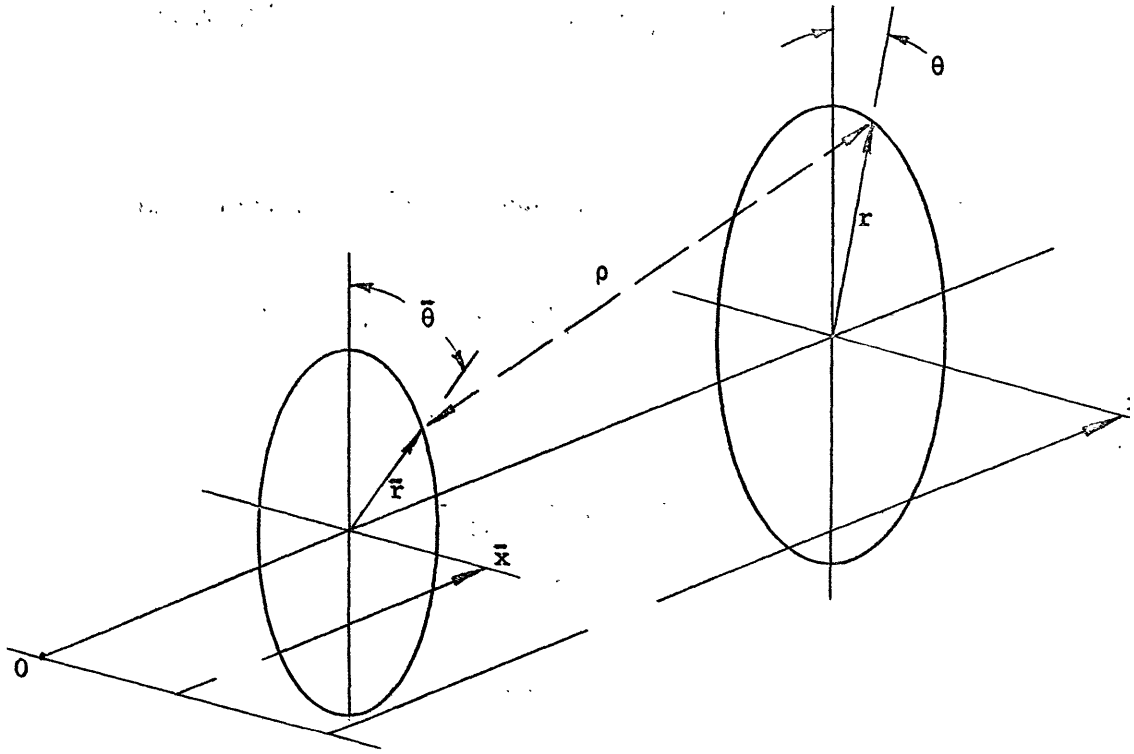

It is evident from symmetry that, since $\vec{\Gamma}$ is a vector of constant magnitude tangential to the circle (x,r), so, along a particular circle $(\bar{x},\bar{r})$, $\vec{S}$ will be of constant magnitude and tangential to this circle, in the same sense as $\vec{\Gamma}$. Hence, from the last equation

$$2\pi\, \Psi(\bar{x},\bar{r}) = 2\pi\, \bar{r}\, |\vec{S}|$$

Hence

$$\Psi(\bar{x},\bar{r}) = \frac{\Gamma}{4\pi}\, r\, \bar{r} \int_0^{2\pi} \frac{\cos\theta\, d\theta}{\rho}$$

where

$$\Gamma = |\vec{\Gamma}|$$

$$\theta' = \theta - \bar{\theta}$$

$$\rho = \left[(x-\bar{x})^2 + (r\cos\theta' - \bar{r})^2 + (r\sin\theta')^2\right]^{\frac{1}{2}}$$

Rearranging terms we obtain Equation [3] of the main text:

$$\Psi(\bar{x},\bar{r}) = \frac{\Gamma}{2\pi}\sqrt{r\,\bar{r}}\,\frac{2}{k}\left[\left(1 - \frac{k^2}{2}\right)K(k) - E(k)\right]$$

where

$$K(k) = \int_0^{\pi/2} \frac{d\alpha}{\sqrt{1 - k^2\sin^2\alpha}}$$

$$E(k) = \int_0^{\pi/2} \sqrt{1 - k^2\sin^2\alpha}\; d\alpha$$

$$k^2 = \frac{4r\bar{r}}{(x-\bar{x})^2 + (r+\bar{r})^2}$$

That is, K(k) and E(k) are the complete elliptic integrals, of the first and second kinds.

The Equation [5] was derived from a velocity field which is continuous and irrotational, except on the circle (x,r), and hence is necessarily a solution of Equation [2'].

REFERENCES

1. Sacks, A. H. and J. A. Burnell. Ducted Propellers; A Critical Review of the State of the Art. In Progress in Aeronautical Sciences, Vol. 3. N.Y., Pergamon Press [1962] p. 85-135

2. Krüger, W. On Wind Tunnel Tests and Computations Concerning the Problem of Shrouded Propellers. Wash., Feb 1949. 79 p. incl. illus. (National Aeronautics & Space Administration. TM 1202) (Translation of Germany. ZWB Deutsche Luftfahrtforschung FB 1949, 21 Jan 1944)

3. Küchemann, Dietrich and Johanna Weber. Aerodynamics of Propulsion. 1st ed. N.Y., McGraw-Hill, 1953. 340 p.

4. Glauert, H. The Elements of Aerofoil and Airscrew Theory. 2d. ed. Cambridge, Eng., Cambridge Univ. Press, 1948. 232 p. incl. illus.

5. Küchemann, Dietrich. Tables for the Stream Function and the Velocity Components of a Source-Ring and a Vortex-Ring. [London?] Nov 1946. 26 l. incl. illus. (Gt. Brit. Ministry of Supply. Rpt. & Translation 308) (Translation from Jahrbuch der deutsche Luftfahrtforschung. 1940, Sec. I, p. 547)

6. Lamb, Horace. Hydrodynamics. 6th ed. N.Y., Dover [1945, c1932] 738 p.

7. Morgan, William B. A Theory of the Ducted Propeller With a Finite Number of Blades. Berkeley, May 1961. 183 l. incl. illus. (California. Univ. Contract Nonr 222(30). Series 82, Issue 19)

8. Kriebel, A. R., A. H. Sacks and J. N. Nielsen. Theoretical Investigation of Dynamic Stability Derivatives of Ducted Propellers [Palo Alto, Calif.] Jan 1963. 120 l. illus. (VIDYA, Inc. Rpt. 167/C-FR-1. Contract NOw 62-0129-c)

9. Aerophysics Development Corp. Aerial Jeep Phase I Final Report, Vol. II. [Pacific Palisades, Calif.] 1 Dec 1957. (U.S. Army Contr. DA-44-177-TC-397, ADC Rpt. 520-3/R24/46)

10. Helmbold, Heinrich B. Range of Application of Shrouded Propellers. Wichita, Aug 1955. 13 1. incl. illus. (Wichita. Univ. Engineering Study 189)

11. Küchemann, Dietrich and Johanna Weber. The Flow Over Annular Aerofoils. [London ?] n.d. 34 1. illus. (Gt. Brit. Ministry of Supply. TIB T 3568. GDC 10/1133T) (Translation of Göttingen. Aerodynamische Versuchsanstalt. Br 42/A/15, Nov 1942 (Germany. ZWB Deutsche Luftfahrtforschung FB 1236/7))

12. Smith, A.M.O. and Jesse Pierce. Exact Solution of the Neumann Problem. Calculation of Non-Circulatory Plane and Axially Symmetric Flows About or Within Arbitrary Boundaries. El Segundo, Apr 1958. 106 1. incl. illus. (Douglas Aircraft Co. Rpt. ES-26988)

13. Weinig, Fritz. Aerodynamics of the Propeller. [Rev., Jul 1947] Dayton [1948] 501 1. illus. (AF F-TR-1157-ND) (Translation of Aerodynamik der Luftshraube. Berlin, Springer 1940)

14. Trefftz, E. Über die Konkraktion kreisformiger Flussigkeitsstrahlen. Zeitshrift für Mathematik and Physik (Leipzig), v. 64, 1916, p. 34-61.

15. Thwaites, Brian. On the Design of Contractions for Wind Tunnels. London, H.M.S.O., 1949. 8 p. incl. illus. (Gt. Brit. Aeronautical Research Council. R & M 2278. 9482)

16. Morgan, William B. and E. B. Caster. Prediction of the Aerodynamic Characteristics of Annular Airfoils. (David Taylor Model Basin. Rpt. 1830) (In preparation)

17. Vandrey, F. A Direct Iteration Method for the Calculation of the Velocity-Distribution of Bodies of Revolution and Symmetrical Profiles. Teddington, Eng., Aug 1951. 28 l. illus. (Gt. Brit. Admiralty Research Lab. R1/G/HY/12/2)

18. Pierce, B. O. A Short Table of Integrals. 3rd rev. ed. N.Y., Ginn and Co. [1929] 156 p.

19. C.R.C. Standard Mathematical Tables. 10th ed. Cleveland, Chemical Rubber Publishing Co. [c1956] 441 p.

20. Good, Sharon E. Matrix Inversion with Accompanying Solution of Linear Equations. [Wash] Nov 1962 (David Taylor Model Basin, LARC Computer Subroutine AM MAT1)

21. Jahnke, Eugene and Fritz Emde. Tables of Functions with Formulae and Curves. 4th ed. N.Y., Dover [1945] 304[76] p.

22. Curtis, Harvey L. and C. Matilda Sparks. Formulas, Tables and Curves for Computing the Mutual Inductance of Two Coaxial Circles [Wash, 1923-1924] (National Bureau of Standards. Scientific Paper 492. In its v. 19, p. 545-565)

23. Meyerhoff, L. and A. B. Finkelstein. On Theories of the Duct Shape for a Ducted Propeller. Brooklyn, Aug 1958. 79 l. incl. illus. (Brooklyn. Polytechnic Institute. PIBAL Rpt. 484 Contract Nonr 839 (07))

Table 1 - Data From a Twenty-Iterative-Cycle Calculation for a Cylindrical Shroud. $\ell = 0.2$, $\bar{r}_N = 1.0$, N = 24, M = 41, U = 0

(a) Input Data

i	x_i	r_i	F_i
1	0.00000000	1.00000000	
2	0.00500000	1.00000000	
3	0.01000000	1.00000000	
4	0.02000000	1.00000000	
5	0.03000000	1.00000000	
6	0.04000000	1.00000000	
7	0.05000000	1.00000000	
8	0.06000000	1.00000000	
9	0.07000000	1.00000000	
10	0.08000000	1.00000000	
11	0.09000000	1.00000000	
12	0.10000000	1.00000000	
13	0.11000000	1.00000000	
14	0.12000000	1.00000000	
15	0.13000000	1.00000000	
16	0.14000000	1.00000000	
17	0.15000000	1.00000000	
18	0.16000000	1.00000000	
19	0.17000000	1.00000000	
20	0.18000000	1.00000000	
21	0.19000000	1.00000000	
22	0.19500000	1.00000000	
23	0.19750000	1.00000000	
24	0.19937500	1.00000000	
25	0.20062500	1.00000000	1.00000000
26	0.20250000	1.00000000	1.00000000
27	0.20500000	1.00000000	1.00000000
28	0.21000000	1.00000000	1.00000000
29	0.22000000	1.00000000	1.00000000
30	0.23000000	1.00000000	1.00000000
31	0.24000000	1.00000000	1.00000000
32	0.26000000	1.00000000	1.00000000
33	0.28000000	1.00000000	1.00000000
34	0.30000000	1.00000000	1.00000000
35	0.32000000	1.00000000	1.00000000
36	0.34000000	1.00000000	1.00000000
37	0.36000000	1.00000000	1.00000000
38	0.40000000	1.00000000	1.00000000
39	0.45000000	1.00000000	1.00000000
40	0.50000000	1.00000000	1.00000000
41	0.60000000	1.00000000	1.00000000
42	0.70000000	1.00000000	1.00000000
43	0.80000000	1.00000000	1.00000000
44	0.90000000	1.00000000	1.00000000
45	1.00000000	1.00000000	1.00000000
46	1.15000000	1.00000000	1.00000000
47	1.30000000	1.00000000	1.00000000
48	1.45000000	1.00000000	1.00000000
49	1.60000000	1.00000000	1.00000000
50	1.75000000	1.00000000	1.00000000
51	1.90000000	1.00000000	1.00000000
52	2.05000000	1.00000000	1.00000000
53	2.20000000	1.00000000	1.00000000
54	2.35000000	1.00000000	1.00000000
55	2.50000000	1.00000000	1.00000000
56	2.65000000	1.00000000	1.00000000
57	2.80000000	1.00000000	1.00000000
58	2.95000000	1.00000000	1.00000000
59	3.10000000	1.00000000	1.00000000
60	3.25000000	1.00000000	1.00000000
61	3.40000000	1.00000000	1.00000000
62	3.55000000	1.00000000	1.00000000
63	3.70000000	1.00000000	1.00000000
64	3.85000000	1.00000000	1.00000000
65	4.00000000	1.00000000	1.00000000

Table 1 (Continued)

(b) First-Cycle Output

i	$\bar{\gamma}_i$	r_i	F_i	$\gamma(\bar{x}_i)V(\bar{x}_i)$	$V(\bar{x}_i)$
1	1.235850	1.000000			0.500000
2	1.226512	1.000000			0.500000
3	0.833518	1.000000			0.500000
4	0.622596	1.000000			0.500000
5	0.507951	1.000000			0.500000
6	0.452613	1.000000			0.500000
7	0.398675	1.000000			0.500000
8	0.378230	1.000000			0.500000
9	0.340082	1.000000			0.500000
10	0.333826	1.000000			0.500000
11	0.302848	1.000000			0.500000
12	0.302252	1.000000			0.500000
13	0.277512	1.000000			0.500000
14	0.277224	1.000000			0.500000
15	0.257619	1.000000			0.500000
16	0.258798	1.000000			0.500000
17	0.241581	1.000000			0.500000
18	0.243413	1.000000			0.500000
19	0.224643	1.000000			0.500000
20	0.229317	1.000000			0.500000
21	0.205870	1.000000			0.500000
22	0.218032	1.000000			0.500000
23	0.191811	1.000000			0.500000
24	0.197717	1.000000		0.088135	0.500000
25	0.197717	1.000000	0.998999	0.088241	0.500059
26	0.197717	0.999972	0.997498	0.088402	0.500121
27	0.197717	0.999938	0.995436	0.088674	0.500313
28	0.197717	0.999849	0.991471	0.089192	0.500732
29	0.197717	0.999639	0.984182	0.089818	0.501439
30	0.197717	0.999389	0.977693	0.090380	0.502234
31	0.197717	0.999109	0.971993	0.091122	0.503582
32	0.197717	0.998485	0.962257	0.091966	0.505554
33	0.197717	0.997815	0.954089	0.092689	0.507641
34	0.197717	0.997115	0.947131	0.093323	0.509787
35	0.197717	0.996393	0.941037	0.093894	0.512001
36	0.197717	0.995661	0.935577	0.094415	0.514190
37	0.197717	0.994926	0.930626	0.095136	0.517492
38	0.197717	0.993453	0.921697	0.096118	0.522323
39	0.197717	0.991628	0.911688	0.097125	0.527480
40	0.197717	0.989844	0.902597	0.098534	0.534712
41	0.197717	0.986402	0.886103	0.100289	0.543417
42	0.197717	0.983135	0.871244	0.101925	0.551068
43	0.197717	0.980100	0.857835	0.103450	0.557800
44	0.197717	0.977305	0.845738	0.104863	0.563723
45	0.197717	0.974771	0.834902	0.106476	0.570135
46	0.197717	0.971599	0.820675	0.108199	0.576630
47	0.197717	0.968472	0.808485	0.109713	0.582043
48	0.197717	0.965954	0.798095	0.111036	0.586621
49	0.197717	0.963785	0.789224	0.112194	0.590489
50	0.197717	0.961925	0.781617	0.113208	0.593759
51	0.197717	0.960325	0.775059	0.114101	0.596560
52	0.197717	0.958924	0.769393	0.114882	0.599030
53	0.197717	0.957700	0.764478	0.115573	0.601130
54	0.197717	0.956642	0.760172	0.116188	0.602958
55	0.197717	0.955714	0.756396	0.116730	0.604557
56	0.197717	0.954895	0.753082	0.117213	0.605973
57	0.197717	0.954175	0.750145	0.117646	0.607199
58	0.197717	0.953533	0.747538	0.118032	0.608320
59	0.197717	0.952957	0.745225	0.118377	0.609299
60	0.197717	0.952445	0.743152	0.118691	0.610184
61	0.197717	0.951994	0.741285	0.118974	0.610936
62	0.197717	0.951584	0.739616	0.119228	0.611674
63	0.197717	0.951204	0.738107	0.119461	0.612313
64	0.197717	0.950871	0.736732	0.119673	0.612880
65	0.197717	0.950871	0.736732		

Table 1 (Continued)
(c) Second-Cycle Output

i	$\bar{\gamma}_i$	r_i	F_i	$\gamma(\bar{s}_i)V(\bar{s}_i)$	$\Psi(\bar{s}_i)$
1	1.269428	1.000000			0.500000
2	1.246234	1.000000			0.500000
3	0.869734	1.000000			0.500000
4	0.631502	1.000000			0.500000
5	0.530308	1.000000			0.500000
6	0.459863	1.000000			0.500000
7	0.419596	1.000000			0.500000
8	0.383804	1.000000			0.500000
9	0.359966	1.000000			0.500000
10	0.339399	1.000000			0.500000
11	0.321057	1.000000			0.500000
12	0.308926	1.000000			0.500000
13	0.295141	1.000000			0.500000
14	0.285924	1.000000			0.500000
15	0.275365	1.000000			0.500000
16	0.268966	1.000000			0.500000
17	0.259780	1.000000			0.500000
18	0.252370	1.000000			0.500000
19	0.248639	1.000000			0.500000
20	0.239475	1.000000			0.500000
21	0.232638	1.000000			0.500000
22	0.232518	1.000000			0.500000
23	0.226330	1.000000			0.500000
24	0.222702	1.000000		0.089219	0.500000
25	0.222479	1.000000	0.996423	0.089443	0.499991
26	0.222144	0.999968	0.991058	0.089939	0.500033
27	0.221685	0.999921	0.984923	0.090215	0.500086
28	0.220802	0.999807	0.977599	0.090622	0.500212
29	0.219179	0.999528	0.966793	0.090773	0.500454
30	0.217734	0.999187	0.958691	0.090950	0.500761
31	0.216464	0.998800	0.950679	0.091399	0.501266
32	0.214296	0.997939	0.936522	0.091722	0.502023
33	0.212477	0.997015	0.925474	0.091997	0.502798
34	0.210928	0.996060	0.916032	0.092247	0.503577
35	0.209570	0.995084	0.907673	0.092487	0.504343
36	0.208355	0.994104	0.900252	0.092684	0.505089
37	0.207252	0.993134	0.893734	0.092943	0.506130
38	0.205263	0.991235	0.882393	0.093227	0.507504
39	0.203034	0.988940	0.870235	0.093457	0.508750
40	0.201010	0.986838	0.859977	0.093638	0.510020
41	0.197337	0.983025	0.842722	0.093760	0.510662
42	0.194027	0.979713	0.828173	0.093728	0.510365
43	0.191041	0.976901	0.816297	0.093557	0.509353
44	0.188347	0.974530	0.806723	0.093279	0.507798
45	0.185934	0.972552	0.799416	0.092769	0.505482
46	0.182766	0.970160	0.791294	0.092111	0.502203
47	0.180051	0.968320	0.785350	0.091392	0.498743
48	0.177737	0.966923	0.781372	0.090662	0.495272
49	0.175761	0.965871	0.778825	0.089945	0.491910
50	0.174067	0.965100	0.777333	0.089254	0.488728
51	0.172607	0.964548	0.776590	0.088603	0.485751
52	0.171345	0.964147	0.776336	0.088004	0.482990
53	0.170250	0.963872	0.776430	0.087446	0.480450
54	0.169291	0.963710	0.776791	0.086930	0.478128
55	0.168451	0.963622	0.777316	0.086459	0.476013
56	0.167712	0.963582	0.777934	0.086028	0.474119
57	0.167058	0.963589	0.778590	0.085638	0.472369
58	0.166478	0.963624	0.779240	0.085287	0.470805
59	0.165963	0.963665	0.779849	0.084974	0.469414
60	0.165501	0.963714	0.780417	0.084688	0.468168
61	0.165085	0.963772	0.780924	0.084437	0.467070
62	0.164714	0.963812	0.781280	0.084228	0.466123
63	0.164377	0.963824	0.781353	0.084076	0.465316
64	0.164071	0.963786	0.781495	0.083955,	0.464813
65	0.164071	0.963786	0.781495		

Table 1 (Continued)
(d) Third-Cycle Output

i	$\bar{\gamma}_i$	r_i	F_i	$\gamma(\bar{s}_i)V(\bar{s}_i)$	$\gamma(\bar{s}_i)$
1	1.266501	1.000000			0.500000
2	1.254028	1.000000			0.500000
3	0.860192	1.000000			0.500000
4	0.634064	1.000000			0.500000
5	0.530733	1.000000			0.500000
6	0.456591	1.000000			0.500000
7	0.421703	1.000000			0.500000
8	0.381936	1.000000			0.500000
9	0.361582	1.000000			0.500000
10	0.336685	1.000000			0.500000
11	0.323336	1.000000			0.500000
12	0.308016	1.000000			0.500000
13	0.296127	1.000000			0.500000
14	0.286836	1.000000			0.500000
15	0.274256	1.000000			0.500000
16	0.273028	1.000000			0.500000
17	0.255299	1.000000			0.500000
18	0.258411	1.000000			0.500000
19	0.244207	1.000000			0.500000
20	0.246893	1.000000			0.500000
21	0.231124	1.000000			0.500000
22	0.238464	1.000000			0.500000
23	0.228856	1.000000			0.500000
24	0.228698	1.000000		0.090103	0.500000
25	0.227880	1.000000	D.996765	0.089857	0.500002
26	0.226653	0.999969	D.991913	0.090137	0.499934
27	0.225250	0.999926	D.984147	0.090269	0.499975
28	0.223575	0.999809	D.974979	0.090466	0.500028
29	0.221103	0.999504	D.962748	0.090484	0.500114
30	0.219250	0.999124	D.953087	0.090647	0.500266
31	0.217418	0.998688	D.943028	0.091084	0.500478
32	0.214181	0.997722	D.925195	0.091334	0.500827
33	0.211654	0.996676	D.911427	0.091585	0.501219
34	0.209494	0.995587	D.899716	0.091801	0.501636
35	0.207583	0.994480	D.889446	0.092004	0.502019
36	0.205885	0.993371	D.880332	0.092185	0.502419
37	0.204395	0.992270	D.872578	0.092367	0.503017
38	0.201801	0.990134	D.859650	0.092576	0.503759
39	0.199021	0.987608	D.845919	0.092764	0.504486
40	0.196675	0.985279	D.835114	0.092782	0.505327
41	0.192728	0.981202	D.818114	0.092838	0.505868
42	0.189401	0.977791	D.803883	0.092813	0.505973
43	0.186685	0.974984	D.792570	0.092773	0.505874
44	0.184496	0.972664	D.783438	0.092776	0.505686
45	0.182825	0.970749	D.776226	0.092809	0.505461
46	0.180967	0.968445	D.767479	0.092973	0.505205
47	0.179608	0.966669	D.760141	0.093184	0.505082
48	0.178698	0.965284	D.754204	0.093458	0.505147
49	0.178116	0.964176	D.749268	0.093779	0.505444
50	0.177774	0.963287	D.745097	0.094128	0.505892
51	0.177604	0.962568	D.741498	0.094495	0.506496
52	0.177546	0.961961	D.738303	0.094874	0.507191
53	0.177568	0.961456	D.735444	0.095250	0.507951
54	0.177650	0.961036	D.732906	0.095615	0.508808
55	0.177770	0.960678	D.730620	0.095972	0.509651
56	0.177912	0.960364	D.728528	0.096314	0.510526
57	0.178062	0.960096	D.726626	0.096635	0.511371
58	0.178210	0.959865	D.724891	0.096935	0.512189
59	0.178350	0.959650	D.723292	0.097215	0.512965
60	0.178480	0.959460	D.721832	0.097468	0.513678
61	0.178596	0.959300	D.720524	0.097689	0.514316
62	0.178677	0.959147	D.719320	0.097876	0.514873
63	0.178694	0.958997	D.718118	0.098057	0.515319
64	0.178726	0.958824	D.716949	0.098218	0.515708
65	0.178726	0.958824	D.716949		

Table 1 (Continued)
(e) Fourth-Cycle Output

i	$\bar{\gamma}_i$	r_i	F_i	$\gamma(\bar{s}_i)V(\bar{s}_i)$	$\Psi(\bar{s}_i)$
1	1.271917	1.000000			0.500000
2	1.256058	1.000000			0.500000
3	0.868949	1.000000			0.500000
4	0.634431	1.000000			0.500000
5	0.531479	1.000000			0.500000
6	0.462507	1.000000			0.500000
7	0.421748	1.000000			0.500000
8	0.384453	1.000000			0.500000
9	0.362553	1.000000			0.500000
10	0.341738	1.000000			0.500000
11	0.323672	1.000000			0.500000
12	0.310633	1.000000			0.500000
13	0.297019	1.000000			0.500000
14	0.290412	1.000000			0.500000
15	0.276336	1.000000			0.500000
16	0.273387	1.000000			0.500000
17	0.259625	1.000000			0.500000
18	0.261688	1.000000			0.500000
19	0.245839	1.000000			0.500000
20	0.251166	1.000000			0.500000
21	0.233806	1.000000			0.500000
22	0.243518	1.000000			0.500000
23	0.229782	1.000000			0.500000
24	0.234388	1.000000		0.091112	0.500000
25	0.233629	1.000000	0.997240	0.090902	0.499994
26	0.232492	0.999973	0.993101	0.090981	0.499977
27	0.230672	0.999935	0.986846	0.090794	0.499962
28	0.229523	0.999822	0.978536	0.090908	0.499963
29	0.225656	0.999518	0.965327	0.090864	0.499955
30	0.223392	0.999133	0.954610	0.090964	0.499990
31	0.221034	0.998690	0.943433	0.091263	0.500002
32	0.216854	0.997709	0.924031	0.091296	0.500080
33	0.213627	0.996696	0.909034	0.091420	0.500163
34	0.210882	0.995518	0.896102	0.091523	0.500252
35	0.208475	0.994380	0.884925	0.091603	0.500351
36	0.206339	0.993237	0.875097	0.091695	0.500459
37	0.204521	0.992101	0.866754	0.091786	0.500612
38	0.201491	0.989903	0.853150	0.091856	0.500809
39	0.198273	0.987312	0.839009	0.091935	0.500987
40	0.195740	0.984936	0.828282	0.091834	0.501160
41	0.191756	0.980847	0.812182	0.091777	0.501011
42	0.188420	0.977533	0.799102	0.091611	0.500579
43	0.185769	0.974890	0.789167	0.091436	0.500003
44	0.183628	0.972772	0.781378	0.091294	0.499327
45	0.181938	0.971082	0.775415	0.091092	0.498439
46	0.179888	0.969144	0.768486	0.090891	0.497248
47	0.178168	0.967761	0.762973	0.090656	0.496015
48	0.176776	0.966778	0.758849	0.090430	0.494775
49	0.175619	0.966066	0.755708	0.090206	0.493600
50	0.174642	0.965557	0.753334	0.089979	0.492468
51	0.173798	0.965205	0.751536	0.089754	0.491385
52	0.173049	0.964950	0.750150	0.089532	0.490354
53	0.172379	0.964782	0.749097	0.089311	0.489383
54	0.171784	0.964682	0.748340	0.089091	0.488465
55	0.171248	0.964627	0.747779	0.088884	0.487604
56	0.170758	0.964600	0.747350	0.088683	0.486795
57	0.170312	0.964604	0.747052	0.088490	0.486036
58	0.169906	0.964624	0.746842	0.088308	0.485353
59	0.169531	0.964639	0.746672	0.088140	0.484726
60	0.169188	0.964660	0.746535	0.087984	0.484159
61	0.168882	0.964694	0.746439	0.087841	0.483637
62	0.168600	0.964715	0.746321	0.087712	0.483184
63	0.168318	0.964719	0.746040	0.087615	0.482772
64	0.168044	0.964660	0.745738	0.087567	0.482555
65	0.168044	0.964660	0.745738		

Table 1 (Continued)
(f) Fifth-Cycle Output

i	$\bar{\gamma}_i$	r_i	F_i	$\gamma(\bar{s}_i)V(\bar{s}_i)$	$\Psi(\bar{s}_i)$
1	1.269060	1.000000			0.500000
2	1.263636	1.000000			0.500000
3	0.856072	1.000000			0.500000
4	0.643949	1.000000			0.500000
5	0.522249	1.000000			0.500000
6	0.469546	1.000000			0.500000
7	0.412426	1.000000			0.500000
8	0.392607	1.000000			0.500000
9	0.359942	1.000000			0.500000
10	0.344056	1.000000			0.500000
11	0.322808	1.000000			0.500000
12	0.310298	1.000000			0.500000
13	0.297629	1.000000			0.500000
14	0.287643	1.000000			0.500000
15	0.278381	1.000000			0.500000
16	0.272735	1.000000			0.500000
17	0.260087	1.000000			0.500000
18	0.259569	1.000000			0.500000
19	0.247389	1.000000			0.500000
20	0.249807	1.000000			0.500000
21	0.234399	1.000000			0.500000
22	0.241476	1.000000			0.500000
23	0.238547	1.000000			0.500000
24	0.234110	1.000000		0.091507	0.500000
25	0.233464	1.000000	0.998496	0.091229	0.500000
26	0.232494	0.999976	0.996239	0.091179	0.499982
27	0.231030	0.999945	0.991613	0.091047	0.499943
28	0.229085	0.999845	0.983635	0.091166	0.499901
29	0.225992	0.999552	0.970279	0.091033	0.499891
30	0.223483	0.999174	0.959335	0.091060	0.499862
31	0.220867	0.998742	0.947904	0.091243	0.499804
32	0.216324	0.997774	0.928225	0.091154	0.499801
33	0.212814	0.996701	0.912886	0.091188	0.499807
34	0.209786	0.995582	0.899572	0.091209	0.499805
35	0.207169	0.994438	0.888072	0.091228	0.499840
36	0.204869	0.993287	0.877886	0.091285	0.499857
37	0.202915	0.992142	0.869197	0.091343	0.499923
38	0.199731	0.989909	0.855091	0.091392	0.500060
39	0.196420	0.987266	0.840415	0.091498	0.500221
40	0.193909	0.984836	0.829330	0.091469	0.500474
41	0.190140	0.980667	0.812872	0.091552	0.500631
42	0.187077	0.977316	0.799559	0.091536	0.500700
43	0.184751	0.974661	0.789465	0.091535	0.500705
44	0.182928	0.972548	0.781430	0.091577	0.500706
45	0.181532	0.970855	0.775108	0.091617	0.500694
46	0.179910	0.968920	0.767483	0.091725	0.500691
47	0.178619	0.967540	0.761169	0.091812	0.500678
48	0.177654	0.966551	0.756164	0.091918	0.500737
49	0.176919	0.965804	0.752042	0.092042	0.500891
50	0.176363	0.965241	0.748590	0.092174	0.501074
51	0.175942	0.964822	0.745661	0.092314	0.501310
52	0.175617	0.964486	0.743115	0.092460	0.501585
53	0.175371	0.964223	0.740882	0.092609	0.501899
54	0.175194	0.964019	0.738933	0.092755	0.502234
55	0.175062	0.963850	0.737202	0.092901	0.502613
56	0.174962	0.963702	0.735642	0.093042	0.502990
57	0.174892	0.963588	0.734245	0.093178	0.503350
58	0.174843	0.963492	0.732977	0.093309	0.503721
59	0.174803	0.963392	0.731791	0.093437	0.504073
60	0.174771	0.963301	0.730724	0.093548	0.504419
61	0.174748	0.963230	0.729778	0.093651	0.504733
62	0.174721	0.963159	0.728902	0.093734	0.504993
63	0.174655	0.963086	0.728006	0.093820	0.505224
64	0.174584	0.962954	0.727081	0.093917	0.505445
65	0.174584	0.962954	0.727081		

Table 1 (Continued)
(g) Sixth-Cycle Output

i	$\bar{Y}_i$	r_i	R_i	$\gamma(\mathbb{E}_i)V(\mathbb{E}_i)$	$V(\mathbb{E}_i)$
1	1.271653	1.000000			0.500000
2	1.261810	1.000000			0.500000
3	0.860971	1.000000			0.500000
4	0.640558	1.000000			0.500000
5	0.525443	1.000000			0.500000
6	0.468872	1.000000			0.500000
7	0.416131	1.000000			0.500000
8	0.389889	1.000000			0.500000
9	0.358224	1.000000			0.500000
10	0.343261	1.000000			0.500000
11	0.322768	1.000000			0.500000
12	0.312304	1.000000			0.500000
13	0.295905	1.000000			0.500000
14	0.291081	1.000000			0.500000
15	0.276124	1.000000			0.500000
16	0.273313	1.000000			0.500000
17	0.262290	1.000000			0.500000
18	0.258825	1.000000			0.500000
19	0.251251	1.000000			0.500000
20	0.244392	1.000000			0.500000
21	0.241633	1.000000			0.500000
22	0.233672	1.000000			0.500000
23	0.240628	1.000000			0.500000
24	0.234083	1.000000		0.091708	0.500000
25	0.233731	1.000000	0.998900	0.091607	0.500005
26	0.233203	0.999975	0.997250	0.091543	0.499999
27	0.232120	0.999944	0.994622	0.091253	0.500009
28	0.230252	0.999844	0.988657	0.091324	0.499992
29	0.227126	0.999559	0.975544	0.091203	0.499971
30	0.224564	0.999190	0.964492	0.091197	0.499933
31	0.221888	0.998749	0.953223	0.091321	0.499893
32	0.217282	0.997816	0.933692	0.091213	0.499856
33	0.213691	0.996745	0.918148	0.091235	0.499818
34	0.210575	0.995648	0.904662	0.091226	0.499790
35	0.207883	0.994509	0.893055	0.091221	0.499782
36	0.205498	0.993361	0.882767	0.091247	0.499774
37	0.203465	0.992217	0.873951	0.091285	0.499772
38	0.200162	0.989981	0.859505	0.091313	0.499769
39	0.196727	0.987334	0.844450	0.091404	0.499795
40	0.194132	0.984896	0.833128	0.091350	0.499859
41	0.190280	0.980723	0.816602	0.091382	0.499799
42	0.187163	0.977408	0.803495	0.091303	0.499637
43	0.184801	0.974817	0.793747	0.091230	0.499409
44	0.182920	0.972772	0.786100	0.091186	0.499185
45	0.181440	0.971161	0.780186	0.091096	0.498862
46	0.179655	0.969366	0.773207	0.091030	0.498386
47	0.178177	0.968143	0.767585	0.090923	0.497885
48	0.177005	0.967320	0.763298	0.090824	0.497359
49	0.176040	0.966737	0.759880	0.090733	0.496875
50	0.175232	0.966327	0.757150	0.090634	0.496415
51	0.174547	0.966056	0.754964	0.090538	0.495965
52	0.173951	0.965862	0.753171	0.090441	0.495539
53	0.173428	0.965735	0.751708	0.090344	0.495132
54	0.172972	0.965663	0.750518	0.090248	0.494739
55	0.172567	0.965617	0.749505	0.090161	0.494375
56	0.172202	0.965586	0.748640	0.090074	0.494031
57	0.171874	0.965580	0.747944	0.089984	0.493717
58	0.171577	0.965587	0.747343	0.089904	0.493404
59	0.171300	0.965584	0.746781	0.089831	0.493133
60	0.171050	0.965583	0.746281	0.089763	0.492865
61	0.170829	0.965591	0.745858	0.089697	0.492654
62	0.170624	0.965586	0.745475	0.089634	0.492464
63	0.170414	0.965574	0.744975	0.089596	0.492284
64	0.170198	0.965485	0.744420	0.089598	0.492210
65	0.170198	0.965485	0.744420		

Table 1 (Continued)

(h) Seventh-Cycle Output

i	$\bar{\gamma}_j$	r_i	F_i	$\gamma(\bar{s}_i)V(\bar{s}_i)$	$\Psi(\bar{s}_i)$
1	1.271061	1.000000			0.500000
2	1.254481	1.000000			0.500000
3	0.866262	1.000000			0.500000
4	0.635018	1.000000			0.500000
5	0.530354	1.000000			0.500000
6	0.461876	1.000000			0.500000
7	0.422413	1.000000			0.500000
8	0.382045	1.000000			0.500000
9	0.364705	1.000000			0.500000
10	0.339105	1.000000			0.500000
11	0.324460	1.000000			0.500000
12	0.308764	1.000000			0.500000
13	0.300068	1.000000			0.500000
14	0.284999	1.000000			0.500000
15	0.281494	1.000000			0.500000
16	0.269821	1.000000			0.500000
17	0.265322	1.000000			0.500000
18	0.253623	1.000000			0.500000
19	0.253222	1.000000			0.500000
20	0.242353	1.000000			0.500000
21	0.240902	1.000000			0.500000
22	0.236942	1.000000			0.500000
23	0.232114	1.000000			0.500000
24	0.232609	1.000000		0.091379	0.500000
25	0.232353	1.000000	0.998683	0.091356	0.500000
26	0.231969	0.999971	0.996708	0.091438	0.500030
27	0.231358	0.999935	0.993788	0.091371	0.500029
28	0.229970	0.999836	0.987656	0.091525	0.500015
29	0.226920	0.999547	0.975060	0.091357	0.500053
30	0.224349	0.999174	0.964639	0.091300	0.500041
31	0.221728	0.998756	0.953791	0.091416	0.500038
32	0.217185	0.997806	0.934536	0.091300	0.500021
33	0.213569	0.996749	0.919129	0.091297	0.500014
34	0.210432	0.995641	0.905726	0.091276	0.500028
35	0.207732	0.994501	0.894086	0.091275	0.500023
36	0.205339	0.993354	0.883698	0.091304	0.500017
37	0.203288	0.992209	0.874765	0.091343	0.500032
38	0.199928	0.989965	0.860088	0.091364	0.500071
39	0.196426	0.987303	0.844797	0.091451	0.500120
40	0.193793	0.984880	0.833261	0.091423	0.500273
41	0.189949	0.980622	0.816384	0.091502	0.500343
42	0.186900	0.977290	0.803084	0.091474	0.500377
43	0.184632	0.974691	0.793214	0.091465	0.500395
44	0.182854	0.972639	0.785401	0.091496	0.500427
45	0.181478	0.971017	0.779278	0.091505	0.500478
46	0.179854	0.969211	0.771976	0.091564	0.500478
47	0.178547	0.967985	0.766016	0.091589	0.500504
48	0.177550	0.967154	0.761364	0.091627	0.500524
49	0.176755	0.966556	0.757541	0.091678	0.500602
50	0.176120	0.966123	0.754352	0.091732	0.500668
51	0.175611	0.965826	0.751676	0.091791	0.500762
52	0.175194	0.965597	0.749385	0.091853	0.500884
53	0.174854	0.965429	0.747409	0.091916	0.501023
54	0.174577	0.965310	0.745705	0.091975	0.501172
55	0.174341	0.965217	0.744202	0.092036	0.501322
56	0.174140	0.965138	0.742855	0.092097	0.501486
57	0.173978	0.965077	0.741679	0.092153	0.501650
58	0.173838	0.965033	0.740622	0.092209	0.501802
59	0.173708	0.964980	0.739634	0.092261	0.501962
60	0.173591	0.964934	0.738738	0.092310	0.502083
61	0.173493	0.964898	0.737944	0.092353	0.502232
62	0.173404	0.964851	0.737227	0.092385	0.502351
63	0.173288	0.964808	0.736448	0.092428	0.502428
64	0.173158	0.964687	0.735618	0.092493	0.502543
65	0.173158	0.964687	0.735618		

Table 1 (Continued)
(i) Eighth-Cycle Output

i	$\bar{\gamma}_i$	r_i	F_i	$\gamma(\bar{s}_i)V(\bar{s}_i)$	$\Psi(\bar{s}_i)$
1	1.272407	1.000000			0.500000
2	1.252357	1.000000			0.500000
3	0.870623	1.000000			0.500000
4	0.631619	1.000000			0.500000
5	0.535832	1.000000			0.500000
6	0.457771	1.000000			0.500000
7	0.425033	1.000000			0.500000
8	0.379323	1.000000			0.500000
9	0.371240	1.000000			0.500000
10	0.331458	1.000000			0.500000
11	0.331871	1.000000			0.500000
12	0.304666	1.000000			0.500000
13	0.303313	1.000000			0.500000
14	0.283145	1.000000			0.500000
15	0.284508	1.000000			0.500000
16	0.264419	1.000000			0.500000
17	0.270628	1.000000			0.500000
18	0.250191	1.000000			0.500000
19	0.258779	1.000000			0.500000
20	0.236930	1.000000			0.500000
21	0.249725	1.000000			0.500000
22	0.224583	1.000000			0.500000
23	0.247917	1.000000			0.500000
24	0.232633	1.000000		0.091013	0.500000
25	0.232327	1.000000	0.997384	0.091063	0.499995
26	0.231867	0.999973	0.993458	0.091396	0.499991
27	0.231188	0.999939	0.988986	0.091261	0.499980
28	0.229761	0.999844	0.983462	0.091363	0.499970
29	0.226831	0.999562	0.971168	0.091291	0.499942
30	0.224407	0.999192	0.960573	0.091282	0.499952
31	0.221883	0.998774	0.949926	0.091390	0.499930
32	0.217404	0.997832	0.931175	0.091269	0.499917
33	0.213819	0.996780	0.916003	0.091269	0.499897
34	0.210702	0.995681	0.902651	0.091259	0.499863
35	0.207994	0.994551	0.891040	0.091248	0.499833
36	0.205577	0.993411	0.880809	0.091247	0.499826
37	0.203499	0.992269	0.871991	0.091272	0.499807
38	0.200085	0.990032	0.857333	0.091271	0.499782
39	0.196528	0.987377	0.842051	0.091342	0.499769
40	0.193844	0.984913	0.830485	0.091294	0.499798
41	0.189918	0.980702	0.813632	0.091334	0.499711
42	0.186824	0.977397	0.800522	0.091263	0.499633
43	0.184528	0.974828	0.790899	0.091211	0.499527
44	0.182710	0.972810	0.783304	0.091199	0.499415
45	0.181286	0.971224	0.777375	0.091150	0.499280
46	0.179587	0.969483	0.770385	0.091130	0.499043
47	0.178200	0.968325	0.764782	0.091068	0.498852
48	0.177118	0.967560	0.760494	0.091018	0.498638
49	0.176229	0.967029	0.757016	0.090975	0.498431
50	0.175487	0.966666	0.754174	0.090928	0.498205
51	0.174865	0.966435	0.751858	0.090880	0.498022
52	0.174332	0.966271	0.749915	0.090839	0.497806
53	0.173872	0.966164	0.748278	0.090795	0.497642
54	0.173475	0.966099	0.746905	0.090754	0.497471
55	0.173126	0.966061	0.745722	0.090714	0.497302
56	0.172812	0.966030	0.744692	0.090677	0.497159
57	0.172539	0.966013	0.743819	0.090636	0.497020
58	0.172293	0.966020	0.743053	0.090602	0.496877
59	0.172063	0.966008	0.742343	0.090569	0.496764
60	0.171855	0.966001	0.741710	0.090538	0.496640
61	0.171670	0.965998	0.741153	0.090509	0.496561
62	0.171503	0.965978	0.740645	0.090477	0.496475
63	0.171322	0.965964	0.740048	0.090464	0.496382
64	0.171129	0.965861	0.739388	0.090489	0.496367
65	0.171129	0.965861	0.739388		

Table 1 (Continued)
(j) Ninth-Cycle Output

i	$\bar{\gamma}_i$	r_i	F_i	$\gamma(\bar{s}_i)V(\bar{s}_i)$	$\Psi(\bar{s}_i)$
1	1.270074	1.000000			0.500000
2	1.260353	1.000000			0.500000
3	0.860434	1.000000			0.500000
4	0.640344	1.000000			0.500000
5	0.525406	1.000000			0.500000
6	0.466176	1.000000			0.500000
7	0.416626	1.000000			0.500000
8	0.390584	1.000000			0.500000
9	0.355112	1.000000			0.500000
10	0.346906	1.000000			0.500000
11	0.317994	1.000000			0.500000
12	0.316176	1.000000			0.500000
13	0.291004	1.000000			0.500000
14	0.294754	1.000000			0.500000
15	0.273336	1.000000			0.500000
16	0.274944	1.000000			0.500000
17	0.258086	1.000000			0.500000
18	0.261792	1.000000			0.500000
19	0.245253	1.000000			0.500000
20	0.250829	1.000000			0.500000
21	0.233095	1.000000			0.500000
22	0.242606	1.000000			0.500000
23	0.229599	1.000000			0.500000
24	0.233399	1.000000		0.091545	0.500000
25	0.232788	1.000000	0.997828	0.091402	0.499997
26	0.231872	0.999972	0.994569	0.091493	0.500013
27	0.230828	0.999933	0.990671	0.091290	0.500029
28	0.229539	0.999883	0.985459	0.091385	0.500044
29	0.226670	0.999815	0.973563	0.091296	0.500057
30	0.224196	0.999736	0.962894	0.091312	0.500041
31	0.221711	0.999656	0.952051	0.091455	0.500079
32	0.217335	0.999548	0.933213	0.091364	0.500087
33	0.213794	0.999453	0.918017	0.091371	0.500074
34	0.210678	0.999363	0.904749	0.091341	0.500093
35	0.207968	0.999278	0.893266	0.091324	0.500073
36	0.205580	0.999202	0.883024	0.091342	0.500101
37	0.203522	0.999133	0.874116	0.091380	0.500125
38	0.200100	0.999027	0.859340	0.091380	0.500150
39	0.196534	0.998927	0.843924	0.091460	0.500154
40	0.193834	0.998852	0.832196	0.091429	0.500247
41	0.189901	0.998686	0.815117	0.091489	0.500278
42	0.186841	0.998586	0.801884	0.091447	0.500285
43	0.184595	0.998490	0.792155	0.091431	0.500318
44	0.182822	0.998425	0.784438	0.091455	0.500336
45	0.181438	0.998371	0.778384	0.091450	0.500364
46	0.179807	0.998301	0.771217	0.091488	0.500391
47	0.178499	0.998243	0.765425	0.091492	0.500426
48	0.177498	0.998196	0.760934	0.091507	0.500465
49	0.176687	0.998155	0.757240	0.091533	0.500493
50	0.176023	0.998121	0.754174	0.091555	0.500532
51	0.175483	0.998092	0.751629	0.091580	0.500572
52	0.175029	0.998068	0.749455	0.091608	0.500651
53	0.174647	0.998045	0.747594	0.091633	0.500708
54	0.174327	0.998028	0.746005	0.091657	0.500774
55	0.174051	0.998013	0.744597	0.091686	0.500822
56	0.173810	0.997999	0.743336	0.091715	0.500910
57	0.173606	0.997988	0.742247	0.091737	0.500992
58	0.173428	0.997979	0.741279	0.091762	0.501054
59	0.173262	0.997968	0.740380	0.091786	0.501126
60	0.173114	0.997961	0.739569	0.091806	0.501171
61	0.172984	0.997954	0.738842	0.091827	0.501234
62	0.172866	0.997947	0.738184	0.091835	0.501305
63	0.172726	0.997939	0.737466	0.091859	0.501304
64	0.172572	0.997928	0.736685	0.091911	0.501392
65	0.172572	0.997928	0.736685		

Table 1 (Continued)
(k) Tenth-Cycle Output

i	$\bar{Y}_i$	r_i	F_i	$\gamma(\bar{\varepsilon}_i)V(\bar{\varepsilon}_i)$	$\gamma(\bar{\varepsilon}_i)$
1	1.271933	1.000000			0.500000
2	1.255608	1.000000			0.500000
3	0.865692	1.000000			0.500000
4	0.635234	1.000000			0.500000
5	0.530549	1.000000			0.500000
6	0.462688	1.000000			0.500000
7	0.419093	1.000000			0.500000
8	0.387701	1.000000			0.500000
9	0.359217	1.000000			0.500000
10	0.342057	1.000000			0.500000
11	0.324140	1.000000			0.500000
12	0.308984	1.000000			0.500000
13	0.299204	1.000000			0.500000
14	0.287723	1.000000			0.500000
15	0.278590	1.000000			0.500000
16	0.270595	1.000000			0.500000
17	0.262117	1.000000			0.500000
18	0.257866	1.000000			0.500000
19	0.250952	1.000000			0.500000
20	0.243708	1.000000			0.500000
21	0.239481	1.000000			0.500000
22	0.235581	1.000000			0.500000
23	0.233050	1.000000			0.500000
24	0.233106	1.000000		0.091216	0.500000
25	0.232599	1.000000	0.997512	0.091101	0.500026
26	0.231840	0.999966	0.993780	0.091383	0.500004
27	0.230931	0.999927	0.988629	0.091339	0.500041
28	0.229716	0.999818	0.982495	0.091496	0.500051
29	0.226943	0.999521	0.970573	0.091400	0.500092
30	0.224456	0.999143	0.960284	0.091364	0.500105
31	0.221929	0.998722	0.949560	0.091533	0.500094
32	0.217537	0.997769	0.930477	0.091449	0.500115
33	0.213995	0.996713	0.915384	0.091442	0.500129
34	0.210902	0.995608	0.902304	0.091416	0.500138
35	0.208225	0.994476	0.890992	0.091389	0.500149
36	0.205838	0.993331	0.880799	0.091418	0.500158
37	0.203761	0.992181	0.871798	0.091463	0.500156
38	0.200317	0.989935	0.856989	0.091448	0.500160
39	0.196724	0.987276	0.841663	0.091511	0.500149
40	0.193990	0.984799	0.829968	0.091468	0.500193
41	0.190009	0.980556	0.812910	0.091508	0.500175
42	0.186924	0.977256	0.799787	0.091443	0.500129
43	0.184656	0.974694	0.790181	0.091406	0.500088
44	0.182857	0.972682	0.782557	0.091408	0.500051
45	0.181446	0.971099	0.776607	0.091371	0.500021
46	0.179775	0.969269	0.769610	0.091371	0.499930
47	0.178425	0.968231	0.763964	0.091336	0.499834
48	0.177378	0.967485	0.759610	0.091311	0.499738
49	0.176517	0.966975	0.756079	0.091288	0.499640
50	0.175802	0.966632	0.753193	0.091262	0.499544
51	0.175209	0.966418	0.750823	0.091238	0.499457
52	0.174702	0.966262	0.748811	0.091220	0.499378
53	0.174268	0.966160	0.747092	0.091201	0.499291
54	0.173898	0.966102	0.745643	0.091181	0.499212
55	0.173570	0.966069	0.744397	0.091160	0.499145
56	0.173276	0.966039	0.743293	0.091144	0.499074
57	0.173022	0.966020	0.742333	0.091125	0.499014
58	0.172796	0.966018	0.741494	0.091109	0.498958
59	0.172587	0.966003	0.740723	0.091094	0.498898
60	0.172398	0.965997	0.740038	0.091078	0.498836
61	0.172228	0.965992	0.739420	0.091066	0.498804
62	0.172075	0.965963	0.738854	0.091047	0.498760
63	0.171908	0.965956	0.738221	0.091045	0.498687
64	0.171725	0.965844	0.737518	0.091080	0.498732
65	0.171725	0.965844	0.737518		

Table 1 (Concluded)

(A) Final (Twentieth-Cycle) Output

i	x_i	r_i	$\bar{V}_i$	$\bar{s}_i$	$\left(\frac{\bar{V}}{U+2\pi\,\bar{r}_{N+M}}\right)^2$	*sin α'_i	sin α_i	$\gamma(\bar{s}_i)V(\bar{s}_i)$	$\gamma(\bar{s}_i)$
1	0.000000	1.000000	1.269665	0.000000	0.000000	0.062358	0.000000	0.517916	0.500000
2	0.005000	1.000000	1.261699	0.007500	12.013343	0.147602	0.000000	0.438584	0.500000
3	0.010000	1.000000	0.860013	0.015000	6.551842	-0.064486	0.000000	0.307662	0.500000
4	0.020000	1.000000	0.640107	0.025000	4.306665	0.005643	0.000000	0.239184	0.500000
5	0.030000	1.000000	0.526870	0.035000	3.317649	-0.012457	0.000000	0.203586	0.500000
6	0.040000	1.000000	0.465122	0.045000	2.762868	0.007284	0.000000	0.181245	0.500000
7	0.050000	1.000000	0.416988	0.055000	2.405936	-0.015210	0.000000	0.165678	0.500000
8	0.060000	1.000000	0.388368	0.065000	2.158437	0.006419	0.000000	0.154170	0.500000
9	0.070000	1.000000	0.360364	0.075000	1.966182	-0.003285	0.000000	0.144759	0.500000
10	0.080000	1.000000	0.342079	0.085000	1.812671	0.012065	0.000000	0.136901	0.500000
11	0.090000	1.000000	0.321737	0.095000	1.696353	-0.012417	0.000000	0.130709	0.500000
12	0.100000	1.000000	0.311728	0.105000	1.604567	0.006940	0.000000	0.125660	0.500000
13	0.110000	1.000000	0.297068	0.115000	1.520221	-0.004749	0.000000	0.120873	0.500000
14	0.120000	1.000000	0.288489	0.125000	1.449964	0.004493	0.000000	0.116767	0.500000
15	0.130000	1.000000	0.277282	0.135000	1.395153	-0.011213	0.000000	0.113475	0.500000
16	0.140000	1.000000	0.272803	0.145000	1.340128	0.013181	0.000000	0.110080	0.500000
17	0.150000	1.000000	0.261355	0.155000	1.287070	-0.008146	0.000000	0.106706	0.500000
18	0.160000	1.000000	0.257333	0.165000	1.251960	-0.001137	0.000000	0.104372	0.500000
19	0.170000	1.000000	0.251294	0.175000	1.207944	0.005081	0.000000	0.101379	0.500000
20	0.180000	1.000000	0.244714	0.185000	1.161174	0.004614	0.000000	0.098054	0.500000
21	0.190000	1.000000	0.238244	0.192500	1.126238	-0.003945	0.000000	0.095376	0.500000
22	0.195000	1.000000	0.235811	0.196250	1.103045	-0.004133	0.000000	0.093499	0.500000
23	0.197500	1.000000	0.232826	0.198438	1.092163	-0.023321	0.000000	0.092414	0.500000
24	0.199375	1.000000	0.234459	0.200000	1.081505	-0.015608	0.000000	0.091020	0.500000
25	0.200625	1.000000	0.233421	0.201563	1.080242	-0.014347	-0.023013	0.091311	0.500019
26	0.202500	0.999957	0.231863	0.203751	1.079515	-0.021464	-0.013384	0.091619	0.500008
27	0.205000	0.999923	0.231058	0.207501	1.074577	-0.028474	-0.021278	0.091341	0.500031
28	0.210000	0.999817	0.229945	0.215004	1.070274	-0.032537	-0.029850	0.091522	0.500041
29	0.220000	0.999518	0.226735	0.225010	1.061789	-0.040048	-0.037691	0.091395	0.500045
30	0.230000	0.999141	0.224264	0.235018	1.055513	-0.044109	-0.042339	0.091384	0.500056
31	0.240000	0.998717	0.221826	0.250034	1.048560	-0.048495	-0.047781	0.091537	0.500074
32	0.260000	0.997761	0.217432	0.270059	1.038622	-0.053639	-0.052759	0.091437	0.500073
33	0.280000	0.996704	0.213896	0.290089	1.031540	-0.056242	-0.055360	0.091443	0.500073
34	0.300000	0.995595	0.210816	0.310120	1.025727	-0.057627	-0.056600	0.091442	0.500096
35	0.320000	0.994461	0.208196	0.330152	1.020651	-0.057734	-0.056959	0.091414	0.500069
36	0.340000	0.993320	0.205836	0.350185	1.016610	-0.057394	-0.057816	0.091424	0.500098
37	0.360000	0.992162	0.203702	0.380234	1.012398	-0.056348	-0.056483	0.091494	0.500096
38	0.400000	0.989899	0.200238	0.425301	1.006498	-0.052990	-0.052701	0.091459	0.500092
39	0.450000	0.987260	0.196718	0.475367	1.002402	-0.049003	-0.049819	0.091507	0.500100
40	0.500000	0.984766	0.193963	0.550444	0.997863	-0.042115	-0.042800	0.091495	0.500110
41	0.600000	0.980482	0.189907	0.650516	0.994112	-0.032020	-0.032646	0.091521	0.500093
42	0.700000	0.977216	0.186860	0.750559	0.990853	-0.025466	-0.025737	0.091451	0.500086
43	0.800000	0.974642	0.184626	0.850586	0.988893	-0.020027	-0.020085	0.091426	0.500073
44	0.900000	0.972633	0.182831	0.950602	0.987749	-0.015653	-0.015977	0.091433	0.500066
45	1.000000	0.971035	0.181415	1.075614	0.986529	-0.011229	-0.011562	0.091413	0.500064
46	1.150000	0.969300	0.179757	1.225621	0.985734	-0.007406	-0.007324	0.091419	0.500035
47	1.300000	0.968202	0.178443	1.375624	0.984856	-0.004952	-0.004912	0.091391	0.500031
48	1.450000	0.967465	0.177420	1.525625	0.984325	-0.003215	-0.003343	0.091380	0.500012
49	1.600000	0.966963	0.176578	1.675626	0.983964	-0.002090	-0.002236	0.091373	0.500000
50	1.750000	0.966628	0.175886	1.825626	0.983638	-0.001360	-0.001431	0.091363	0.499970
51	1.900000	0.966413	0.175310	1.975626	0.983428	-0.000878	-0.001032	0.091359	0.499956
52	2.050000	0.966258	0.174822	2.125626	0.983239	-0.000592	-0.000567	0.091353	0.499949
53	2.200000	0.966173	0.174411	2.275626	0.983052	-0.000388	-0.000376	0.091345	0.499948
54	2.350000	0.966117	0.174057	2.425626	0.982956	-0.000235	-0.000303	0.091343	0.499925
55	2.500000	0.966072	0.173742	2.575626	0.982859	-0.000166	-0.000178	0.091340	0.499908
56	2.650000	0.966045	0.173467	2.725626	0.982757	-0.000148	-0.000085	0.091335	0.499908
57	2.800000	0.966032	0.173230	2.875626	0.982657	-0.000105	-0.000041	0.091329	0.499895
58	2.950000	0.966026	0.173016	3.025626	0.982605	-0.000088	-0.000193	0.091327	0.499894
59	3.100000	0.965997	0.172818	3.175626	0.982568	-0.000167	-0.000062	0.091327	0.499887
60	3.250000	0.965988	0.172645	3.325626	0.982484	-0.000191	-0.000075	0.091321	0.499874
61	3.400000	0.965976	0.172487	3.475626	0.982529	-0.000309	-0.000273	0.091327	0.499878
62	3.550000	0.965936	0.172348	3.625626	0.982355	-0.000395	0.000122	0.091312	0.499874
63	3.700000	0.965954	0.172204	3.775626	0.982398	-0.000566	-0.000968	0.091318	0.499845
64	3.850000	0.965809	0.172020	3.925626	0.982939	-0.001538	0.000000	0.091370	0.499868
65	4.000000	0.965809	0.172020	0.000000	0.000000	0.000000	0.000000	0.000000	0.000000

*$\sin \alpha'_i$ is the sine of the angle between the axis of symmetry and the velocity V, considered a vector.

Table 2

Summary of Results of Calculations of Slipstream Contraction in the Static Case

	Slipstream Contraction Ratio, ϕ						
	Cylindrical Shrouds	Conical Shrouds			Parabolic-Cambered Shrouds		
$\ell/\bar{r}_N$ \ $\tan \alpha_N$	0	0.08	0.16	0.24	0.08	0.16	0.24
0.05	((0.835))						
0.10	0.884			((1.008))			0.945
0.20	0.934						
0.40	0.974	1.016	1.062	1.111	1.000	1.027	1.056
1.00	0.998	1.041	1.087	1.136	1.030	1.064	1.099
2.00				(1.136)			(1.117)

The results are for twenty-iterative-cycle calculations, except that data in single parentheses are from ten-cycle calculations, in cases giving rapid convergence; and data in double parentheses are from ten-cycle calculations, with good estimate of slipstream representation at first cycle, in cases giving slow convergence.

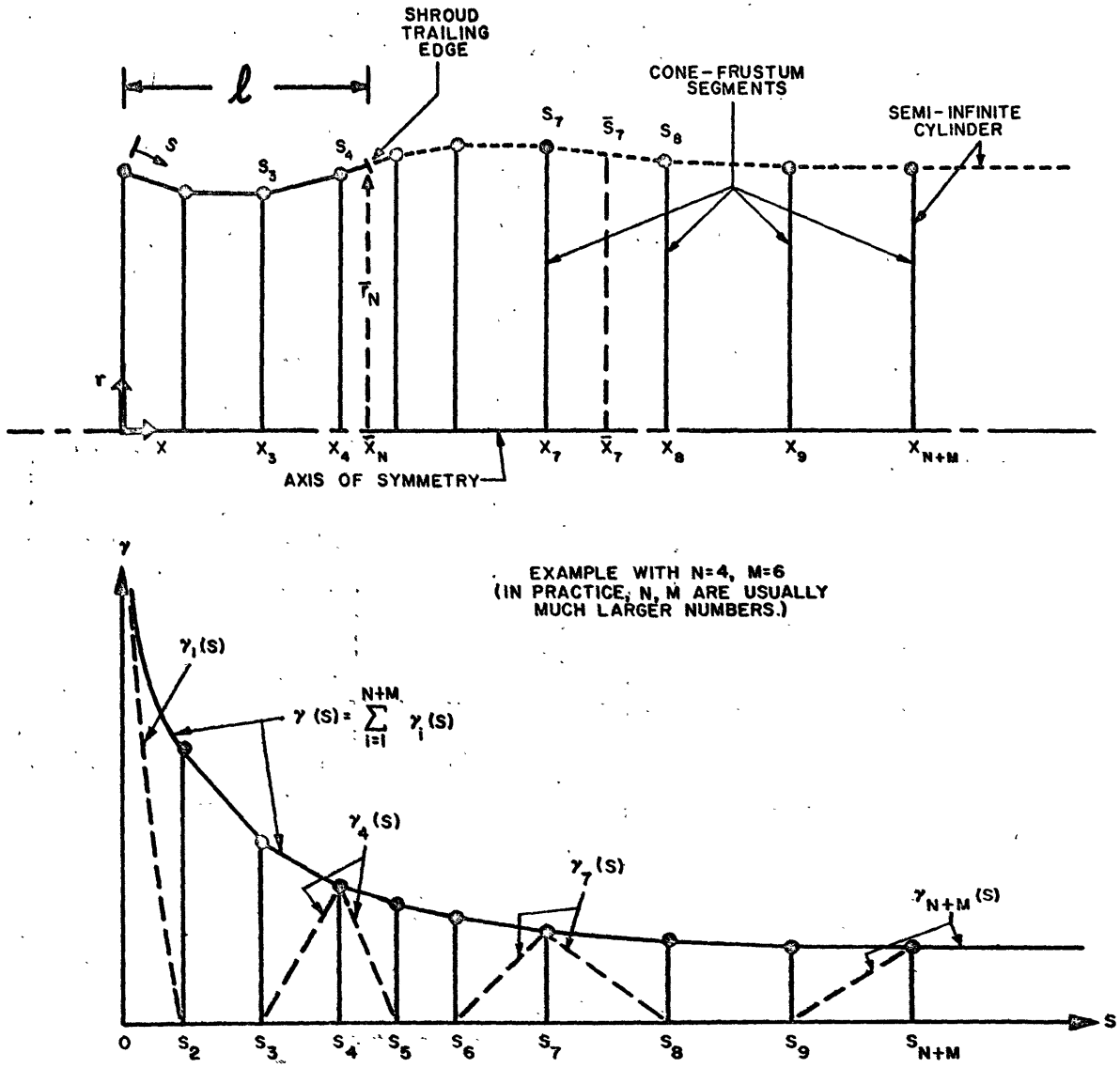

Figure 1 - Approximation of the Vortex Distribution on a Shroud and Slipstream by a Vortex Distribution on a System of Cone-Frustum Segments

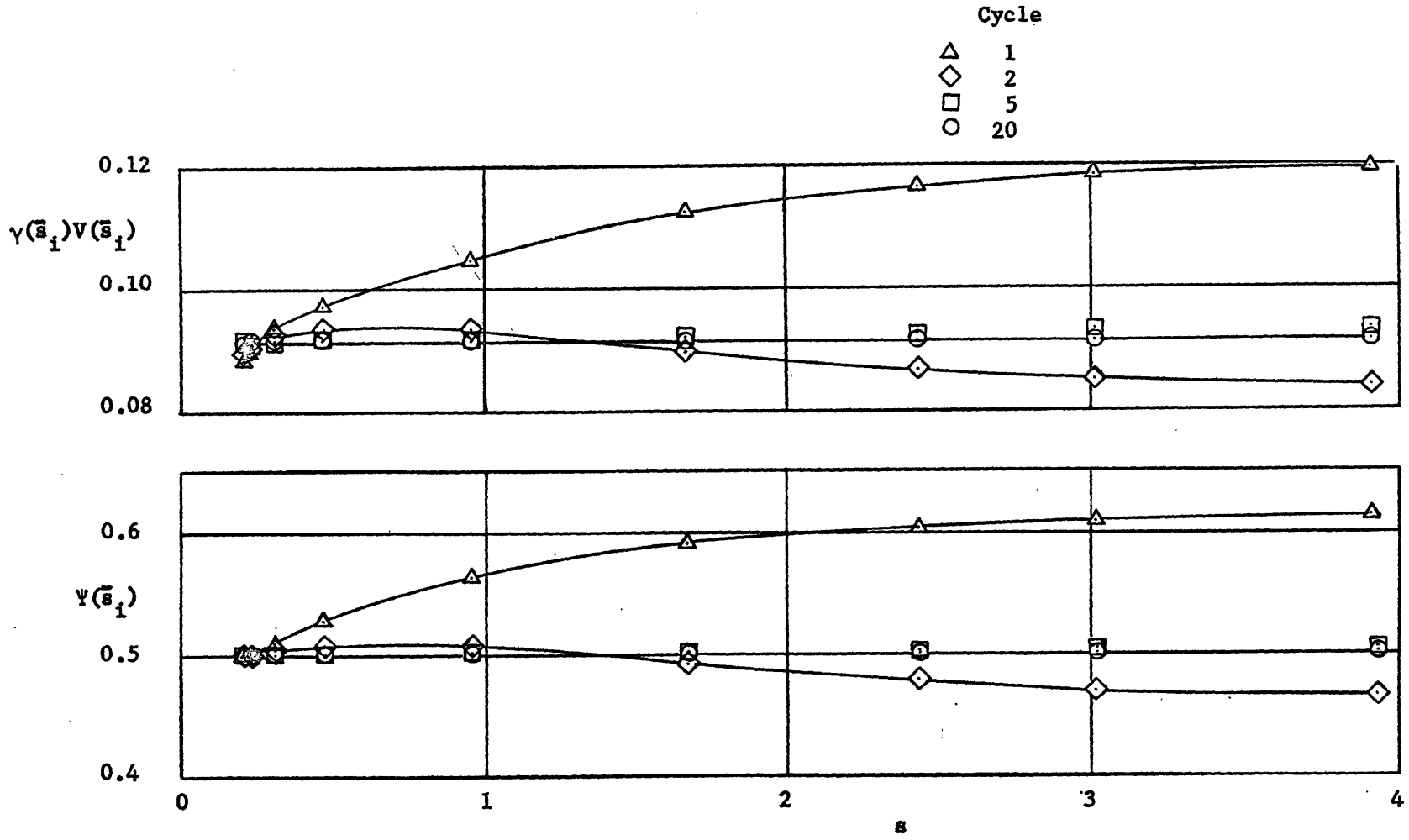

Figure 2 - Approximation of Slipstream Boundary Conditions at Various Stages of a Twenty-Iterative-Cycle Calculation. Cylindrical Shroud; $\ell/\bar{r}_N = 0.2$; U = 0

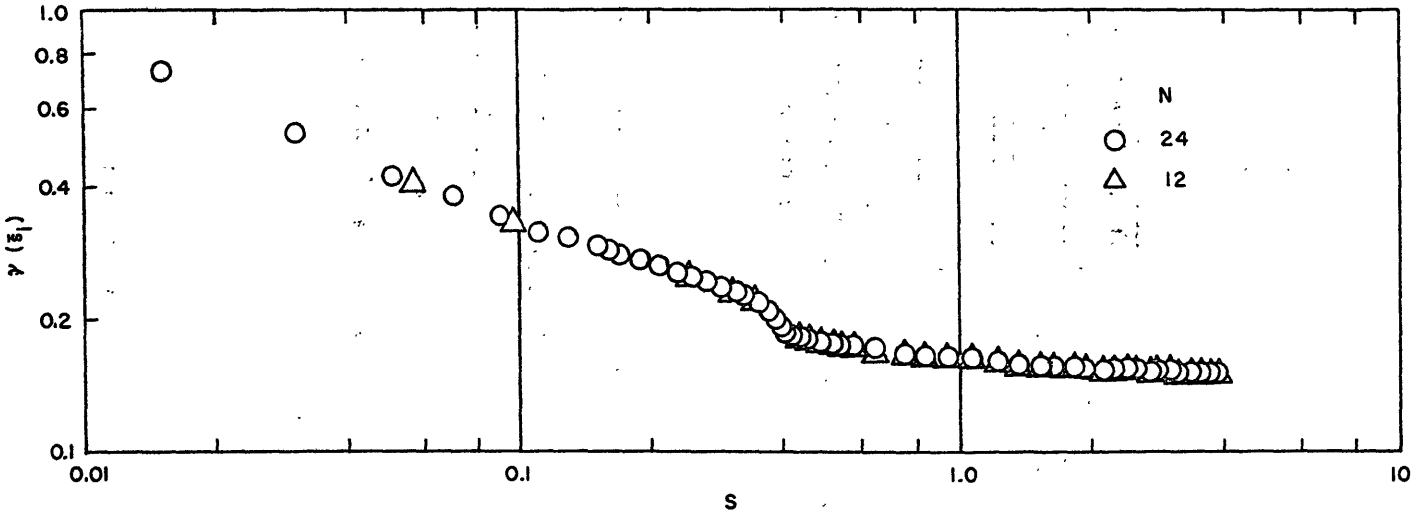

Figure 3 - Effect of Halving the Number, N, of Cone-Frustum Segments Used to Approximate the Shroud. Parabolic-Cambered Shroud; $\ell = 0.4$; $\bar{r}_N = 1.0$; $\tan \alpha_N = 0.24$; $\Psi_o = \frac{1}{2}$; $U = 0$

(a) Vortex Distributions After 20 Cycles

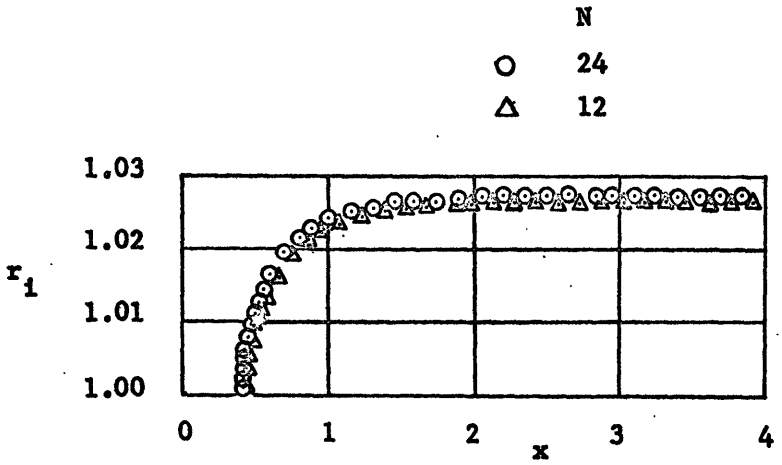

(b) Slipstream Shapes After 20 Cycles
(Note exaggerated r-scale)

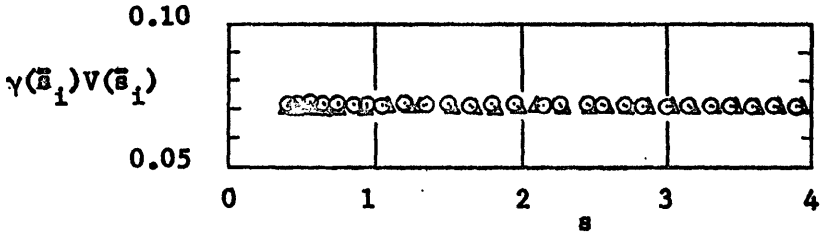

(c) $\gamma(\vec{s}_i)V(\vec{s}_i)$ After 20 Cycles

Figure 3 (Concluded)

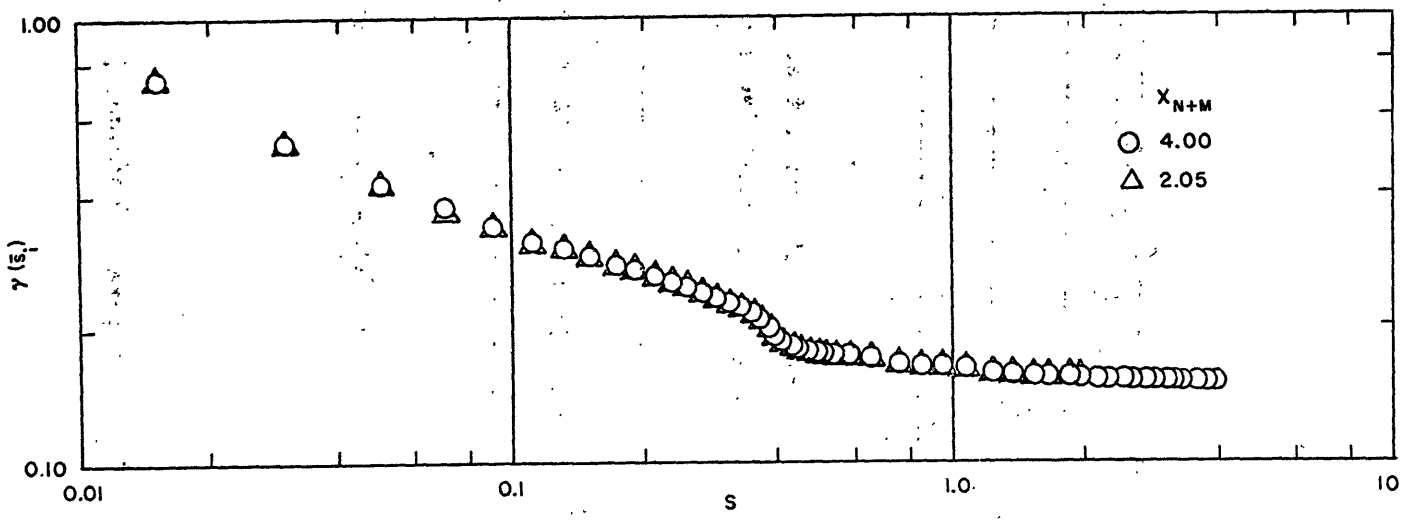

Figure 4 - Effect of Halving the Length, x_{N+M}, of the System of Cone-Frustum Segments.

Parabolic-Cambered Shroud; $\ell = 0.4$; $\bar{r}_N = 1.0$; $\tan \alpha_N = 0.24$; $\Psi_o = \frac{1}{2}$; $U = 0$

(a) Vortex Distributions After 20 Cycles

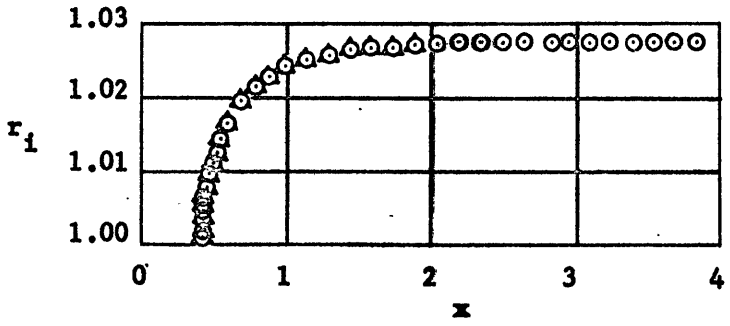

(b) Slipstream Shape After 20 Cycles
(Note exaggerated r-scale)

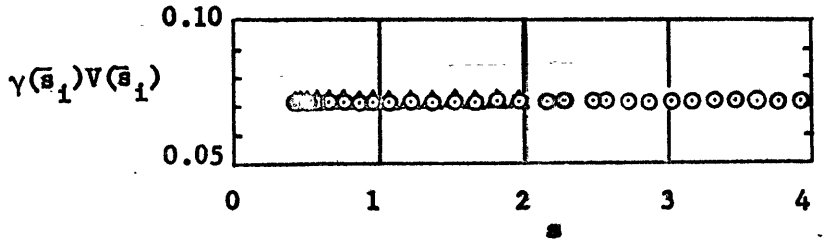

(c) $\gamma(\bar{s}_i)V(\bar{s}_i)$ After 20 Cycles

Figure 4 (Concluded)

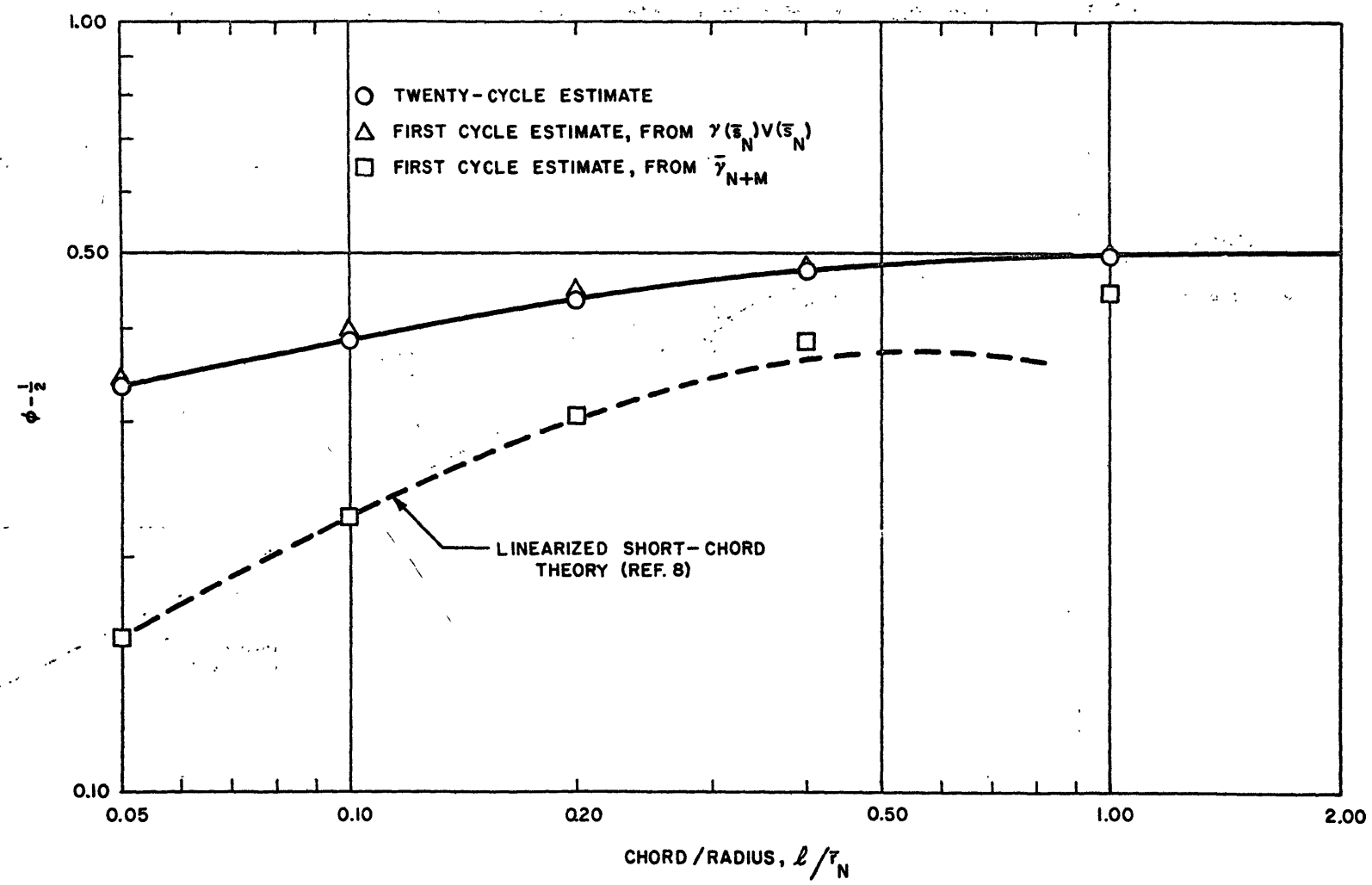

Figure 5 - Slipstream Contraction Ratio for Cylindrical Shrouds. (Static Case)

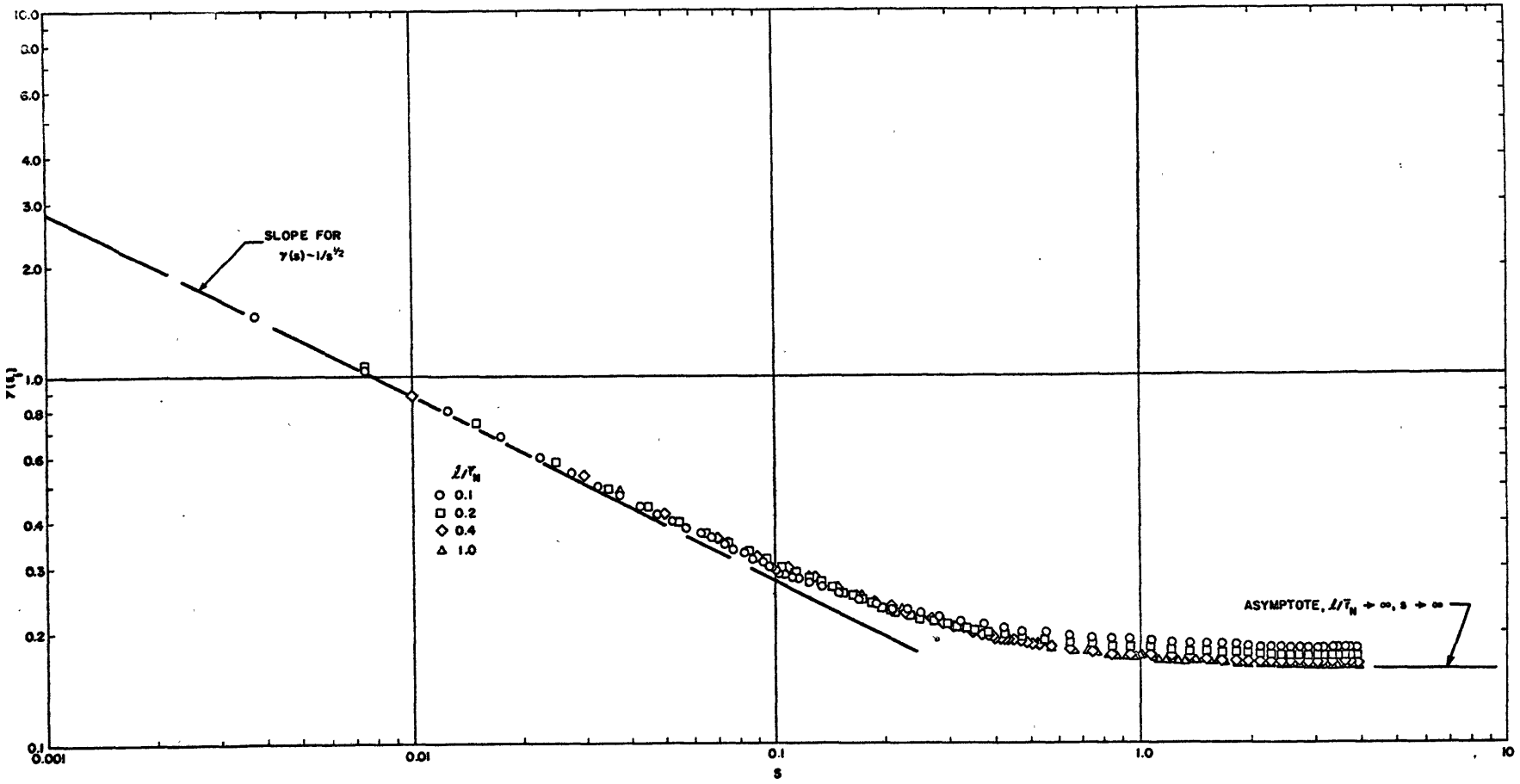

Figure 6 - Vortex Distributions on Cylindrical Shrouds and Their Slipstream (20-Cycle Calculations). $\Psi_o = \frac{1}{2}$; $U = 0$; $\bar{r}_N = 1.0$

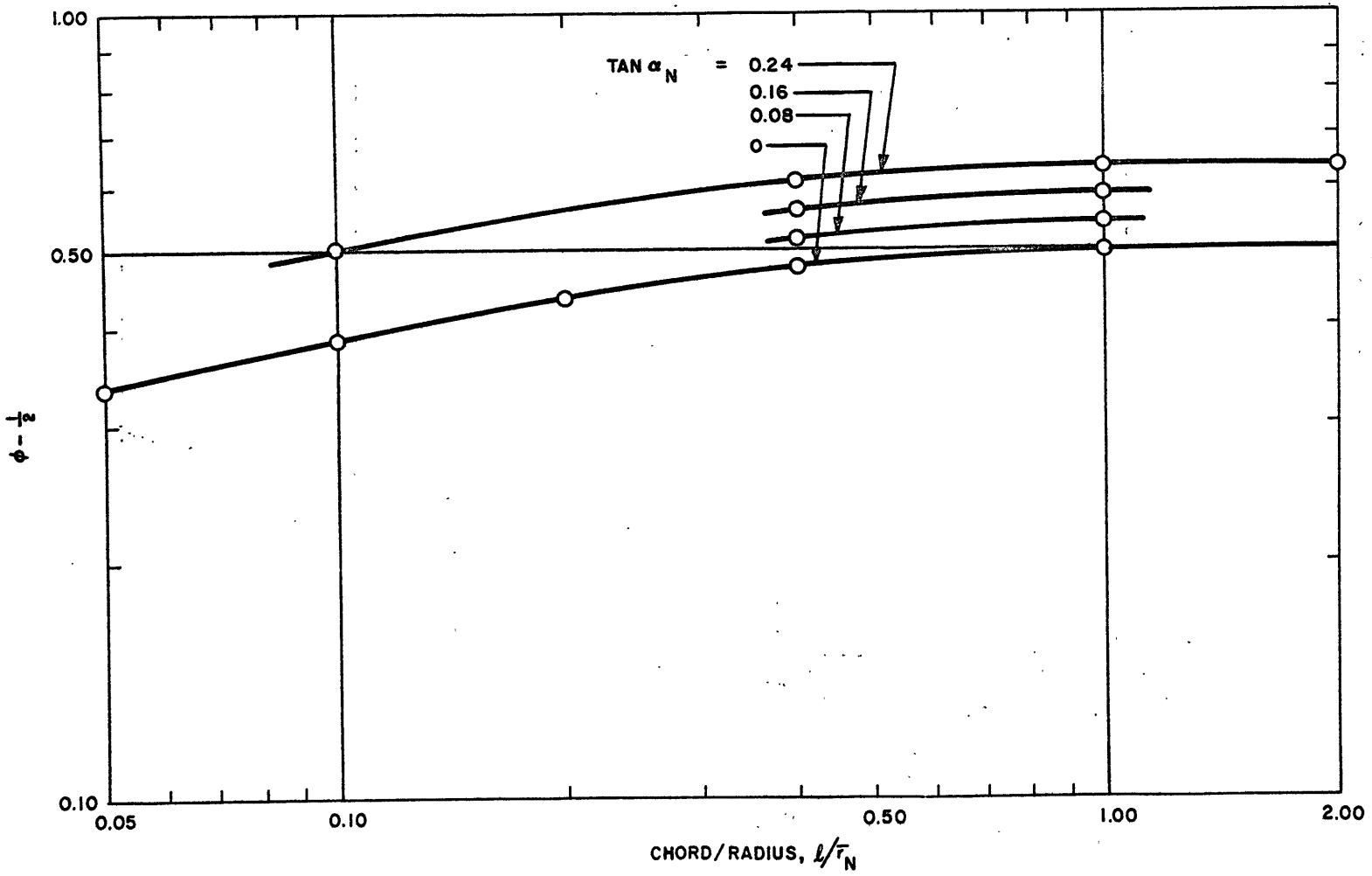

Figure 7 - Slipstream Contraction Ratio for Conical Shrouds. (Static Case)

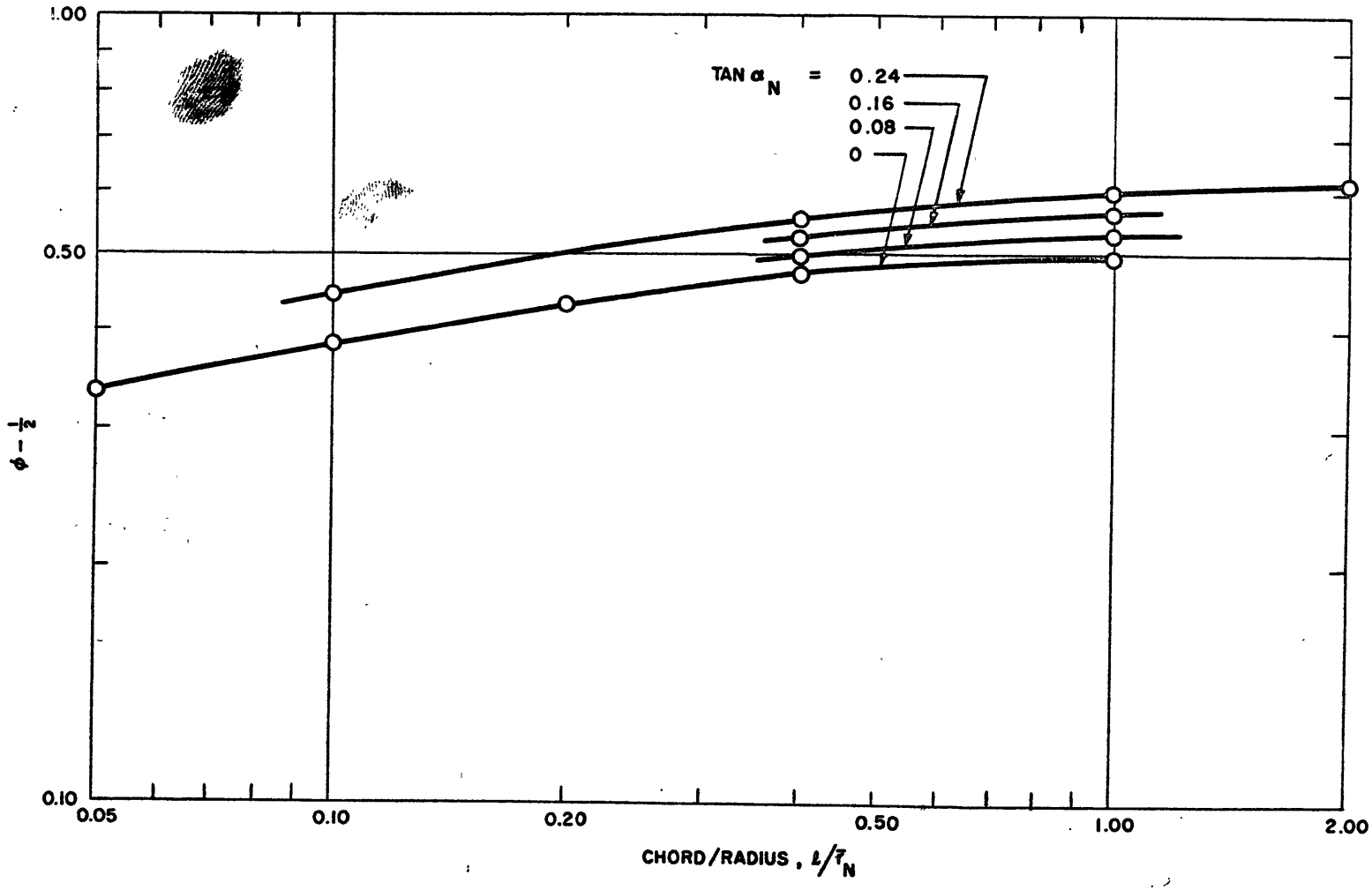

Figure 8 - Slipstream Contraction Ratio for Parabolic-Cambered Shrouds. (Static Case)

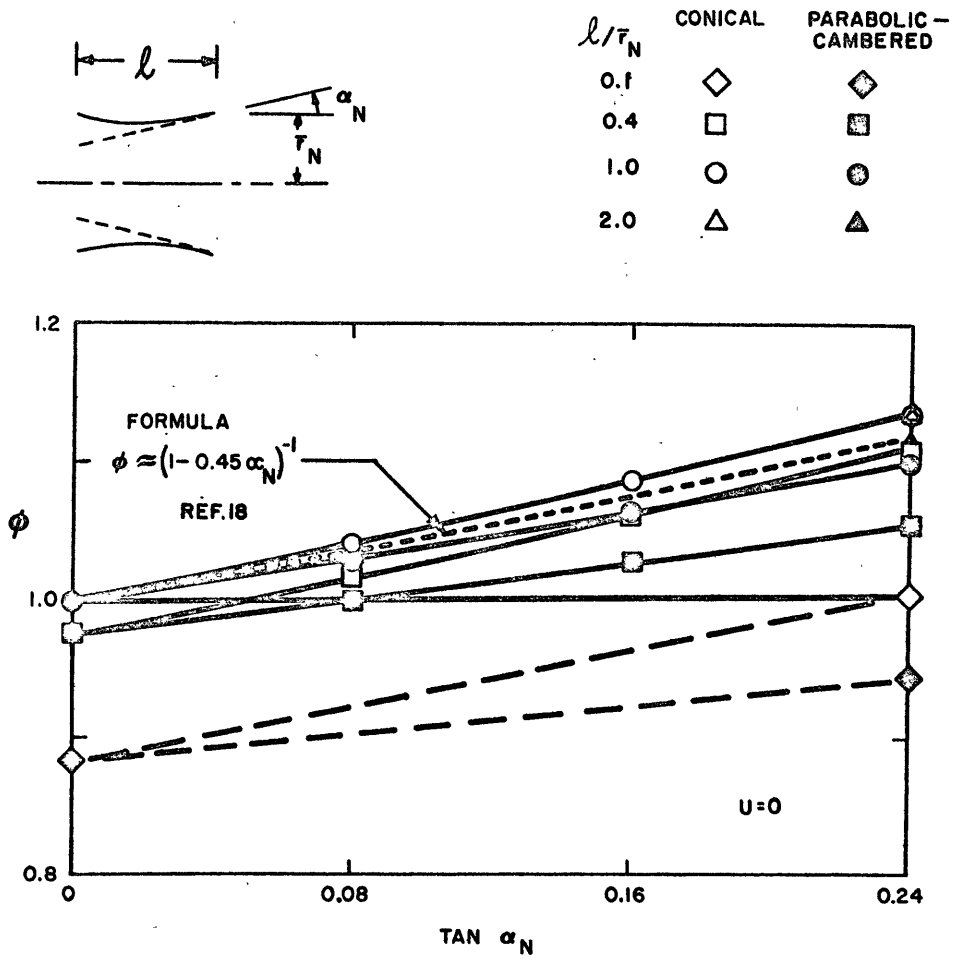

Figure 9 - Effect of Trailing-Edge Divergence Angle on Slipstream Contraction Ratio (Data From Table 2)

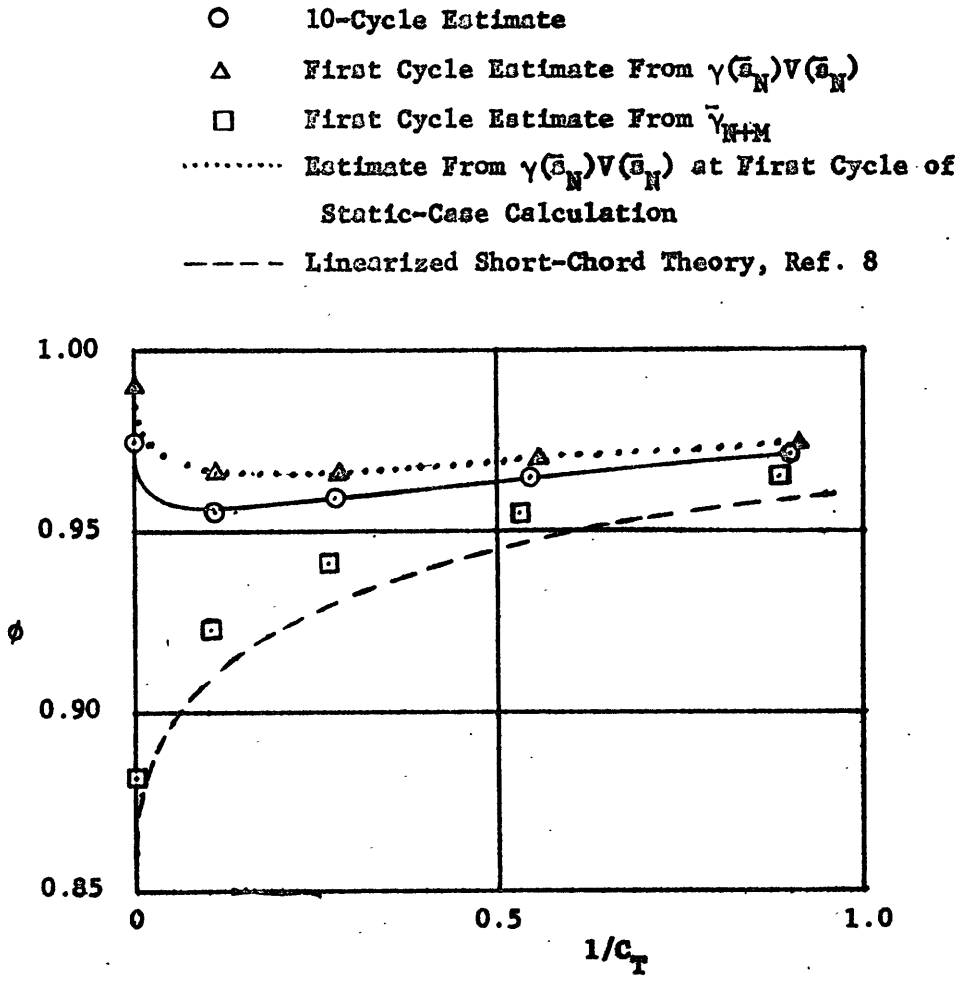

Figure 10 - Slipstream Contraction at Finite Thrust Coefficients. Cylindrical Shrouds
(a) Various Estimates; $\ell/\bar{r}_N = 0.4$

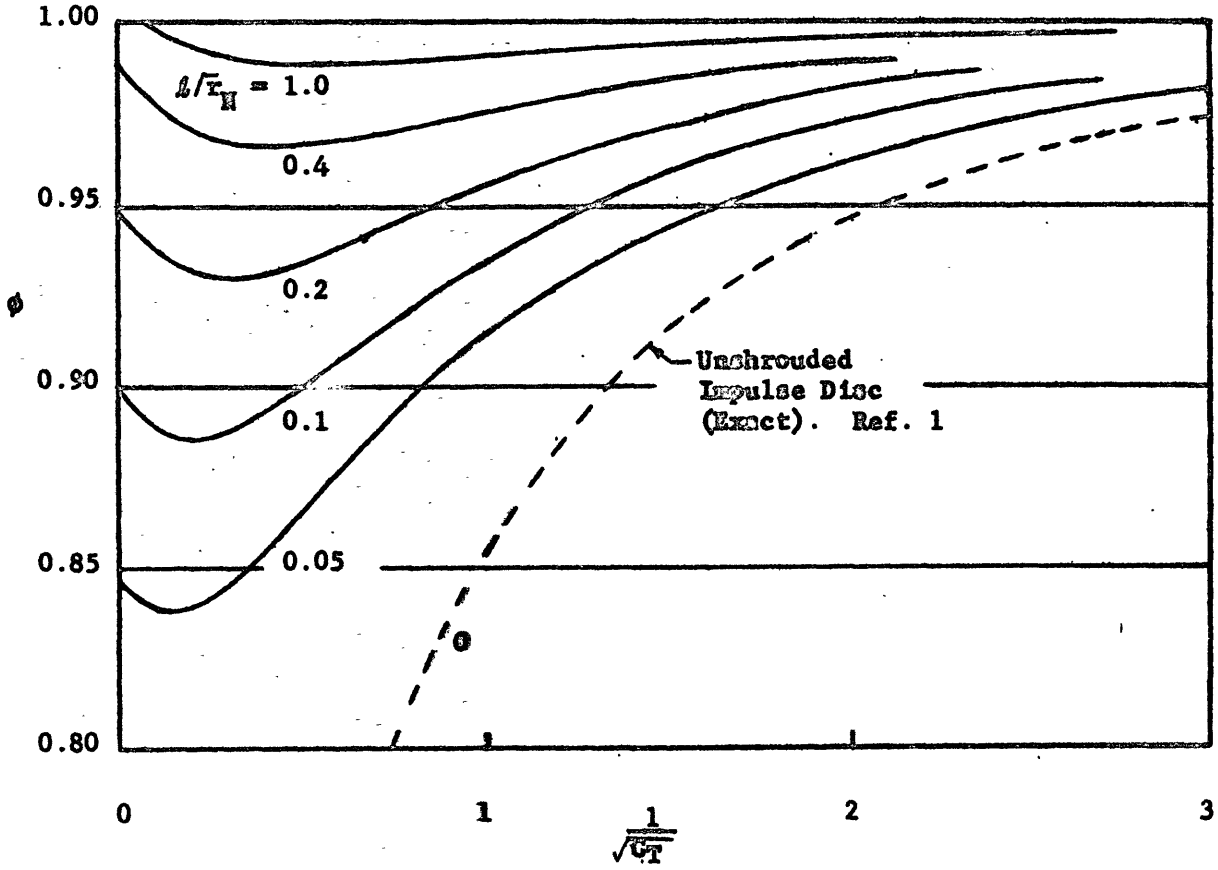

Figure 10 (Concluded)

(b) Estimates From $\gamma(\bar{s}_N)V(\bar{s}_N)$ at First Cycle of Static-Case Calculation

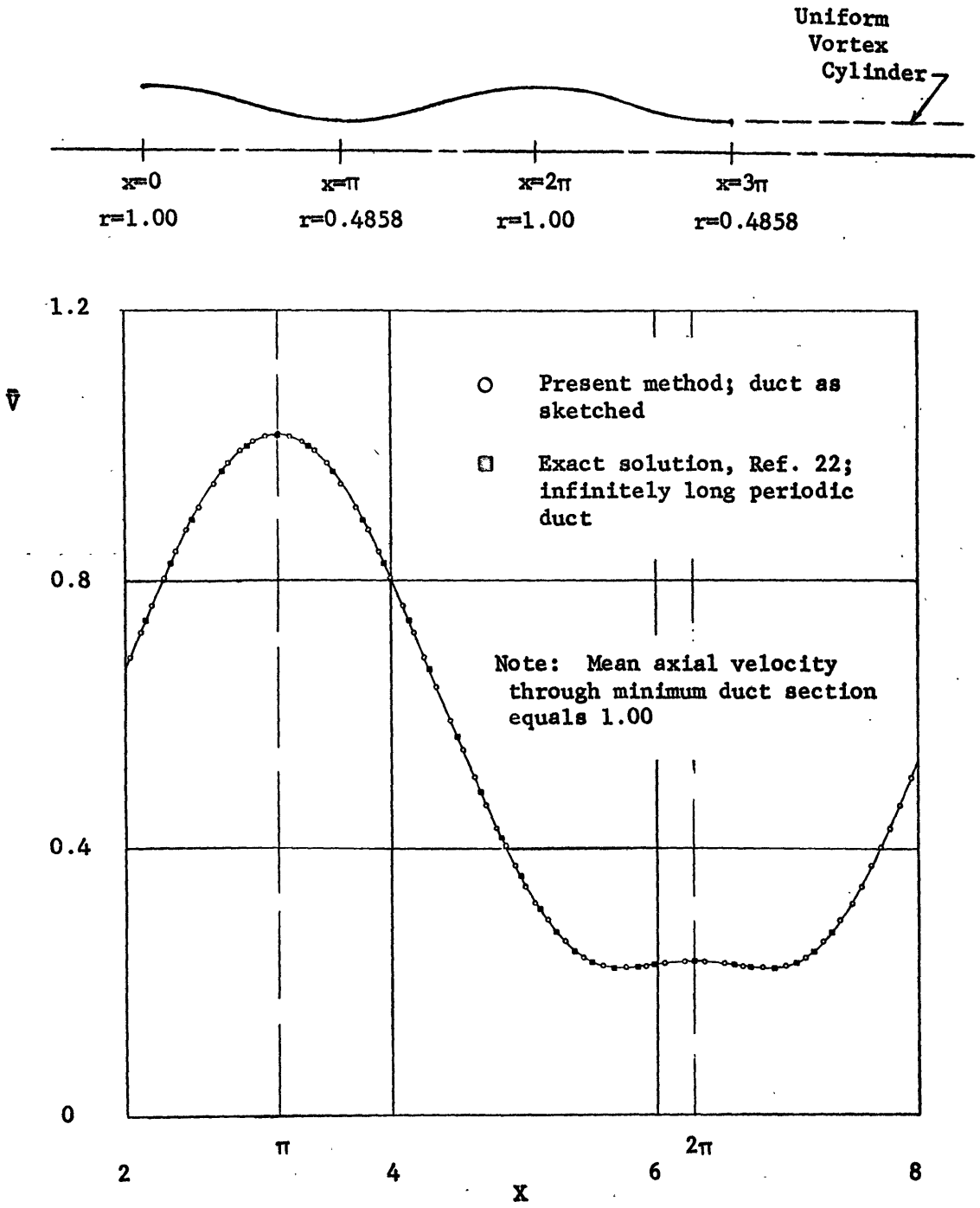

Figure 11 - Velocity Distribution Along the Interior Wall of a Duct

(a) Section of a Periodic Duct

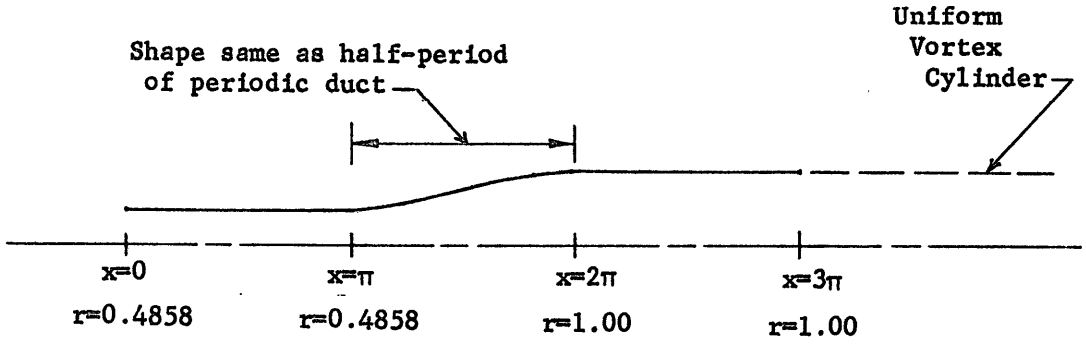

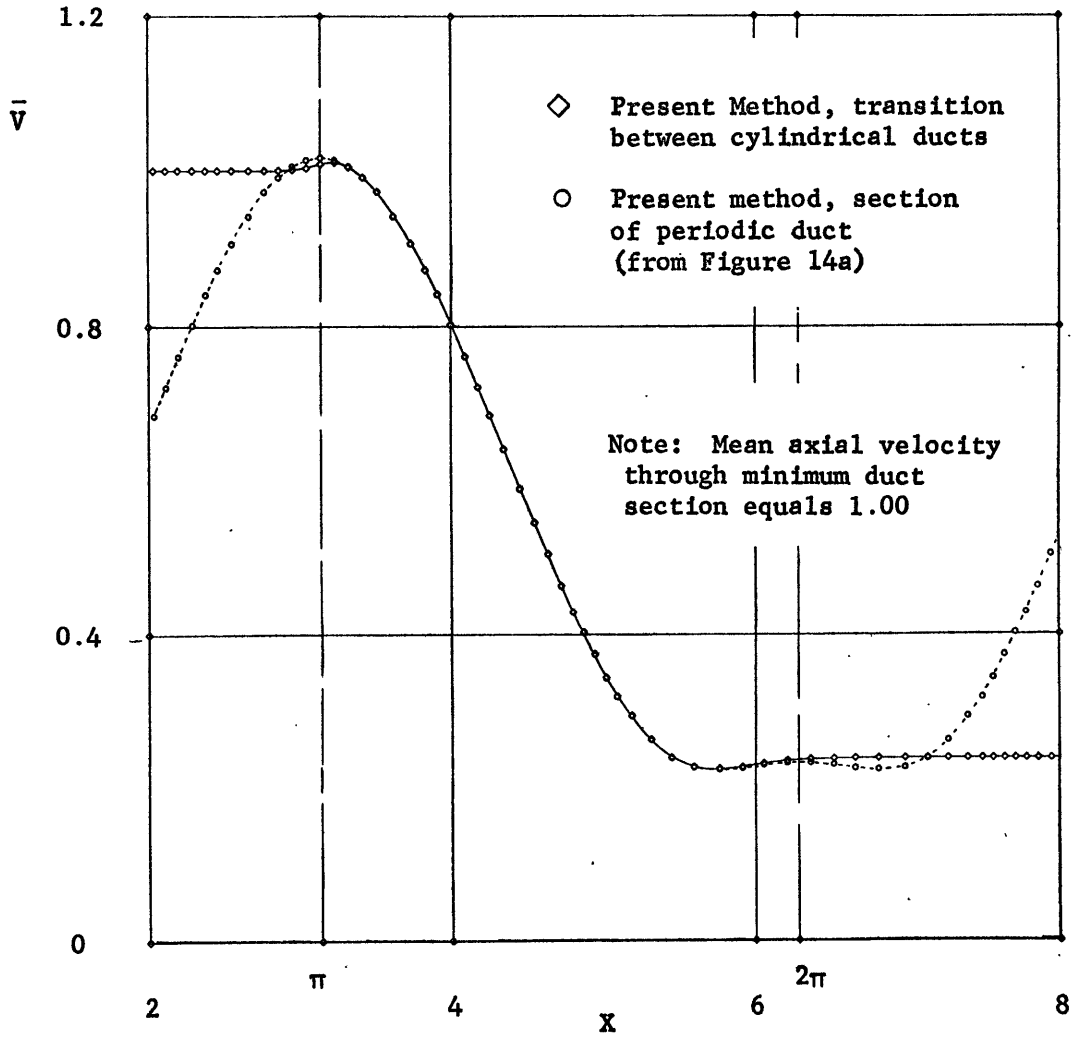

Figure 11 (Concluded)

(b) Transition Between Cylindrical Ducts

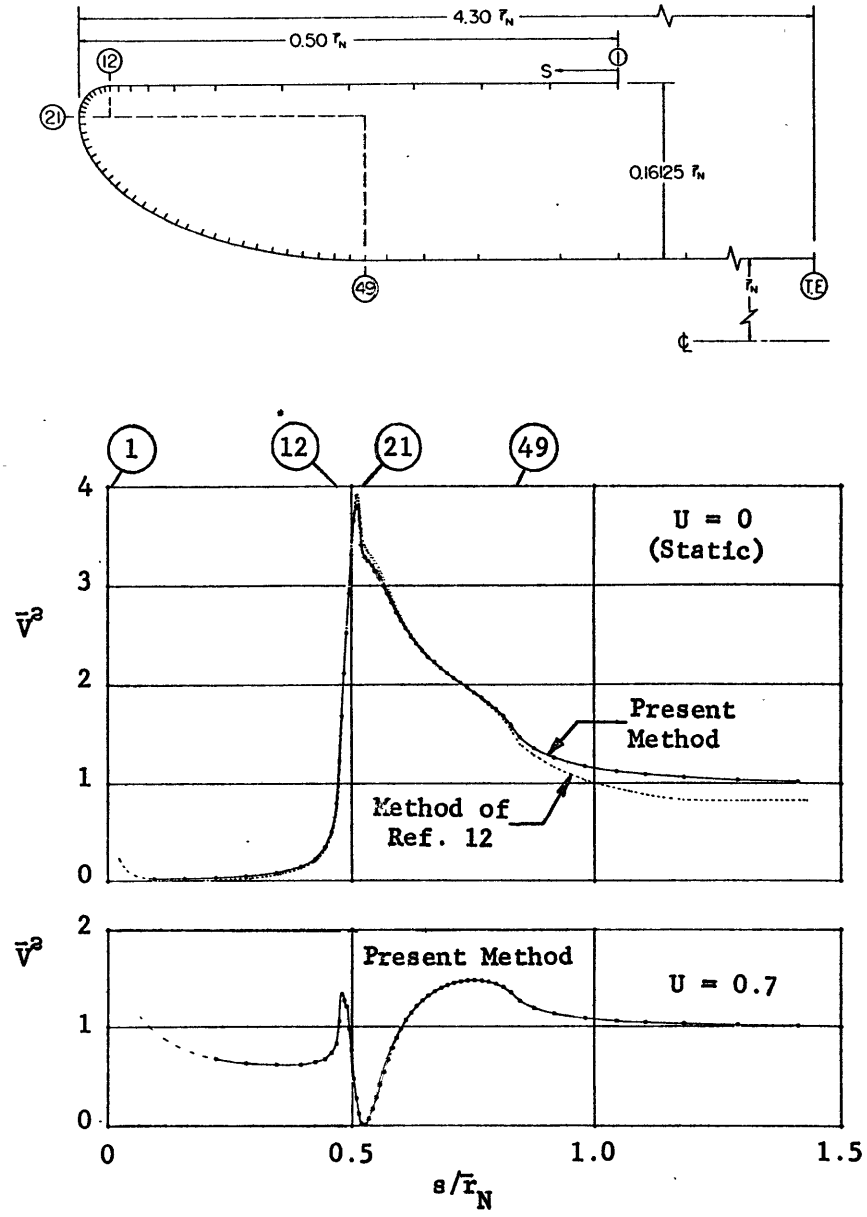

Figure 12 - Velocity Distribution on the Inlet to a Circular Cylindrical Duct. Mean Internal Axial Velocity = 1.0

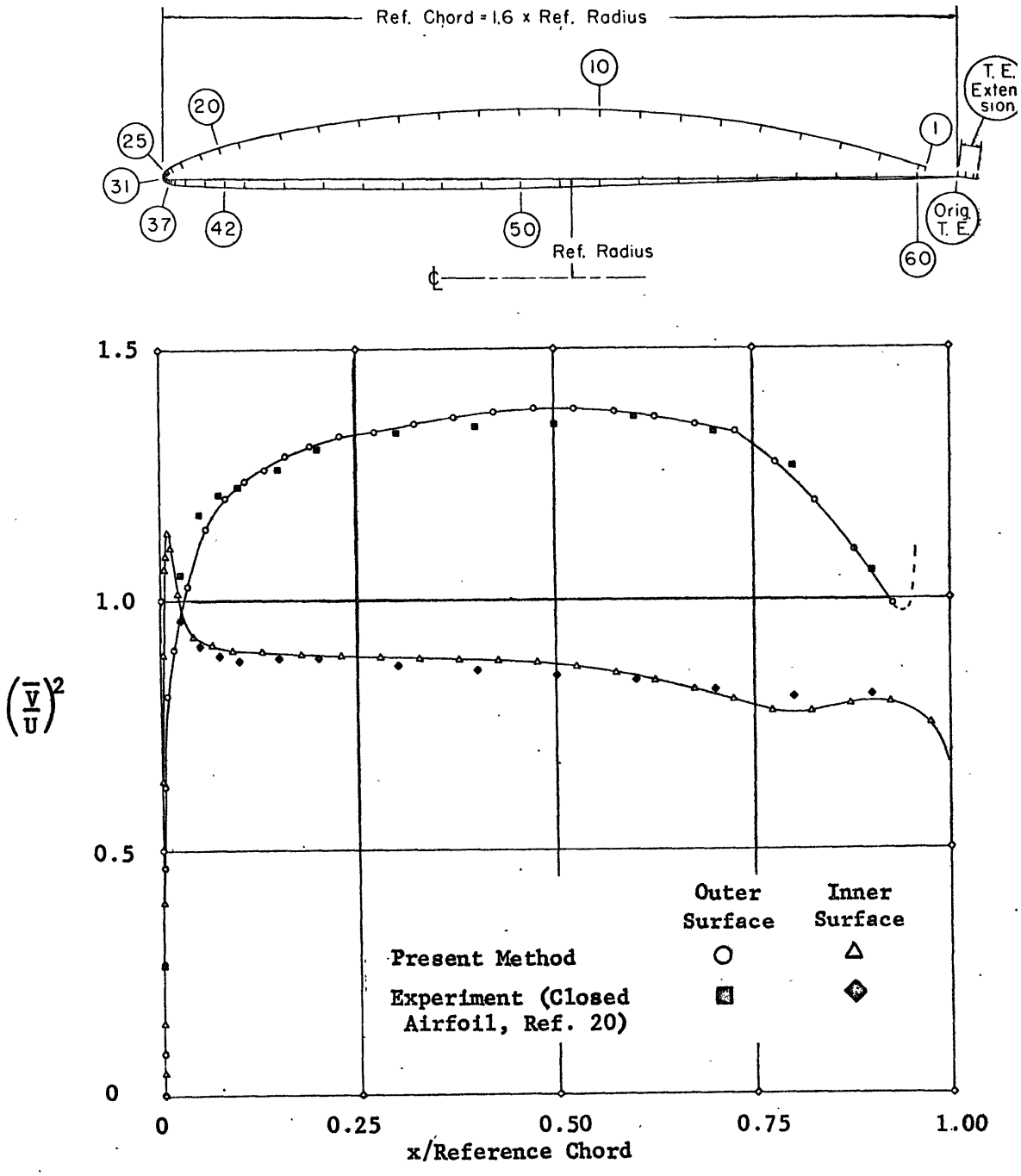

Figure 13 - Velocity Distribution on a Nearly Closed Annular Airfo

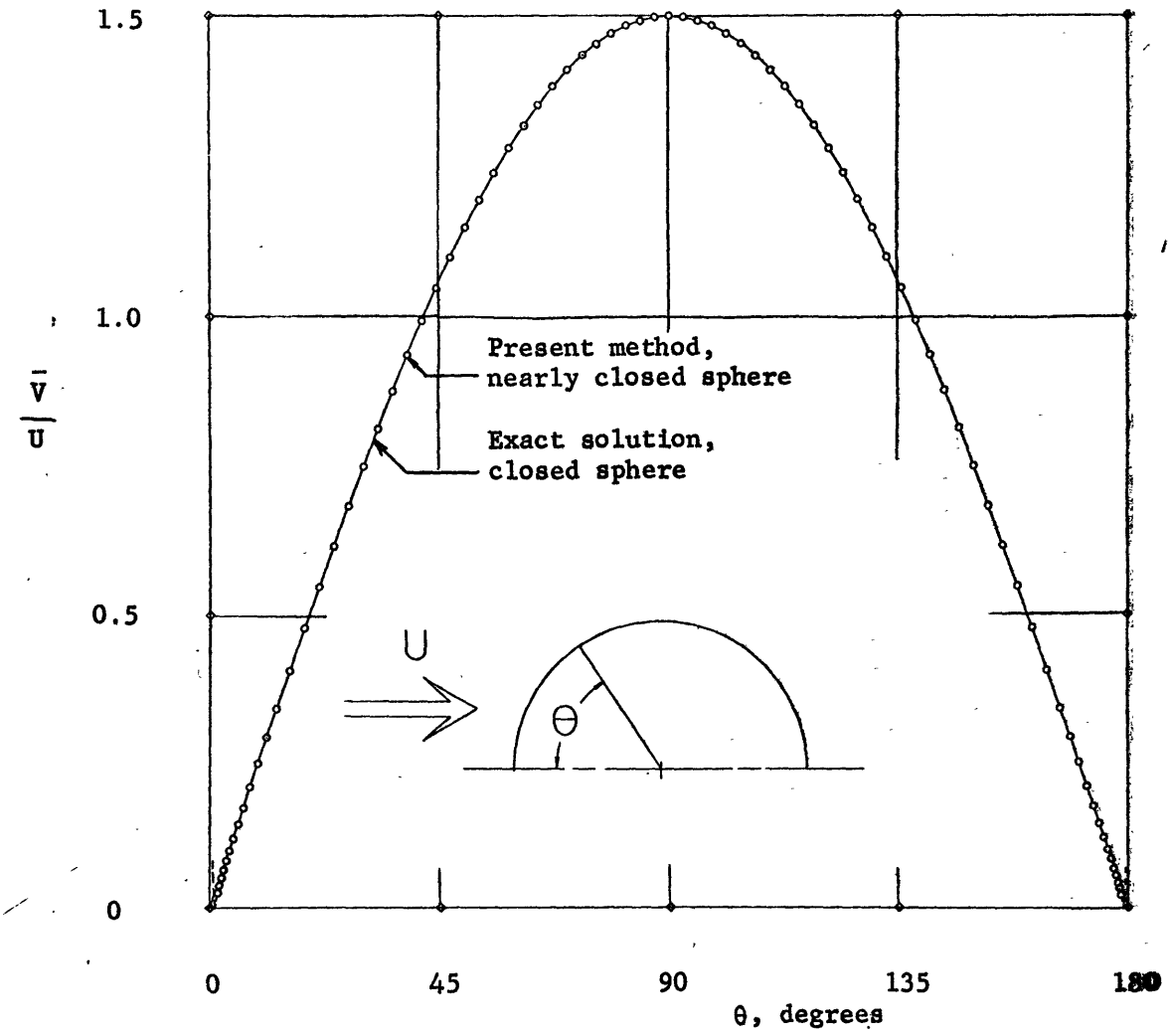

Figure 14 - Velocity Distribution on a Nearly Closed Sphere

DTMB Aero Report 1077

David Taylor Model Basin. Report 1857.
A METHOD FOR NUMERICAL CALCULATION OF SLIPSTREAM CONTRACTION OF A SHROUDED IMPULSE DISC IN THE STATIC CASE WITH APPLICATION TO OTHER AXISYMMETRIC POTENTIAL FLOW PROBLEMS, by Harvey R. Chaplin. Wash., Jun 1964. 138p. incl. illus. 23 refs. (Aerodynamics Lab. Aero Rpt 1077)
Thesis (Ph.D.)--Catholic University.

Digital computer method developed to calculate axisymmetric potential flow through shrouded propeller with uniform disc loading, no swirl. Slipstream shape approached by successive approximations, and calculations made for cylindrical, conical and parabolic-cambered shrouds. Method of singularities used also applicable to other axisymmetric flow problems. Examples given for annular airfoil, body of revolution, duct and inlet flow.

Slipstream--Contraction Ratio
Propellers, Shrouded
Wings, Ring
Propellers--Efficiency
Propellers--Thrust
Ducts, Circular
Inlets, Circular
Bodies of Revolution
Flow, Axisymmetric
Flow, One-Dimensional
Propeller Shrouds--Configurations
Computer Methods
Propeller Theory, Momentum
Chaplin, Harvey R.
Catholic Univ. Thesis

DTMB Aero Report 1077

David Taylor Model Basin. Report 1857.
A METHOD FOR NUMERICAL CALCULATION OF SLIPSTREAM CONTRACTION OF A SHROUDED IMPULSE DISC IN THE STATIC CASE WITH APPLICATION TO OTHER AXISYMMETRIC POTENTIAL FLOW PROBLEMS, by Harvey R. Chaplin. Wash., Jun 1964. 138p. incl. illus. 23 refs. (Aerodynamics Lab. Aero Rpt 1077)
Thesis (Ph.D.)--Catholic University.

Digital computer method developed to calculate axisymmetric potential flow through shrouded propeller with uniform disc loading, no swirl. Slipstream shape approached by successive approximations, and calculations made for cylindrical, conical and parabolic-cambered shrouds. Method of singularities used also applicable to other axisymmetric flow problems. Examples given for annular airfoil, body of revolution, duct and inlet flow.

Slipstream--Contraction Ratio
Propellers, Shrouded
Wings, Ring
Propellers--Efficiency
Propellers--Thrust
Ducts, Circular
Inlets, Circular
Bodies of Revolution
Flow, Axisymmetric
Flow, One-Dimensional
Propeller Shrouds--Configurations
Computer Methods
Propeller Theory, Momentum
Chaplin, Harvey R.
Catholic Univ. Thesis

DTMB Aero Report 1077

David Taylor Model Basin. Report 1857.
A METHOD FOR NUMERICAL CALCULATION OF SLIPSTREAM CONTRACTION OF A SHROUDED IMPULSE DISC IN THE STATIC CASE WITH APPLICATION TO OTHER AXISYMMETRIC POTENTIAL FLOW PROBLEMS, by Harvey R. Chaplin. Wash., Jun 1964. 138p. incl. illus. 23 refs. (Aerodynamics Lab. Aero Rpt 1077)
Thesis (Ph.D.)--Catholic University.

Digital computer method developed to calculate axisymmetric potential flow through shrouded propeller with uniform disc loading, no swirl. Slipstream shape approached by successive approximations, and calculations made for cylindrical, conical and parabolic-cambered shrouds. Method of singularities used also applicable to other axisymmetric flow problems. Examples given for annular airfoil, body of revolution, duct and inlet flow.

Slipstream--Contraction Ratio
Propellers, Shrouded
Wings, Ring
Propellers--Efficiency
Propellers--Thrust
Ducts, Circular
Inlets, Circular
Bodies of Revolution
Flow, Axisymmetric
Flow, One-Dimensional
Propeller Shrouds--Configurations
Computer Methods
Propeller Theory, Momentum
Chaplin, Harvey R.
Catholic Univ. Thesis

DTMB Aero Report 1077

David Taylor Model Basin. Report 1857.
A METHOD FOR NUMERICAL CALCULATION OF SLIPSTREAM CONTRACTION OF A SHROUDED IMPULSE DISC IN THE STATIC CASE WITH APPLICATION TO OTHER AXISYMMETRIC POTENTIAL FLOW PROBLEMS, by Harvey R. Chaplin. Wash., Jun 1964. 138p. incl. illus. 23 refs. (Aerodynamics Lab. Aero Rpt 1077)
Thesis (Ph.D.)--Catholic University.

Digital computer method developed to calculate axisymmetric potential flow through shrouded propeller with uniform disc loading, no swirl. Slipstream shape approached by successive approximations, and calculations made for cylindrical, conical and parabolic-cambered shrouds. Method of singularities used also applicable to other axisymmetric flow problems. Examples given for annular airfoil, body of revolution, duct and inlet flow.

Slipstream--Contraction Ratio
Propellers, Shrouded
Wings, Ring
Propellers--Efficiency
Propellers--Thrust
Ducts, Circular
Inlets, Circular
Bodies of Revolution
Flow, Axisymmetric
Flow, One-Dimensional
Propeller Shrouds--Configurations
Computer Methods
Propeller Theory, Momentum
Chaplin, Harvey R.
Catholic Univ. Thesis

DTMB Aero Report 1077

David Taylor Model Basin. Report 1857.
A METHOD FOR NUMERICAL CALCULATION OF SLIPSTREAM CONTRACTION OF A SHROUDED IMPULSE DISC IN THE STATIC CASE WITH APPLICATION TO OTHER AXISYMMETRIC POTENTIAL FLOW PROBLEMS, by Harvey R. Chaplin. Wash., Jun 1964. 138p. incl. illus. 23 refs. (Aerodynamics Lab. Aero Rpt 1077)
Thesis (Ph.D.)--Catholic University.

Digital computer method developed to calculate axisymmetric potential flow through shrouded propeller with uniform disc loading, no swirl. Slipstream shape approached by successive approximations, and calculations made for cylindrical, conical and parabolic-cambered shrouds. Method of singularities used also applicable to other axisymmetric flow problems. Examples given for annular airfoil, body of revolution, duct and inlet flow.

Slipstream--Contraction Ratio
Propellers, Shrouded
Wings, Ring
Propellers--Efficiency
Propellers--Thrust
Ducts, Circular
Inlets, Circular
Bodies of Revolution
Flow, Axisymmetric
Flow, One-Dimensional
Propeller Shrouds--Configurations
Computer Methods
Propeller Theory, Momentum
Chaplin, Harvey R.
Catholic Univ. Thesis

DTMB Aero Report 1077

David Taylor Model Basin. Report 1857.
A METHOD FOR NUMERICAL CALCULATION OF SLIPSTREAM CONTRACTION OF A SHROUDED IMPULSE DISC IN THE STATIC CASE WITH APPLICATION TO OTHER AXISYMMETRIC POTENTIAL FLOW PROBLEMS, by Harvey R. Chaplin. Wash., Jun 1964. 138p. incl. illus. 23 refs. (Aerodynamics Lab. Aero Rpt 1077)
Thesis (Ph.D.)--Catholic University.

Digital computer method developed to calculate axisymmetric potential flow through shrouded propeller with uniform disc loading, no swirl. Slipstream shape approached by successive approximations, and calculations made for cylindrical, conical and parabolic-cambered shrouds. Method of singularities used also applicable to other axisymmetric flow problems. Examples given for annular airfoil, body of revolution, duct and inlet flow.

Slipstream--Contraction Ratio
Propellers, Shrouded
Wings, Ring
Propellers--Efficiency
Propellers--Thrust
Ducts, Circular
Inlets, Circular
Bodies of Revolution
Flow, Axisymmetric
Flow, One-Dimensional
Propeller Shrouds--Configurations
Computer Methods
Propeller Theory, Momentum
Chaplin, Harvey R.
Catholic Univ. Thesis

DTMB Aero Report 1077

David Taylor Model Basin. Report 1857.
A METHOD FOR NUMERICAL CALCULATION OF SLIPSTREAM CONTRACTION OF A SHROUDED IMPULSE DISC IN THE STATIC CASE WITH APPLICATION TO OTHER AXISYMMETRIC POTENTIAL FLOW PROBLEMS, by Harvey R. Chaplin. Wash., Jun 1964. 138p. incl. illus. 23 refs. (Aerodynamics Lab. Aero Rpt 1077)
Thesis (Ph.D.)--Catholic University.

Digital computer method developed to calculate axisymmetric potential flow through shrouded propeller with uniform disc loading, no swirl. Slipstream shape approached by successive approximations, and calculations made for cylindrical, conical and parabolic-cambered shrouds. Method of singularities used also applicable to other axisymmetric flow problems. Examples given for annular airfoil, body of revolution, duct and inlet flow.

Slipstream--Contraction Ratio
Propellers, Shrouded
Wings, Ring
Propellers--Efficiency
Propellers--Thrust
Ducts, Circular
Inlets, Circular
Bodies of Revolution
Flow, Axisymmetric
Flow, One-Dimensional
Propeller Shrouds--Configurations
Computer Methods
Propeller Theory, Momentum
Chaplin, Harvey R.
Catholic Univ. Thesis

DTMB Aero Report 1077

David Taylor Model Basin. Report 1857.
A METHOD FOR NUMERICAL CALCULATION OF SLIPSTREAM CONTRACTION OF A SHROUDED IMPULSE DISC IN THE STATIC CASE WITH APPLICATION TO OTHER AXISYMMETRIC POTENTIAL FLOW PROBLEMS, by Harvey R. Chaplin. Wash., Jun 1964. 138p. incl. illus. 23 refs. (Aerodynamics Lab. Aero Rpt 1077)
Thesis (Ph.D.)--Catholic University.

Digital computer method developed to calculate axisymmetric potential flow through shrouded propeller with uniform disc loading, no swirl. Slipstream shape approached by successive approximations, and calculations made for cylindrical, conical and parabolic-cambered shrouds. Method of singularities used also applicable to other axisymmetric flow problems. Examples given for annular airfoil, body of revolution, duct and inlet flow.

Slipstream--Contraction Ratio
Propellers, Shrouded
Wings, Ring
Propellers--Efficiency
Propellers--Thrust
Ducts, Circular
Inlets, Circular
Bodies of Revolution
Flow, Axisymmetric
Flow, One-Dimensional
Propeller Shrouds--Configurations
Computer Methods
Propeller Theory, Momentum
Chaplin, Harvey R.
Catholic Univ. Thesis

DTMB Aero Report 1077

David Taylor Model Basin. Report 1857.
A METHOD FOR NUMERICAL CALCULATION OF SLIPSTREAM CONTRACTION OF A SHROUDED IMPULSE DISC IN THE STATIC CASE WITH APPLICATION TO OTHER AXISYMMETRIC POTENTIAL FLOW PROBLEMS, by Harvey R. Chaplin. Wash., Jun 1964. 138p. incl. illus. 23 refs. (Aerodynamics Lab. Aero Rpt 1077)
Thesis (Ph.D.)--Catholic University.

Digital computer method developed to calculate axisymmetric potential flow through shrouded propeller with uniform disc loading, no swirl. Slipstream shape approached by successive approximations, and calculations made for cylindrical, conical and parabolic-cambered shrouds. Method of singularities used also applicable to other axisymmetric flow problems. Examples given for annular airfoil, body of revolution, duct and inlet flow.

Slipstream--Contraction Ratio
Propellers, Shrouded
Wings, Ring
Propellers--Efficiency
Propellers--Thrust
Ducts, Circular
Inlets, Circular
Bodies of Revolution
Flow, Axisymmetric
Flow, One-Dimensional
Propeller Shrouds--
Configurations
Computer Methods
Propeller Theory, Momentum
Chaplin, Harvey R.
Catholic Univ. Thesis

DTMB Aero Report 1077

David Taylor Model Basin. Report 1857.
A METHOD FOR NUMERICAL CALCULATION OF SLIPSTREAM CONTRACTION OF A SHROUDED IMPULSE DISC IN THE STATIC CASE WITH APPLICATION TO OTHER AXISYMMETRIC POTENTIAL FLOW PROBLEMS, by Harvey R. Chaplin. Wash., Jun 1964. 138p. incl. illus. 23 refs. (Aerodynamics Lab. Aero Rpt 1077)
Thesis (Ph.D.)--Catholic University.

Digital computer method developed to calculate axisymmetric potential flow through shrouded propeller with uniform disc loading, no swirl. Slipstream shape approached by successive approximations, and calculations made for cylindrical, conical and parabolic-cambered shrouds. Method of singularities used also applicable to other axisymmetric flow problems. Examples given for annular airfoil, body of revolution, duct and inlet flow.

Slipstream--Contraction Ratio
Propellers, Shrouded
Wings, Ring
Propellers--Efficiency
Propellers--Thrust
Ducts, Circular
Inlets, Circular
Bodies of Revolution
Flow, Axisymmetric
Flow, One-Dimensional
Propeller Shrouds--
Configurations
Computer Methods
Propeller Theory, Momentum
Chaplin, Harvey R.
Catholic Univ. Thesis

DTMB Aero Report 1077

David Taylor Model Basin. Report 1857.
A METHOD FOR NUMERICAL CALCULATION OF SLIPSTREAM CONTRACTION OF A SHROUDED IMPULSE DISC IN THE STATIC CASE WITH APPLICATION TO OTHER AXISYMMETRIC POTENTIAL FLOW PROBLEMS, by Harvey R. Chaplin. Wash., Jun 1964. 138p. incl. illus. 23 refs. (Aerodynamics Lab. Aero Rpt 1077)
Thesis (Ph.D.)--Catholic University.

Digital computer method developed to calculate axisymmetric potential flow through shrouded propeller with uniform disc loading, no swirl. Slipstream shape approached by successive approximations, and calculations made for cylindrical, conical and parabolic-cambered shrouds. Method of singularities used also applicable to other axisymmetric flow problems. Examples given for annular airfoil, body of revolution, duct and inlet flow.

Slipstream--Contraction Ratio
Propellers, Shrouded
Wings, Ring
Propellers--Efficiency
Propellers--Thrust
Ducts, Circular
Inlets, Circular
Bodies of Revolution
Flow, Axisymmetric
Flow, One-Dimensional
Propeller Shrouds--
Configurations
Computer Methods
Propeller Theory, Momentum
Chaplin, Harvey R.
Catholic Univ. Thesis

DTMB Aero Report 1077

David Taylor Model Basin. Report 1857.
A METHOD FOR NUMERICAL CALCULATION OF SLIPSTREAM CONTRACTION OF A SHROUDED IMPULSE DISC IN THE STATIC CASE WITH APPLICATION TO OTHER AXISYMMETRIC POTENTIAL FLOW PROBLEMS, by Harvey R. Chaplin. Wash., Jun 1964. 138p. incl. illus. 23 refs. (Aerodynamics Lab. Aero Rpt 1077)
Thesis (Ph.D.)--Catholic University.

Digital computer method developed to calculate axisymmetric potential flow through shrouded propeller with uniform disc loading, no swirl. Slipstream shape approached by successive approximations, and calculations made for cylindrical, conical and parabolic-cambered shrouds. Method of singularities used also applicable to other axisymmetric flow problems. Examples given for annular airfoil, body of revolution, duct and inlet flow.

Slipstream--Contraction Ratio
Propellers, Shrouded
Wings, Ring
Propellers--Efficiency
Propellers--Thrust
Ducts, Circular
Inlets, Circular
Bodies of Revolution
Flow, Axisymmetric
Flow, One-Dimensional
Propeller Shrouds--
Configurations
Computer Methods
Propeller Theory, Momentum
Chaplin, Harvey R.
Catholic Univ. Thesis